Doctoral Thesis

Experimental Study
of Photo-induced Voltage
in Random Nanoporous Thin Metal Films

(ランダムナノ多孔性金属薄膜における
光誘起起電力の実験的研究)

MARJAN AKBARI

Department of Physics
Graduate School of Science
Tohoku University

October 2017

To my husband

Mohammad

Acknowledgment

Contents

CHAPTER 1

Introduction

1.1 Photo-induced voltage

Solar cell is a familiar example of interaction of light with matter. Mechanism that generates voltage in such solar cell is different from that of we will discuss in this thesis for metallic nanoporous thin films. In a p-n junction solar cell energy of sunlight is converted to voltage and generating voltage with high efficiency is the purpose of the interaction(Fig. 1.1, top). In a different mechanism, by interaction of a light source, for example, laser with conductive material like a metal film, electric and magnetic fields of light beam apply force on the conduction electrons and we can observe it as photo-induced voltage (Fig. 1.1, down). In this case, manipulating amplitude and sign of the voltage by wavelength, polarization or incidence angle is main purpose and is of interest for the development of fast response photodetectors and angle sensors. This force can be estimated using momentum conservation, that is, momentum from photons transfers to the free carriers of the material and this effect manifests itself as a pulsed voltage (or emf) signal [1].

This phenomenon has been explained as photon drag effect in semiconductors. This effect was first experimentally observed during carbon dioxide laser excitation on holes and electrons in bulk germanium crystals [2]. This effect, caused by different optical excitation mechanisms, has been investigated by other groups in various materials, for example, Ge, Si and GaP [3]. Semiconductors such as Ge and Te have already found applications as photon drag detectors[4]. In principle, photon
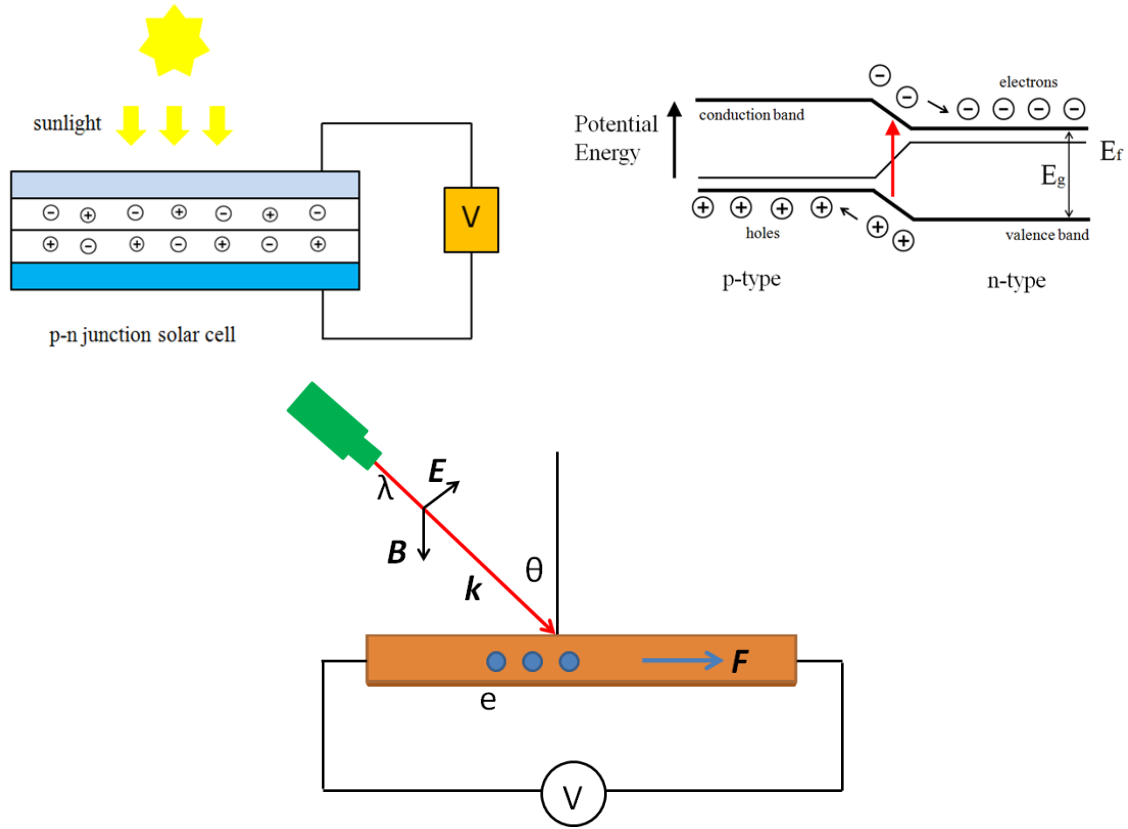
Figure 1.1: Top: Left: p-n junction solar cell, right: p-n junction energy levels. Down: Force on the free electrons from incident light in a conductive material and generation of photo-induced voltage.

drag effect is also expected for surface of metals like gold. In metals, this effect can be observed as the surface current that depend on the incidence angle and the polarization of the exciting light[5]. The photon drag effect induced current in metals without surface plasmon resonance has been described using equation of motion for the electrons within a hydrodynamic model[6]. This effect is significant in semiconductors [7] but very small in bulk metals[8].

Vengurlekar and Ishihara have reported enhanced photon drag effect in a thin gold film when the incident light excited surface plasmon. As surface plasmon cannot be excited by photons in free space, they used Kretschmann-Raether configuration to have surface plasmon at the metal-air surface by p- polarized light (Fig. 1.2). They showed that the observed photo-voltage depends on the incidence angle and polarization of light [4].

In the field of subwavelength structures, like photonic crystal and metamaterials, there is a possibility for excitation of surface plasmon polariton and it can enhance photo-induced voltage observed in these materials. Photo-induced voltage in semiconductor or metallic photonic crystal and metamaterials has been investigated [2, 9, 10, 11, 12, 13].

In systems with inversion symmetry, depending on the polarization of the light, it is possible
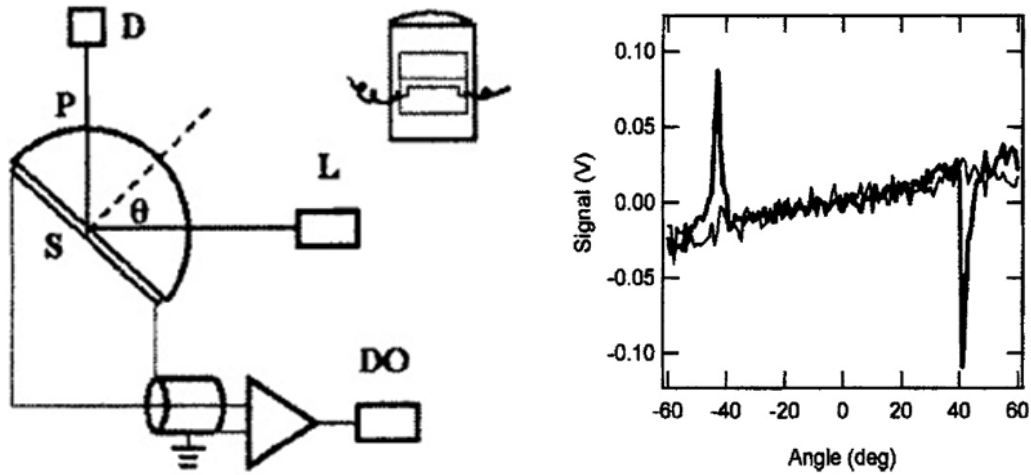
Figure 1.2: Photo-voltage induced in flat metallic film by Kretchmann-Raether configuration [4].

to break the symmetry by applying obliquely incident light. In such systems, light can induce DC polarization in the structure that is second order in terms of electric field, $P \propto E^2$. This term is referred to as optical rectification and is responsible for the voltage.

Hatano et al. measured photo-voltage in a symmetric grating structure. When laser beam is obliquely incident to the sample, they can break the symmetry in the system and generate voltage for non zero incident angles. For this structure by balancing the force from momentum flux against the electrostatic force in the structure on the electrons they estimated the longitudinal voltage (Fig. 1.3).

When a circularly polarized light beam is irradiated on gyrotropic crystals, voltage depending on the sense of circular polarization is generated, which is sometimes referred to as a circular photogalvanic effect. Similar effect is observed when the beam is incident obliquely on a conductive sample: a transverse voltage is generated perpendicular to the plane of incidence [14]. The effect is believed to be based on the transfer of angular momentum of photon to the sample and even incident beam with linear polarized light except for s- and p-polarized light may generate it.

The phenomena have been observed in many systems such as quantum wells [15], metallic photonic crystal slabs [16], Ag-Pd film [17], single walled carbon nanotube film [18], graphene [19] and spongy nanoporous gold thin film [20]. It is generated perpendicular to the plane of incidence and by changing the sense of polarization, its sign is reversed.

Hatano et al. have reported transverse and longitudinal voltage in a photonic crystal slab [11]. Transmission spectrum on this structure for p- polarization shows a dip for excitation of surface plasmon that depending on the incidence angle, the position of this dip changes. For this resonant
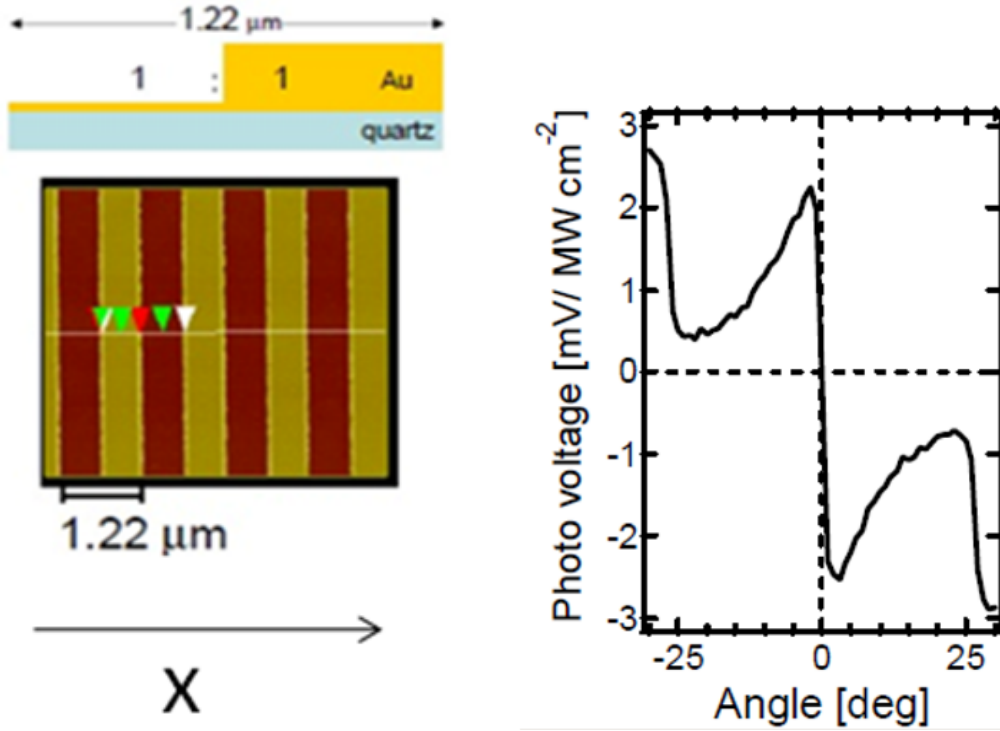
Figure 1.3: Photo-voltage induced in 1D metallic photonic crystal with symmetry structure [10].

wavelength in the spectrum, a large longitudinal photo-voltage is observed. For transverse voltage there is sign change from right hand to left hand circular polarized light. Transverse photo-voltage has a dispersive behavior at resonance due to dispersive change of phase of p- polarization at resonant points (Fig. 1.4 and 1.5).

For this photonic crystal, calculation of electric field distribution around circular holes shows breaking symmetry of the fields along y- axis, which can explain this transverse voltage and its sign change by change of sense of rotation. They showed this voltage can be estimated using integral of DC force along y- axis for all unit cells in the volume of the film (Fig. 1.5 and 1.6).
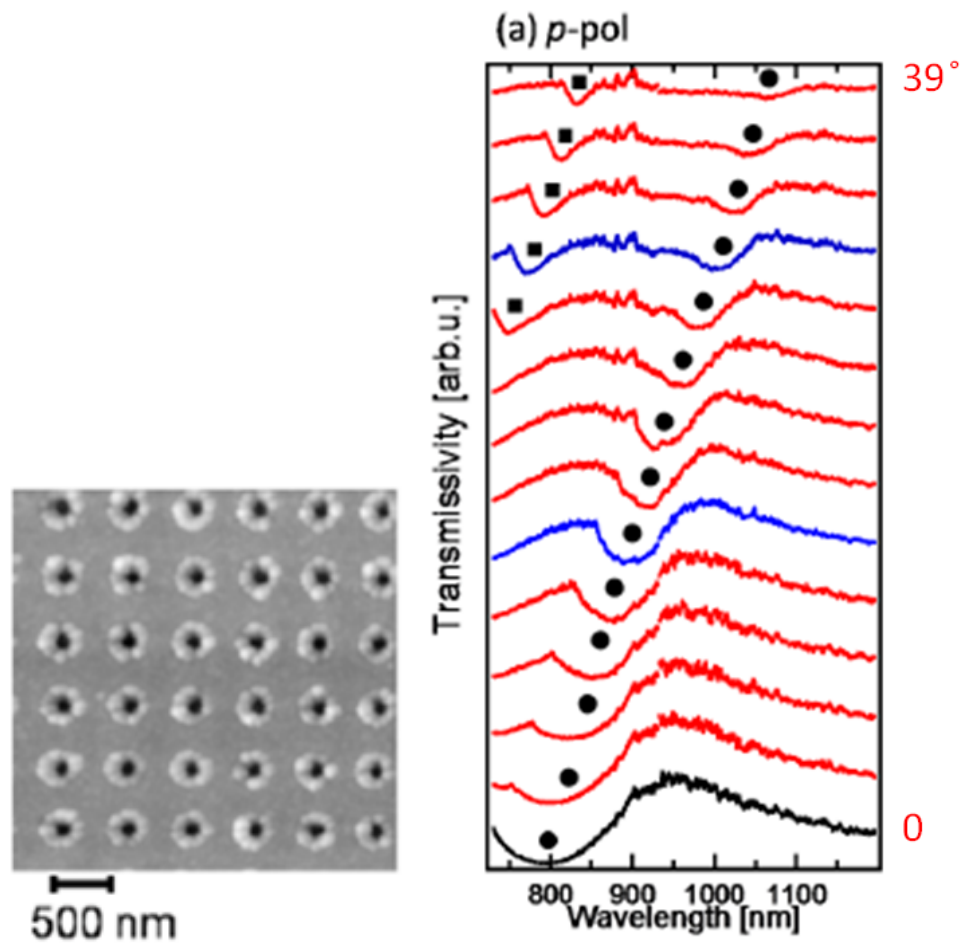
Figure 1.4: Transmission spectrum for p- polarization for photonic crystal slab [11].
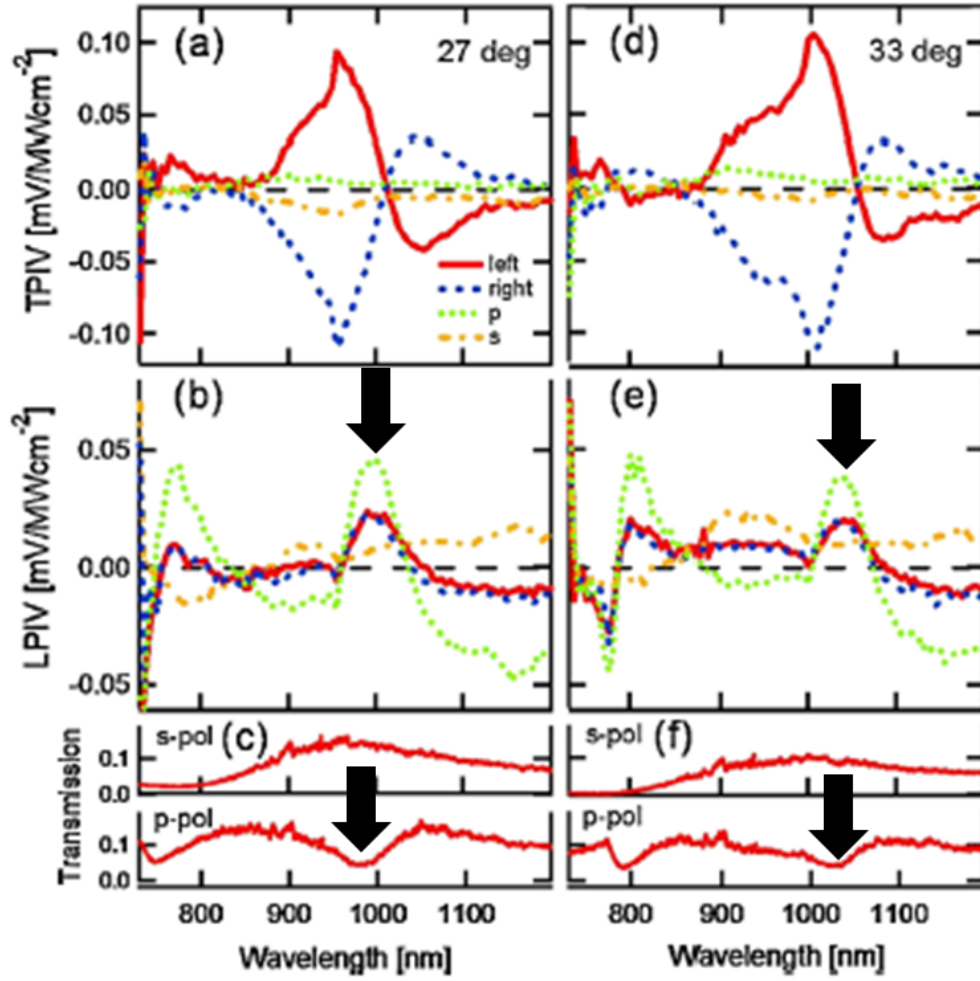
Figure 1.5: Longitudinal and transverse photo-voltage induced in metallic photonic crystal slab [11].
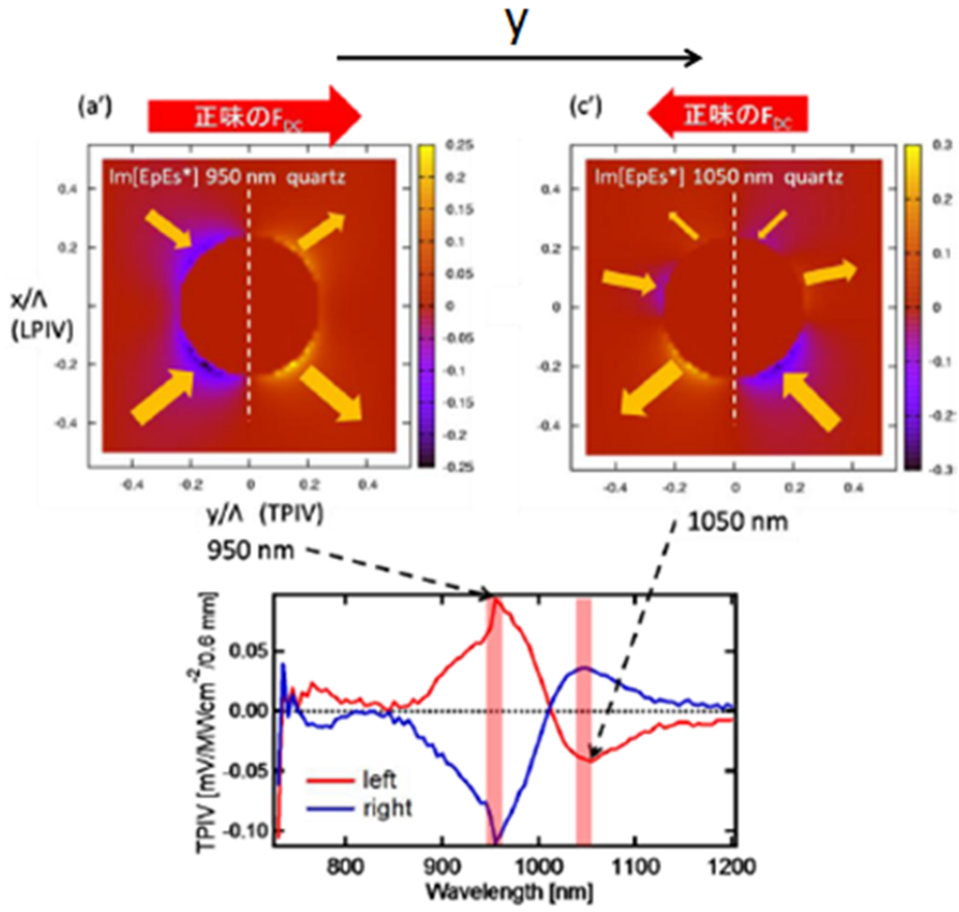
Figure 1.6: Transverse photo-voltage induced in metallic photonic crystal slab due breaking symmetry of electric fields for a circular hole [11].
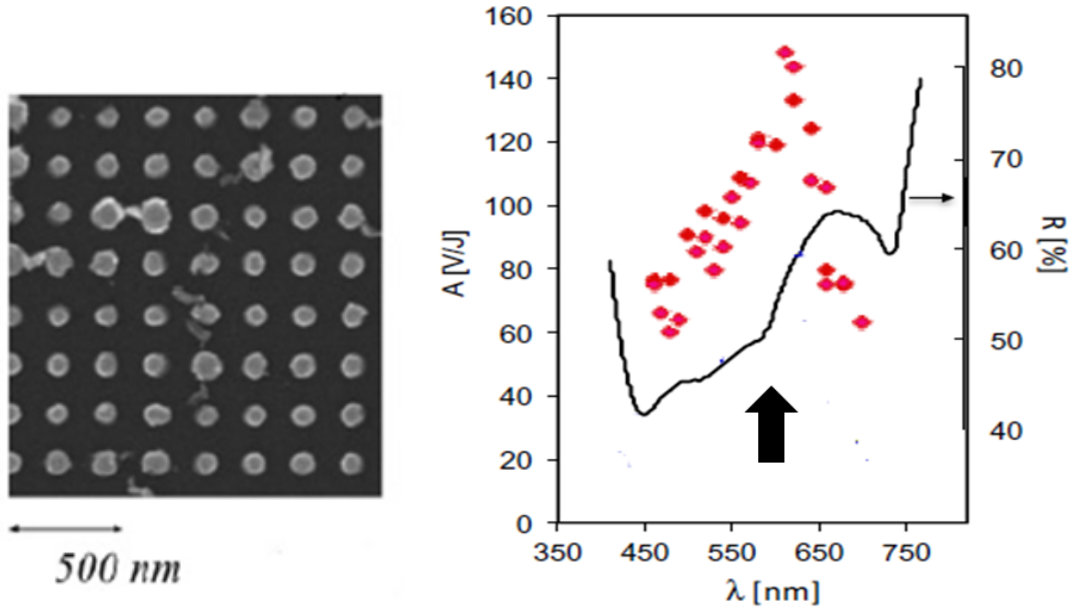
Figure 1.7: Strong longitudinal voltage in gold-coated silicon nanopillars on silicon substrate due to excitation of localized surface plasmon resonance [21].

Longitudinal voltage generated by p- polarization in gold-coated silicon nanopillars on silicon substrate was reported by Noginova et al. [21]. They reported that the peak in the wavelength dependence longitudinal voltage for p- polarization locates in the wavelength that localized surface plasmon resonance happens, as can be seen in the reflection spectrum as a dip (Fig. 1.7).

For a 2D plasmonic crystal, reflection spectrum for different incidence angles shows surface plasmon modes in the shaded area of the spectrum (Fig. 1.8). Proscia et al. have calculated transverse photo-voltage using Lorentz force and its components for total length of the sample with different polarized light for this narrow shaded area [22]. As the graph in Fig.1.8 shows, there are opposite signs for right hand and left hand circular polarized light that are consistent with experimental measurements.

They also calculated the transverse voltages generated by gradient force and scattering force separately. As the graph shows the scattering force is almost zero and the gradient force from breaking symmetry of electric field distribution around holes has the main role in generating voltage. This electric filed distribution changes by sense of rotation and it results in opposite forces or voltages for these polarized lights with opposite sense of rotations.
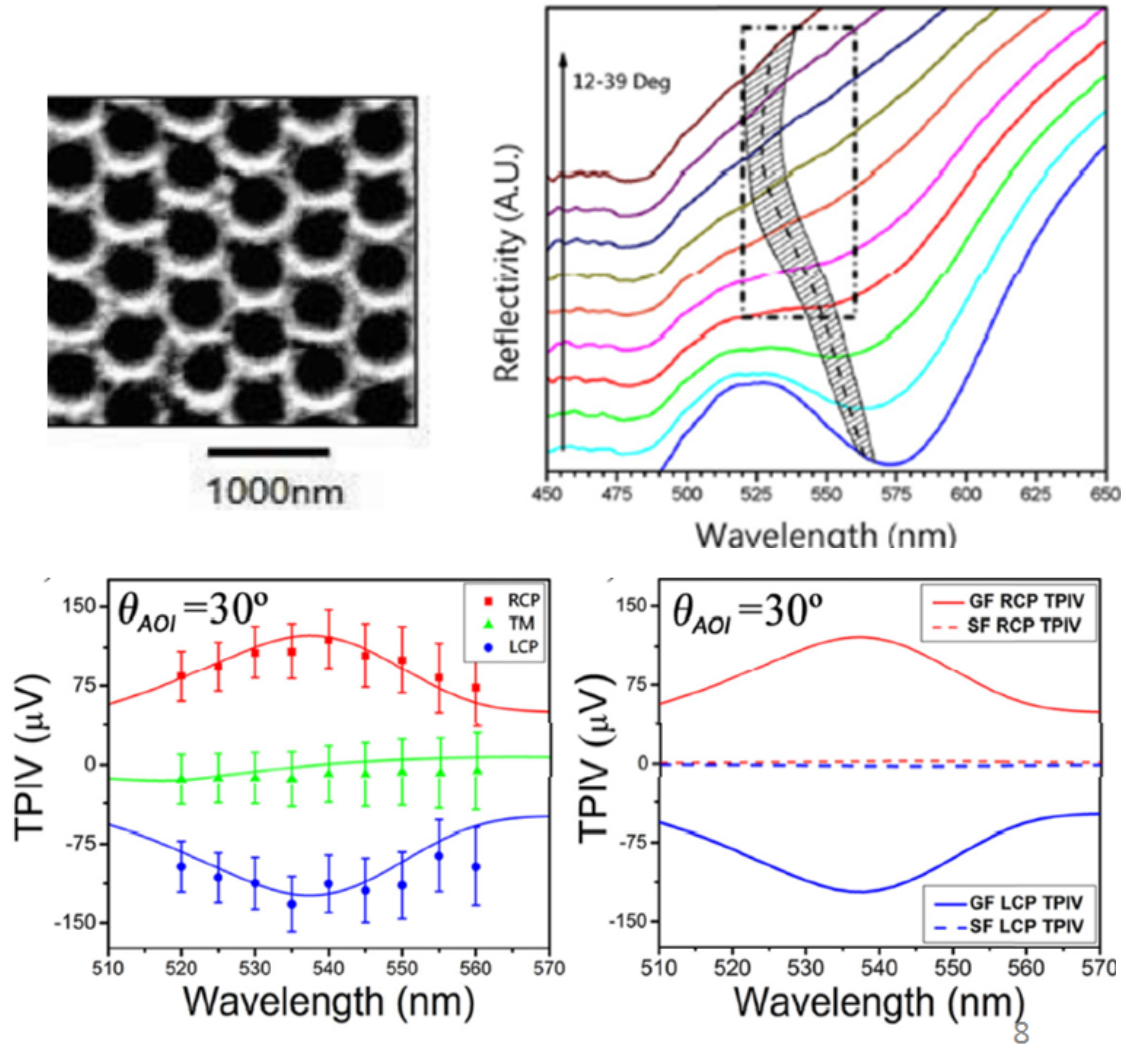
Figure 1.8: Photo-voltage induced in 2D plasmonic crystal by circularly polarized light [22].

1.2   Lorentz force

When light impinges on the material, electric and magnetic fields of the light apply a force (Lorentz force) on the free carriers and we could measure this force as voltage or photocurrent. To show how we could calculate voltage from Lorentz force we start with equation of motion for electrons:

$$m\ddot{\mathbf{r}} + m\gamma\dot{\mathbf{r}} = e(\mathbf{E} + \dot{\mathbf{r}} \times \mathbf{B}) = f \tag{1.1}$$

Second order $f^{(2)}$ can be shown as

$$f^{(2)} = e\left[(\mathbf{r} \cdot \nabla)\mathbf{E} + (\dot{\mathbf{r}} \times \mathbf{B})\right] = f_{\text{DC}}^{(2)} + f_{\text{SHG}}^{(2)} \tag{1.2}$$

and for DC force we have

$$f_{\text{DC}}^{(2)} = Re\frac{\alpha}{2}\left[(\mathbf{E} \cdot \nabla)\mathbf{E}^* + (-i\omega)\mathbf{E} \times \mathbf{B}^*\right] \tag{1.3}$$

Using

$$\nabla \times \mathbf{E} = -(-i\omega)\mathbf{B} = (i\omega)\mathbf{B}) \tag{1.4}$$

we have

$$f_{\text{DC}}^{(2)} = Re\frac{\alpha}{2}\left[(\mathbf{E} \cdot \nabla)\mathbf{E}^* + \mathbf{E} \times (\nabla \times \mathbf{E}^*)\right] \tag{1.5}$$

and for α

$$\alpha = \frac{-e^2}{m(\omega^2 + i\gamma\omega)} \tag{1.6}$$

so

$$f_{\text{DC}}^{(2)} = Re\frac{e^2}{2m(\omega^2 + i\gamma\omega)})\left[(\mathbf{E} \cdot \nabla)\mathbf{E}^* + \mathbf{E} \times (\nabla \times \mathbf{E}^*)\right] \tag{1.7}$$

After some manipulation we have

$$f_{\text{DC}}^{(2)} = -\frac{e^2}{4m(\omega^2 + \gamma^2)}\{\nabla|\mathbf{E}|^{\mathbf{2}} + \frac{2\gamma}{\omega}Im(\sum E_j\nabla E_j^*)\} \tag{1.8}$$

Where the first and the second terms are called as gradient and scattering force, respectively.

So, $f_{\text{DC}}^{(2)}$ can be shown as

$$f_{\text{DC}}^{(2)} = Re\left[\alpha \sum_j E_j \nabla E_j^*\right] \tag{1.9}$$

and force in total volume of the film is

$$F_{\text{DC}}^{(2)} = \int_V f_{\text{DC}}^{(2)} dv \tag{1.10}$$

Now for microscopic field in material $\mathbf{E}(\mathbf{r})$, and incident plane wave with a polarization (s-, p-, circular or diagonal), E_{inc};

$$\mathbf{E}(\mathbf{r}) = A(\mathbf{r}, \theta, \omega)\mathbf{E}_{inc} \tag{1.11}$$

A is a matrix describing the structure. When static force inside the material and Lorentz force are balanced

$$-Ne\mathbf{E}_{\text{DC}} + \mathbf{F}_{\text{DC}} = 0 \tag{1.12}$$

and voltage is related to $\mathbf{E}_{\text{DC}}$ as

$$\mathbf{E}_{\text{DC}} = -\nabla V \tag{1.13}$$

So, voltage along x-axis and y-axis are

$$V_x = -\frac{1}{Ne}\int_0^{Lx} f_{\text{DC},x}dx \int_0^{Ly} dy \int_0^{Lz} dz \tag{1.14}$$

$$V_y = -\frac{1}{Ne}\int_0^{Ly} f_{\text{DC},y}dy \int_0^{Lx} dx \int_0^{Lz} dz \tag{1.15}$$

For oblique incident light

$$\mathbf{E}_j(r) = \mathbf{u}_j(r,\theta)e^{ik_x} \tag{1.16}$$

Where $k_x = \omega \sin\theta/c$ and θ is incidence angle.

By replacing this electric field from (1.22) we have

$$f_{\text{DC},x}^{(2)} = \alpha' \frac{\partial}{\partial x}|\mathbf{u}(r,\theta)|^2/2 + k_x\alpha''|\mathbf{u}(r,\theta)|^2 \tag{1.17}$$
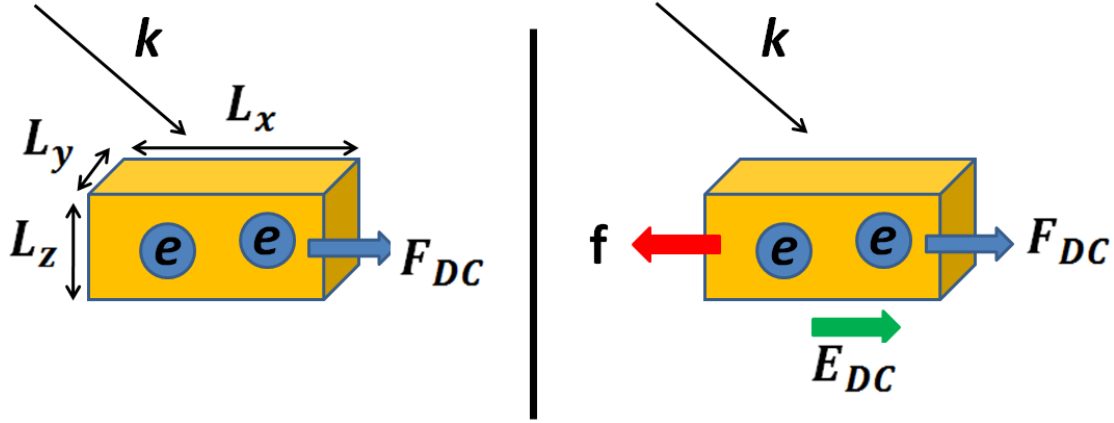
Figure 1.9: Left: Lorentz force on unit cell of the sample, right: Schematic of force of the light in the structure and response of material to this light.

Now for a periodic structure, $\mathbf{u}(r+a) = \mathbf{u}(r)$ and for circular polarized light we have $\mathbf{u}(r) = \mathbf{u}_p(r) \pm i\mathbf{u}_s(r)$. So, for circular hole

$$|u(r,\theta)|^2 = |u_s(r,\theta)|^2 + |u_p(r,\theta)|^2 \pm 2Im(u_p(r).u_s(r)^*) \tag{1.18}$$

So,

$$f_{\text{DC},x} = \alpha'\frac{\partial}{\partial x}|u(r,\theta)|^2/2 + k\alpha''|u(r,\theta)|^2 \tag{1.19}$$

For smooth film

$$F_{\text{DC},x} = \int f_{\text{DC},x}dv = k\alpha''\int |u(r)|^2 dv \tag{1.20}$$

$$\mathbf{f}_{\text{DC},y} = \alpha'\frac{\partial}{\partial y}|\mathbf{u}(r,\theta)|^2/2 \tag{1.21}$$

Here term $Im\ (u_p(r).u_s(r)^*)$ is responsible for opposite sign for voltage for different sense of rotation for right hand and left hand circular polarization [16].

Equation of motion of free electrons in a sample with periodic circular hole is

$$m\ddot{\mathbf{r}} + m\gamma\dot{\mathbf{r}} = \mathbf{F}_{\text{DC}}^{(2)} \tag{1.22}$$

In the balanced state, static force inside the whole film, $\mathbf{f}$ and gradient force in whole film, F_{DC}^L
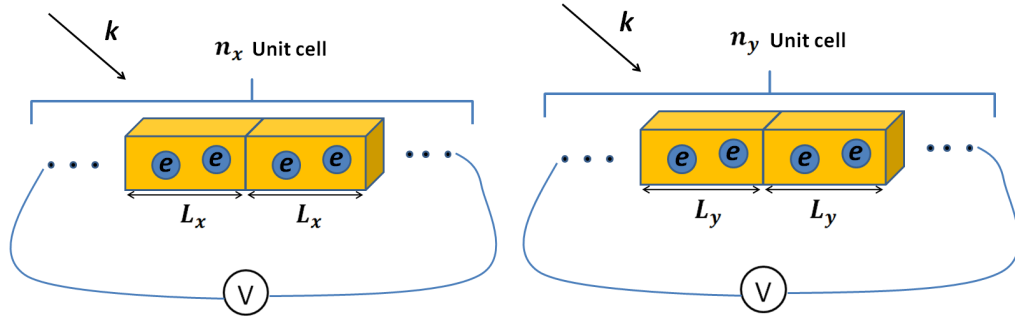
Figure 1.10: Measurement of the LPIV and TPIV.

are equal with opposite directions, so

$$\mathbf{f} + \mathbf{F}_{\text{DC}}^{(2)} = 0 \tag{1.23}$$

on the other hand $\mathbf{f}$ is opposite with the force due to induced electric field inside the whole film

$$\mathbf{f} = -\frac{1}{e}\mathbf{E}_{\text{DC}}^{(2)} \tag{1.24}$$

from eqs. 1.23 and 1.24 we have

$$\mathbf{E}_{\text{DC}}^{L} = \frac{1}{e}\mathbf{F}_{\text{DC}}^{(2)} \tag{1.25}$$

So, we can calculate E_{unit}, electric field in the unit of volume of a periodic structure as

$$\mathbf{E}_{\text{unit}} = \frac{1}{V}\int_{\text{film}}\mathbf{E}_{\text{DC}}dv = \frac{1}{eV}\int_{\text{film}}\mathbf{F}_{\text{DC}}dv \tag{1.26}$$

V is the total volume of the film. Then the voltage is

$$V_{\text{PIVi}} = -\int_{\text{film}}\mathbf{E}_{\text{unit-i}}di = -n_i L_i \mathbf{E}_{\text{unit-i}} \qquad i = x, y \tag{1.27}$$

V_{PIVx} and V_{PIVy} are voltage in the film along x and y-axis, respectively, which correspond to LPIV and TPIV:

$$V_{\text{LPIV}} = -n_x L_x E_{\text{unit-x}} = -\frac{n_x L_x}{eV}\int_{\text{film}}F_{\text{DC-x}}dv = -\frac{n_x}{L_y L_z}\int_{\text{film}}F_{\text{DC-x}}dv = -\frac{n_x}{L_y L_z}\int_{\text{film}}\nabla_x|\mathbf{E}|^2 dv \tag{1.28}$$
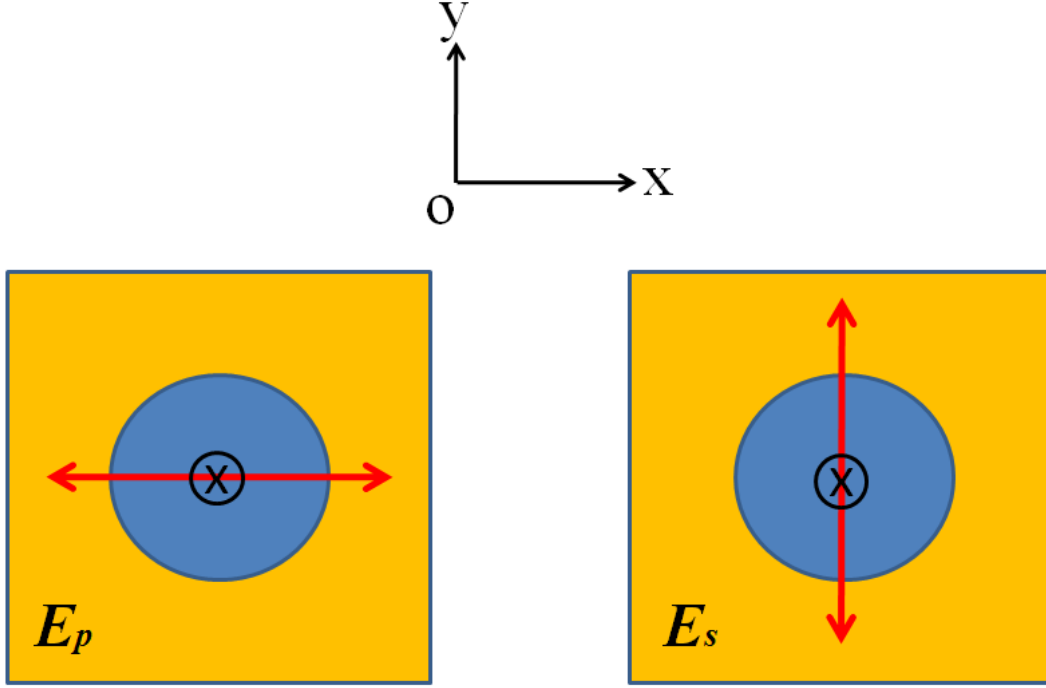
Figure 1.11: s- and p- polarized light fields for normal incident light in a symmetric unit cell of a periodic structure.

$$V_{\text{TPIV}} = -n_y L_y E_{\text{ unit-y}} = -\frac{n_y L_y}{eV} \int_{\text{film}} F_{\text{DC-y}} dv = -\frac{n_y}{L_x L_z} \int_{\text{film}} F_{\text{DC-y}} dv = -\frac{n_y}{L_x L_z} \int_{\text{film}} \nabla_y |\mathbf{E}|^2 dv$$

(1.29)

Here $\mathbf{E}$ is induced electric field in the film.

For incident light we could have $\mathbf{E}_{\text{s}}$, $\mathbf{E}_{\text{p}}$, $\mathbf{E}_{\text{cir}}^{\pm}$ and $\mathbf{E}_{45}^{\pm}$.

In our definition, when electric field is along x-axis we call it p- polarization and when along y-axis we consider it as s- polarization. So, when incident light is normal to the film we have:

$$\mathbf{E}_{\text{s}} = \begin{bmatrix} E_{\text{s}x} \\ E_{\text{s}y} \\ E_{\text{s}z} \end{bmatrix}$$

(1.30)

$$\mathbf{E}_{\text{p}} = \begin{bmatrix} E_{\text{p}x} \\ E_{\text{p}y} \\ E_{\text{p}z} \end{bmatrix}$$

(1.31)
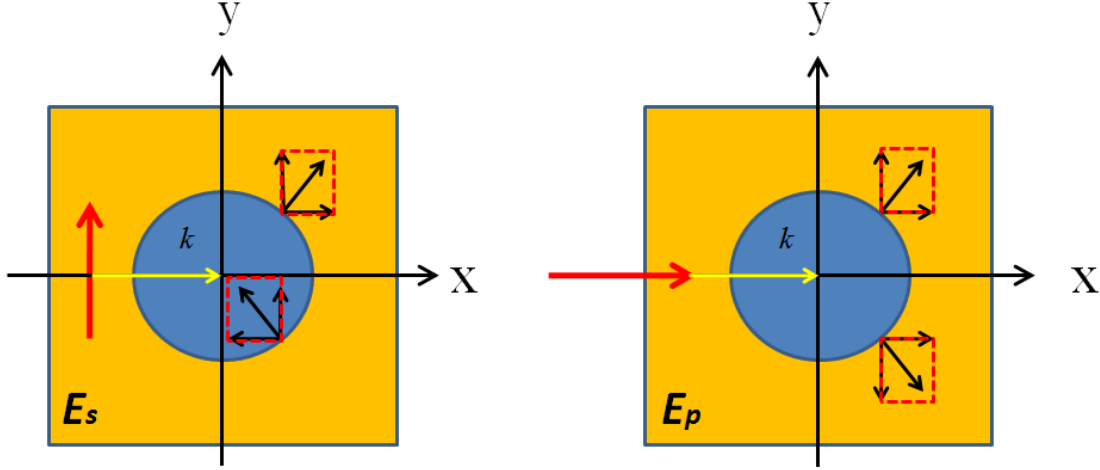
Figure 1.12: s- and p- polarized light fields for obliquely incident light in a symmetric unit cell of a periodic structure.

In this condition, symmetry of electric fields cannot be broken and we have

$$\int_{\text{film}} \nabla |\mathbf{E}|^2 dv = 0 \tag{1.32}$$

By obliquely incident light symmetry of electric fields can be broken and for s- and p- polarization we have

$$\mathbf{E}_s = \begin{bmatrix} E_{sx} \\ E_{sy} \\ E_{sz} \end{bmatrix} \tag{1.33}$$

$$\mathbf{E}_p = \begin{bmatrix} E_{px} \\ E_{py} \\ E_{pz} \end{bmatrix} \tag{1.34}$$

For these components of $\mathbf{E}_s$ and $\mathbf{E}_p$ we have

$$E_{sx}(y) = -E_{sx}(-y) \qquad E_{sy}(y) = E_{sy}(-y) \qquad E_{sz}(y) = -E_{sz}(-y)$$

and

$$E_{px}(y) = E_{px}(-y) \qquad E_{py}(y) = -E_{py}(-y) \qquad E_{pz}(y) = -E_{pz}(-y)$$

So, our odd componnets are E_{py}, E_{sx} and E_{sz}. For even components we have E_{px}, E_{pz} and E_{sy}.

If we use eqs. 1.28 and 1.29

$$V_{\text{LPIV}} \propto - \int_{\text{film}} \nabla_x |\mathbf{E}|^2 dv \tag{1.35}$$

$$V_{\text{TPIV}} \propto - \int_{\text{film}} \nabla_y |\mathbf{E}|^2 dv \tag{1.36}$$

and substitute the eclectic field of the incident light in them as $|\mathbf{E}|$ we explain the voltages in term of electric field of the light:

$\mathbf{V_{LPIV}}$:

1. Oblique incident light with $\mathbf{E_s}$:

Due to obliquely incident light integral in eq. 1.35 is non zero and if we consider odd and even components of s- polarization and knowing that $\nabla(x) = \nabla(-x)$ ($\nabla(x)$ is odd) under integral is an even function so the result is non zero voltage.

$$V_{\text{LPIV}}^s \propto - \int_{\text{film}} \nabla_x |\mathbf{E_s}|^2 dv = \nabla_x (E_{sx} E_{sx}^* + E_{sy} E_{sy}^* + E_{sz} E_{sz}^*) dv \neq 0 \tag{1.37}$$

2. Oblique incident light with $\mathbf{E_p}$:

Similar to the s- polarization

$$V_{\text{LPIV}}^p \propto - \int_{\text{film}} \nabla_x |\mathbf{E_p}|^2 dv = - \int \nabla_x (E_{px} E_{px}^* + E_{py} E_{py}^* + E_{pz} E_{pz}^*) dv \neq 0 \tag{1.38}$$

3. Oblique incident light with $\mathbf{E}_{\text{cir}}^{\pm}$:

For right hand and left hand polarized light we can show them using their s and p components as

$$\mathbf{E}_{\text{circ}}^{\pm} = \frac{1}{\sqrt{2}} (\mathbf{E_p} \pm i\mathbf{E_s}) \tag{1.39}$$

Here + sing is for right hand and - is for left hand circular polarized. By substituting $\mathbf{E}_{cir}^{\pm}$

$$V_{\text{LPIV}}^{\pm \text{circ}} \propto -\frac{1}{2} \int_{\text{film}} \nabla_x |\mathbf{E}_{\text{circ}}^{\pm}|^2 dv \propto -\frac{1}{2} \int_{\text{film}} \nabla_x (|\mathbf{E_p}|^2 + |\mathbf{E_s}|^2 \pm 2Im(\mathbf{E_p} \cdot \mathbf{E_s}^*)) dv \tag{1.40}$$

The third term in this relation $(\nabla_x 2Im(\mathbf{E_p} \cdot \mathbf{E_s}^*)$ is an odd function so

$$V_{\text{LPIV}}^{\pm \text{circ}} \propto -\frac{1}{2} \int_{\text{film}} \nabla_x |\mathbf{E}_{\text{circ}}^{\pm}|^2 dv \propto -\frac{1}{2} \int_{\text{film}} \nabla_x (|\mathbf{E_p}|^2 + |\mathbf{E_s}|^2) dv = \frac{I_p + I_s}{2} \tag{1.41}$$

as we see eq. 1.41 is combination of eqs. 1.37 and 1.38. So, it is consistent with our measurement of LPIV with circular polarized light.

3. Oblique incident light with $\mathbf{E}_{45}^{\pm}$:

Showing diagonal polarized light as

$$\mathbf{E}_{45}^{\pm} = \frac{1}{\sqrt{2}}(\mathbf{E}_{\mathrm{p}} \pm \mathbf{E}_{\mathrm{s}}) \tag{1.42}$$

We reach

$$V_{\mathrm{LPIV}}^{\pm 45} \propto -\frac{1}{2}\int_{\mathrm{film}} \nabla_x |\mathbf{E}_{45}^{\pm}|^2 dv \propto -\frac{1}{2}\int_{\mathrm{film}} \nabla_x (|\mathbf{E}_{\mathrm{p}}|^2 + |\mathbf{E}_{\mathrm{s}}|^2 \pm 2Re(\mathbf{E}_{\mathrm{p}} \cdot \mathbf{E}_{\mathrm{s}}^*))dv \tag{1.43}$$

Similar to circular polarization

$$V_{\mathrm{LPIV}}^{\pm 45} \propto -\frac{1}{2}\int_{\mathrm{film}} \nabla_x |\mathbf{E}_{45}^{\pm}|^2 dv \propto -\frac{1}{2}\int_{\mathrm{film}} \nabla_x (|\mathbf{E}_{\mathrm{p}}|^2 + |\mathbf{E}_{\mathrm{s}}|^2)dv \tag{1.44}$$

$\mathbf{V_{TPIV}}$:

1. Oblique incident light with $\mathbf{E}_{\mathrm{s}}$:

Due to obliquely incident light integral in eq.1.36) is non zero and if we consider odd and even components of s- polarization and knowing that $\nabla(y) = -\nabla(-y)$ ($\nabla(y)$ is odd) under integral is an odd function so the result is zero voltage.

$$V_{\mathrm{TPIV}}^{\mathrm{s}} \propto -\int_{\mathrm{film}} \nabla_y |\mathbf{E}_{\mathrm{s}}|^2 dv = -\int \nabla_y (E_{\mathrm{s}x}E_{\mathrm{s}x}^* + E_{\mathrm{s}y}E_{\mathrm{s}y}^* + E_{\mathrm{s}z}E_{\mathrm{s}z}^*)dv = 0 \tag{1.45}$$

2. Oblique incident light with $\mathbf{E}_{\mathrm{p}}$:

Similar to the s- polarization

$$V_{\mathrm{TPIV}}^{\mathrm{p}} \propto -\int_{\mathrm{film}} \nabla_y |\mathbf{E}_{\mathrm{p}}|^2 dv = \nabla_x (E_{\mathrm{p}x}E_{\mathrm{p}x}^* + E_{\mathrm{p}y}E_{\mathrm{p}y}^* + E_{\mathrm{p}z}E_{\mathrm{p}z}^*)dv = 0 \tag{1.46}$$

3. Oblique incident light with $\mathbf{E}_{\mathrm{cir}}^{\pm}$:

$$V_{\mathrm{TPIV}}^{\pm \mathrm{circ}} \propto -\frac{1}{2}\int_{\mathrm{film}} \nabla_y |\mathbf{E}_{\mathrm{circ}}^{\pm}|^2 dv \propto -\frac{1}{2}\int_{\mathrm{film}} \nabla_y (|\mathbf{E}_{\mathrm{p}}|^2 + |\mathbf{E}_{\mathrm{s}}|^2 \pm 2Im(\mathbf{E}_{\mathrm{p}} \cdot \mathbf{E}_{\mathrm{s}}^*))dv \tag{1.47}$$
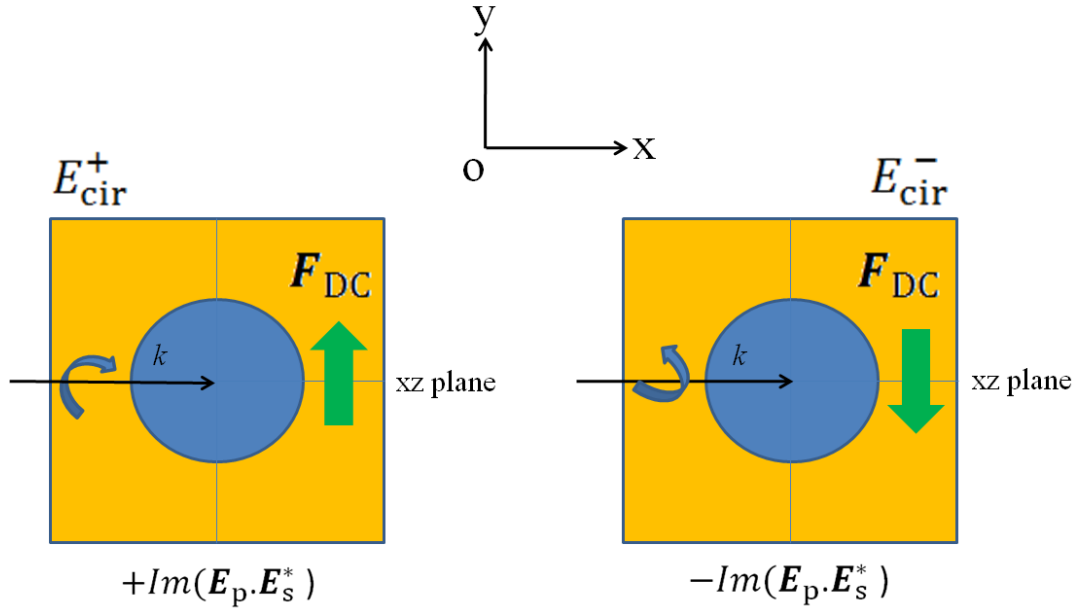
Figure 1.13: Schematics of the force for generating TPIV for right hand and left hand circular polarized light.

The first and second terms in this relation are odd function so

$$V_{\text{TPIV}}^{\pm\text{circ}} \propto -\frac{1}{2}\int_{\text{film}}\nabla_y|\mathbf{E}_{\text{circ}}^{\pm}|^2 dv \propto -\int_{\text{film}}\nabla_y(\pm Im(\mathbf{E}_{\text{p}}\cdot\mathbf{E}_{\text{s}}^*))dv \qquad (1.48)$$

3. Oblique incident light with $\mathbf{E}_{45}^{\pm}$:

$$V_{\text{TPIV}}^{\pm 45} \propto -\frac{1}{2}\int_{\text{film}}\nabla_y|\mathbf{E}_{45}^{\pm}|^2 dv \propto -\int_{\text{film}}\nabla_y(\pm Re(\mathbf{E}_{\text{p}}\cdot\mathbf{E}_{\text{s}}^*))dv \qquad (1.49)$$

1.3   Surface plasmon

Surface plasmons are electromagnetic surface waves at metal-dielectric interfaces. Their specific character is determined by the coupling of the electromagnetic field with the coherent electron oscillations at the metal surface. Surface plasmons have wavelengths shorter than light and exhibit a strong field confinement at the metal-dielectric interface. Because of these properties they form the backbone of current subwavelength optics [23].

1.3.1   Surface plasmon polariton

We consider the interface between a metal and dielectric as shown in Fig. 1.14. Solving Maxwell's equations for this interface with a plane wave excitation, they give two solutions for waves in the system. One is plane wave solution which corresponds to transmittance, reflectance and diffraction.
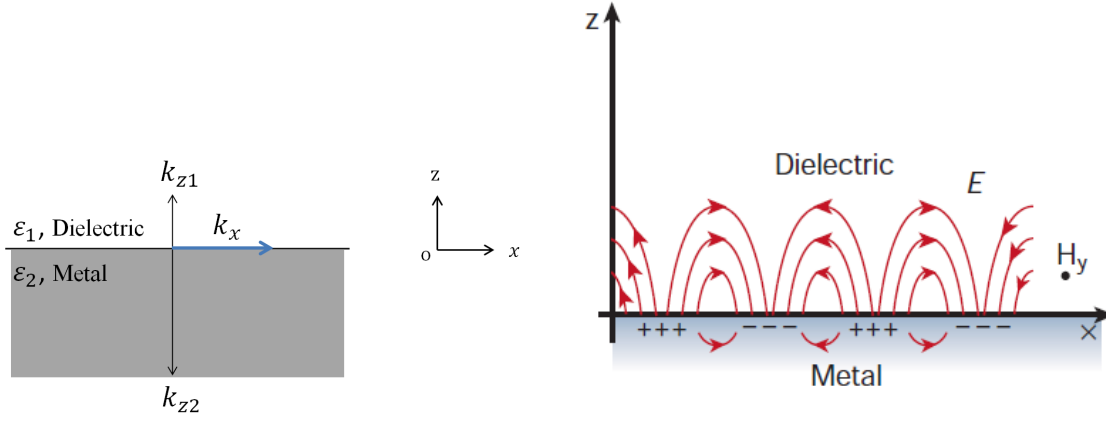
Figure 1.14: Excitation of surface plasmon polariton at the interface of metal-dielectric [23].

The other one is evanescent solution that corresponds to surface mode which is strongly localized near the interface [24].

The magnetic field of a propagating electromagnetic wave localized at interface can be expressed as

$$H_y = H_0 e^{-k|z|} e^{i(k_x x - \omega t)} \tag{1.50}$$

where k is the wave number and ω is the frequency of the wave. Magnetic field of this wave is perpendicular with propagation direction, so, it is a transverse magnetic mode. By solving Maxwell's equations for the electromagnetic wave at the interface between dielectric with permittivity of ε_1 and metal with permittivity of ε_2, and considering the continuity relation for the electric and magnetic fields we have (for TM mode)

$$\frac{\kappa_1}{\varepsilon_1} + \frac{\kappa_2}{\varepsilon_2} = 0 \tag{1.51}$$

and

$$k_x^2 + \kappa_j^2 = \varepsilon_j \left(\frac{\omega}{c}\right)^2 \quad i = 1, 2 \tag{1.52}$$

where c is the speed of light in vacuum, and k_x (wave vector of surface plasmon) is the same for both media at the interface. κ_1 and κ_2 are z components of wave vectors in the dielectric and metal. Solving these two equations, the dispersion relation for a wave propagating on the surface
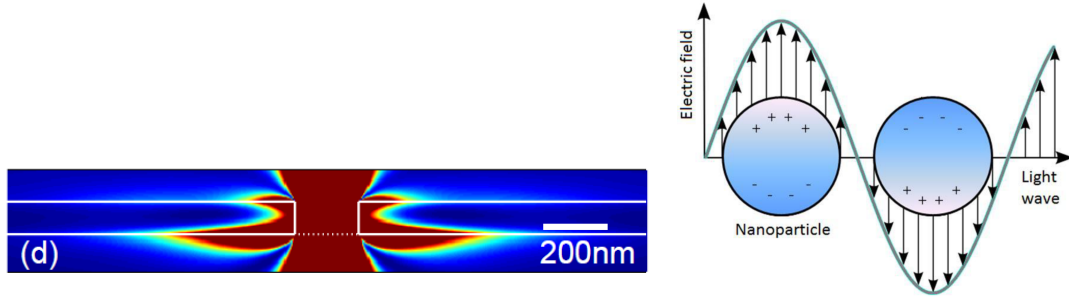
Figure 1.15: Left: Amplification of electric field in the rim of the nanohole due to the localized surface plasmons in nanohole gold [25], right: Excitation of localized surface plasmons in nanoparticles [26].

is

$$k_x = \frac{\omega}{c} \left(\frac{\varepsilon_1 \varepsilon_2}{\varepsilon_1 + \varepsilon_2} \right)^{1/2}.$$ (1.53)

In equation 1.51 considering that $\kappa_1 > 0$ and $\kappa_2 > 0$, this equation is valid only when ε_1 and ε_2 have opposite signs. In this condition there is possibility to have surface plasmon excitation in the interface of the metal and dielectric. For TE configuration (electric field of this wave is perpendicular to the propagation direction)

$$\frac{\kappa_1}{\mu_1} + \frac{\kappa_2}{\mu_2} = 0$$ (1.54)

and equation 1.54 cannot be satisfied with $\kappa_1 > 0$ and $\kappa_2 > 0$, so, there is not any solution for surface wave with s- polarized incident light. These surface plasmons are propagating electromagnetic waves couple to the electron plasma of a conductor at a dielectric interface (Fig. 1.14).

1.3.2   Localized surface plasmons

Localized surface plasmons on the other hand are non-propagating excitations of the conduction electrons of metallic nanostructures coupled to the electromagnetic field. These modes arise naturally from the scattering of a small subwavelength conductive nanoparticles in an oscillating electromagnetic field (Fig. 1.15). The surface of the particle exerts an effective restoring force on the driven electrons, so that a resonance can arise, leading to field amplification both inside and in the near-field zone outside the particle. This resonance is called localized surface plasmon or localized plasmon resonance. Another consequence of the curved surface is that plasmon resonances can be excited by direct light illumination, in contrast to propagating surface plasmon polariton in the previous section, where the phase-matching techniques described have to be employed [27]. In this study we focus on the interaction of visible light with nanoporous metallic thin films with

subwavelength sizes of holes (pores). For these random metamaterials for p- polarized incident light it is possible to couple photons with surface plasmons for all wavelengths of visible range. Here the scattering points are the nanoholes and similar to the curved surface of the nanoparticles, resonance happens and leads to field amplification in the rims of the nanoholes (Fig. 1.15) [25].

1.4   Nonlinear Polarization

Interaction of light with matters result in various responses inside the materials that can be described using Maxwell's equations. The Maxwell's equations for non-magnetic media with no free charges gives:

$$\nabla \cdot \mathbf{D} = 0 \tag{1.55}$$

here $\mathbf{D} = \mathbf{D}(\mathbf{E})$ is the electric displacement, describing the response of the medium to an external electric field, as given by the constitutive relation:

$$= \varepsilon_0 \mathbf{E} + \mathbf{P} \tag{1.56}$$

$\mathbf{P} = \mathbf{P}(\mathbf{E})$ is the polarization, describing the average density of the induced (atomic or molecular) electric dipole moments in the medium. ε_0 is the electric permittivity of free space. In presence of a medium, the Maxwell's equations alone do not determine the field quantities. They should be complemented by the constitutive relation [28].

The constitutive relation $\mathbf{D}(\mathbf{E}) = \varepsilon_0 \mathbf{E} + \mathbf{P}(\mathbf{E})$ plays a key role in optics. It describes the response of a medium to the applied external electric field. For small field strengths the dependence of the induced polarization in a medium on the electric field is linear:

$$\mathbf{P}(\mathbf{E}) = \varepsilon_0 \chi^{(1)} \mathbf{E} = \mathbf{P^{(1)}} \tag{1.57}$$

here χ is susceptibility of the medium. So, for electric displacement we have:

$$\mathbf{D}(\mathbf{E}) = \varepsilon_0 (1 + \chi^{(1)}) \mathbf{E} = \varepsilon_0 \varepsilon \mathbf{E} \tag{1.58}$$

If a strong light (laser) acts on the nonlinear medium, the relationship between $\mathbf{P}$ and $\mathbf{E}$ is

nonlinear, the medium induced $\mathbf{P}$ can be spread out into a power series of E:

$$\mathbf{P}(\mathbf{E}) = \varepsilon_0 \chi^{(1)} \mathbf{E} + \varepsilon_0 \chi^{(2)} \mathbf{EE} + \varepsilon_0 \chi^{(3)} \mathbf{EEE} + ... \tag{1.59}$$

where $\chi^{(n)}$ is n^{th} electric susceptibility, $(n = 1, 2, 3, ...)$ which is a $n+1$ order tensor. Therefore P can be divided into the linear and nonlinear parts. The nonlinear part is just the sum of high-order terms of polarization, which is called as nonlinear polarization noted by P^{NL}, that is:

$$\mathbf{P}^{NL} = \varepsilon_0 \chi^{(2)} \mathbf{EE} + \varepsilon_0 \chi^{(3)} \mathbf{EEE} + ... = \mathbf{P}^{(2)} + \mathbf{P}^{(3)} + ... \tag{1.60}$$

In this relation $\mathbf{E}$ is macroscopic electric filed induced in the material and $\mathbf{P}^{(2)} = \varepsilon_0 \chi^{(2)} \mathbf{EE}$ is second order nonlinear polarization and force on the material could be estimated by integration of $\mathbf{P^{(2)}}$ over total volume of the film.

1.5   Metamaterials

For conventional materials atomic structure of material has an essential role on the interaction between light and material and results in electromagnetic phenomena. Creation of an artificially structured composite consisting of feature sizes of wavelength dimensions is the way to realize novel electromagnetic material and has attracted considerable attentions in last few decades. Such artificial functional materials are referred to as metamaterials.

A metamaterial is an artificially structured material which attains its unusual unique properties from the unit structure rather than the constitute materials. A metamaterial has a feature size that is much smaller than the wavelength of interest and its electromagnetic response is expressed in terms of homogenized material parameters [29]. Metamaterials are mostly repeating pattern of meta-atoms with various shapes, geometries, sizes and arrangements of meta-atoms and are designed to manipulate light in various ways, for example, by blocking, absorbing, enhancing or bending the light.

The idea of metamaterials has been quickly adopted in the optics. Optical metamaterials are by far the most fascinating and most challenging topics in this field. Optical magnetism [30], optical negative index materials [31], super resolution with metamaterials [32] and nonlinear optics [33] are several key research directions in this field. Such electromagnetic properties cannot be found in the natural materials. Like conventional materials, electromagnetic and optical phenomena in
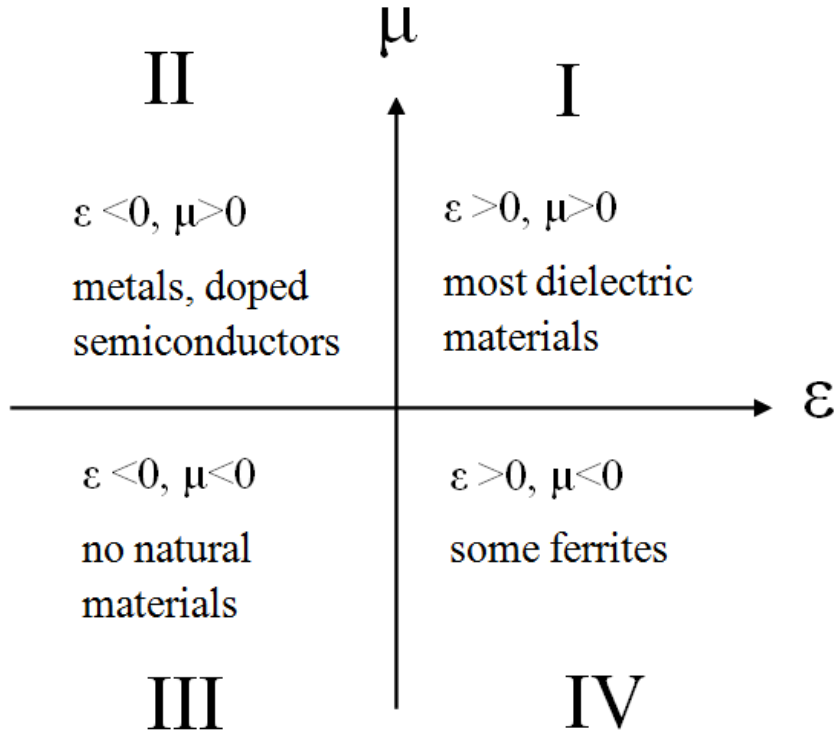
Figure 1.16: The parameter space for ε and μ.

metamaterials can be analyzed by using Maxwell's equations:

$$\nabla{\cdot}\mathbf{D} = \rho, \qquad \nabla{\cdot}\mathbf{B} = 0, \qquad \nabla{\times}\mathbf{E} = -\frac{\partial\mathbf{B}}{\partial t}, \qquad \nabla{\times}\mathbf{H} = \mathbf{J} + \frac{\partial\mathbf{D}}{\partial t}. \qquad (1.61)$$

and their electromagnetic properties are determined by four complex macroscopic effective constitutive parameters (*i.e.* they are used to describe the overall average response of the material as a whole),permittivity ε, permeability μ, refractive index n

$$n = \sqrt{\mu\varepsilon} \qquad (1.62)$$

and impedance Z[29].

$$Z = \sqrt{\frac{\mu}{\varepsilon}} \qquad (1.63)$$

Since the response of a material to external field is largely determined only by the two parameters ε and μ, we can use an electromagnetic space to classify materials based on these two values in Fig. 1.16. In this figure horizontal axis is real part of ε and vertical axis is real part of μ.
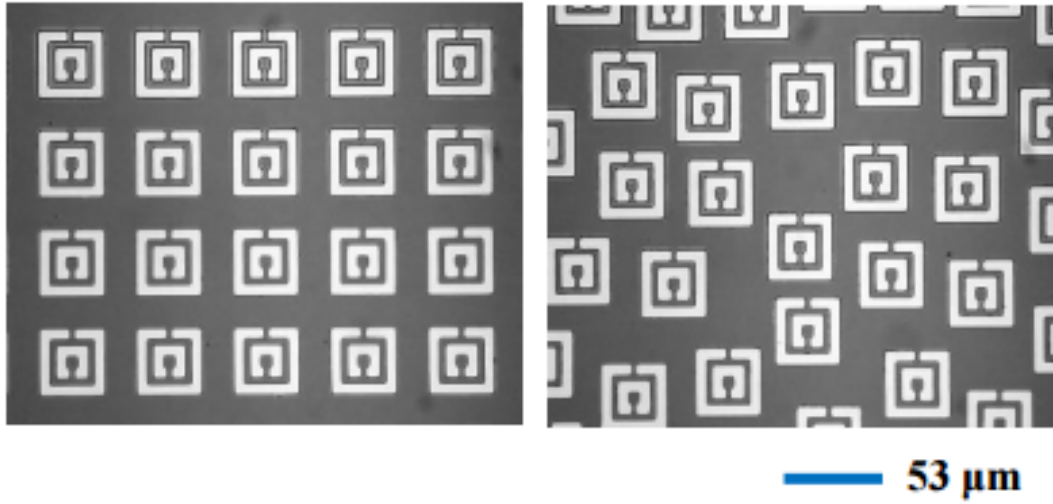
Figure 1.17: Left: periodic arrangement of Split Ring Resonators (SRR) for Terahertz frequencies, right: random arrangement of SRR [36].

First quarter represents conventional materials known as transparent which have both values positive. Second quarter includes metals in optical wavelengths which have negative ε. Noble metals are good example for this quarter. Negative μ can be found in ferromagnetic medium near resonance [34]. In the domain of optics, all conventional materials are confined to a narrow zone around a horizontal line at $\mu=1$ in the above parameter space [35].

The major focus of the metamaterial researchers is to create artificial materials that enter regions of the parameter space that are not forbidden by Maxwell's equations but are not observed in any conventional materials. Taking advantage of this expanded parameter space, they can use it for better control of electromagnetic waves [29]. Photonic metamaterials (optical metamaterials) are structures with features and cell sizes much smaller than wavelength (subwavelength). These materials are homogenous in the applied wavelength and have effective permittivity and permeability.

For Plasmonic metamaterials we can utilize surface plasmon excitations to achieve new optical properties [37]. Many of the previous works on metamaterials were focused on investigating the unique properties of wave propagation through periodic structures. There has been some interest to explore the collective behavior of metamaterials with disorder arrangements of meta-atoms, for example, investigation of the normal incidence transmission through randomly arranged planar split ring resonators (Fig.1.17). In this thesis we study the optical properties and photo response of metallic thin films with random nanoholes where the size of holes are subwavelength in visible wavelength, so we can consider them as random metamaterials in this range. In these metamaterials nanoholes are meta-atoms which are randomly distributed in the film.

1.6   Nanohole metallic thin films

In this thesis we will investigate photo-induced voltage in nanoporous gold thin films with various size and shape of nanoholes. Nanostructured gold can be used in several forms, for example, nanoparticles gold, nanowire gold and spongy nanoporous gold. Spongy nanoporous gold, has an important role in modern technologies. It is a bicontinous interconnected network of holes (with typical feature size of several ten nanometers) and air which can be prepared by dealloying an alloy of gold and a less noble metal. It has applications in biomedicine, solar cells, catalysis and many others.

But some of the applications of spongy nanoporous gold are different from that of the nature of bulk gold. For example, bulk gold is an inert metal but spongy nanoporous gold can be used as a good catalyser in chemical activities. While gold exhibit golden color, spongy nanoporous gold has a copper like color which is result of reduction in reflections of light in this range of wavelength. Thus pores play an essential role for spongy nanoporous gold and its nanostructure is a crucial factor for various applications [38]. One important consequence of pores is the increased surface area, so, it produces a large surface to volume ratio. This implies that nanomaterials and nanostructures are to a large extent governed by their surface properties.

In recent years, the number of publications concerning spongy nanoporous gold steadily increased by about 30 percent per year, from 11 publications in 2001 to more than 100 publications in the year 2009. Spongy nanoporous gold is used in the field of catalysis, sensors, actuators, optics, and many more areas [39]. After 30 min of dealloying a 50% -50% alloy of silver and gold in acid, almost all silver atoms are dissolved and 96.1% of produced thin film is gold and the rest is silver [40]. For this thin film, size of pores is about 30 to 40 nm. Porous materials with various micro or nanostructures have been investigated to utilize their multifunctional features for the applications in modern technology in many length scales [41]. Optimal nanoporous structures for transport properties are being applied to many small sized devices in nanotechnology: nanofluidics, nano-bio, MEMS, and nano electromechanical systems (NEMS) [42].

The presence of nanohole in thin gold films is utilized for the excitation of localized and propagating surface plasmon modes. Conditions can be established to excite a resonance between the localized and propagating surface plasmon modes, which enhanced the local electromagnetic field [43]. Near-field scanning optical microscopy experiments have shown that the hole acts as a scattering center for surface plasmon polariton [44]. Etching techniques and nano sphere lithography allow us to produce this film with low-cost in less time. So, these random nanoporous metallic

films are good candidates to investigate their photo response and possible applications in optical

sensing.

1.7   Motivation and purpose

In the above review of the pervious works on the photo-induced voltage all the samples were periodic nanostructures and excitation of surface plasmon modes can generate a large voltage at the resonance wavelengths. Characterizations of all these periodic structures are: 1. a period, 2. identical feature size (regular holes) and 3. inversion symmetry. Such periodic structures dispersion relation allows us to find the resonant points for diffractions or surface plasmon modes.

Compared to the periodic nanostructures random structures lack all these characterizations. They do not have period, so, such dispersion relation and resonant points do not exist. It is also possible to have non identical features (irregular holes) and lack of inversion symmetry in a random structures. Motivation of this thesis is investigation of photo-induced voltage in such random structures compared to the periodic ones.

Here I present an experimental study of the photo-induced voltage in randomly distributed nanoporous structures. A good candidate for such random structure is spongy nanoporous gold. It is an interconnected network of gold and hole with hole size of 50 nm and thickness of 100nm. This conductive material has a simple fabrication method and has applications, for example, optical sensing. It is not obvious in advance whether LPIV and TPIV are observed in such a random system. Experimental demonstration of these effects is the first purpose of this study. In contrast to the periodic structures, these structures are perfectly random, so, diffraction does not happens and we do not expect any resonance. On the other hand there is a possibility of anomalous response in these subwavelength metallic structures, as we see in metamaterials. As numerical simulations cannot apply for the random structures and electric fields inside the structure is complicated, I try to use conservation rules to investigate its validity and I explore the evidence which shows that spongy nanoporous gold is qualified as a metamaterial under certain condition.

CHAPTER 2

Experimental methods

Photo-induced voltage (PIV) generated by oblique incident light in metallic nanoporous thin films was investigated in this thesis. In this chapter we explain configurations and setups used to perform these measurements in details. In all setups and configurations sample is normal to the z-axis and film is set in xy-plane and voltage is measured across x-axis or y-axis as we explain below.

2.1 Configurations

In order to measure voltages, we employed two configurations:

1.**Longitudinal configuration:** In this configuration two electrodes are oriented perpendicular to the plane of incidence (xz-plane) and the voltage along x-axis is measured.

2.**Transverse configuration:** Two electrodes are oriented parallel to the incidence plane and the voltage along y-axis is measured (Fig. 2.1).

The observed photo-induced voltages; longitudinal photo-induced voltage (LPIV) and transverse photo-induced voltage (TPIV), are measured for a pulse laser. Positive incidence angle is shown by the arrow in Fig. 2.1. Peak of the signal is measured as a voltage.
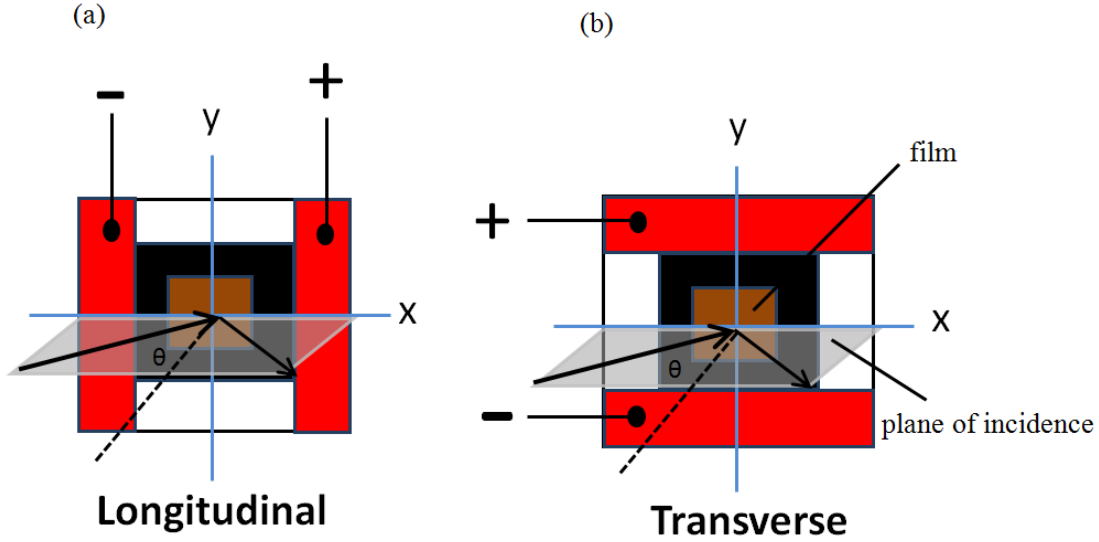
Figure 2.1: Longitudinal and transverse configurations.

2.2   Experimental setups

Light from an optical parametric oscillator (OPO) was pumped by tripled Nd:YAG laser and produced both idler wavelengths (light with 750-2300 nm) and signal wavelengths (light with 450-650 nm). The laser pulse width and repetition rate were 7 ns and 10 Hz, respectively. Energy of laser beam was measured by a joule-meter. The intensity of light for angle dependence and polarization dependence measurements were 900 mV and using 1.58 mJ/V as conversion constant between laser intensity [J] and voltage [V], the energy of laser pulse in Joule is E_{pulse}=1.4 mJ. For calculating intensity of laser beam we use E_{pulse}, pulse width, Δ t = 7 ns and area of laser spot with a diameter of $D = 5$ mm $(A = \pi(D/2)^2 = 0.2\ cm^2)$. So, for incident light we have $I_I = E_{\text{pulse}}/\Delta t \times A$=1 MW/cm^2, while threshold of the laser damage intensity was 2.4 MW/ cm^2. For wavelength dependence measurement intensity of incident light was 0.35 MW/ cm^2 for all wavelengths.

Sample is mounted on a rotational stage, so we can change the incidence angle of the light. A half wave plate on a rotary stage combined with a polarizer works to keep intensity of all wavelengths the same for wavelength resolved measurements. The polarization of light was controlled with a super achromatic half wave plate (HWP) and quarter wave plate (QWP) from Thorlab, which are valid for wavelength between 315 and 2300 nm. We measured peak of photo-induced voltage at a fixed delay for different configurations with a digital oscilloscope (Tektronix TDS3012B with 50 Ω input impedance and pass band of 100 MHz) which is triggered by the Q-switch of the laser. An amplifier with a gain of 125 was used before feeding induced voltage to the oscilloscope. A shield
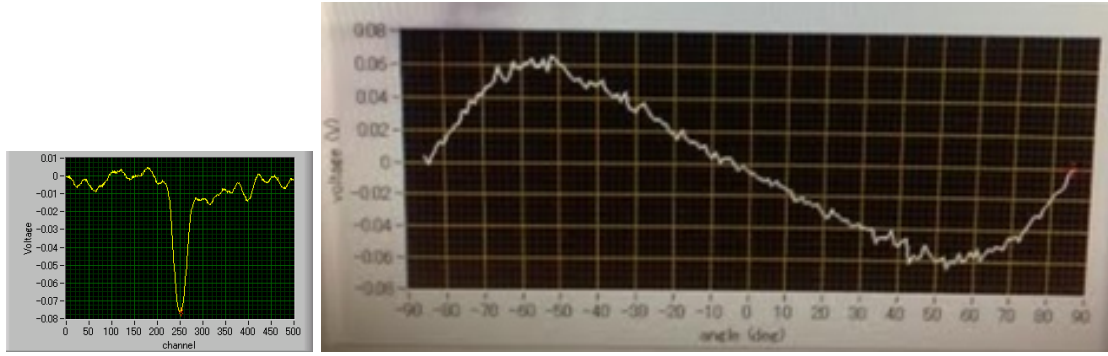
Figure 2.2: Left: peak of generated voltage in the LabVIEW screen, right: Incidence angle resolved voltage measured by LabVIEW program.
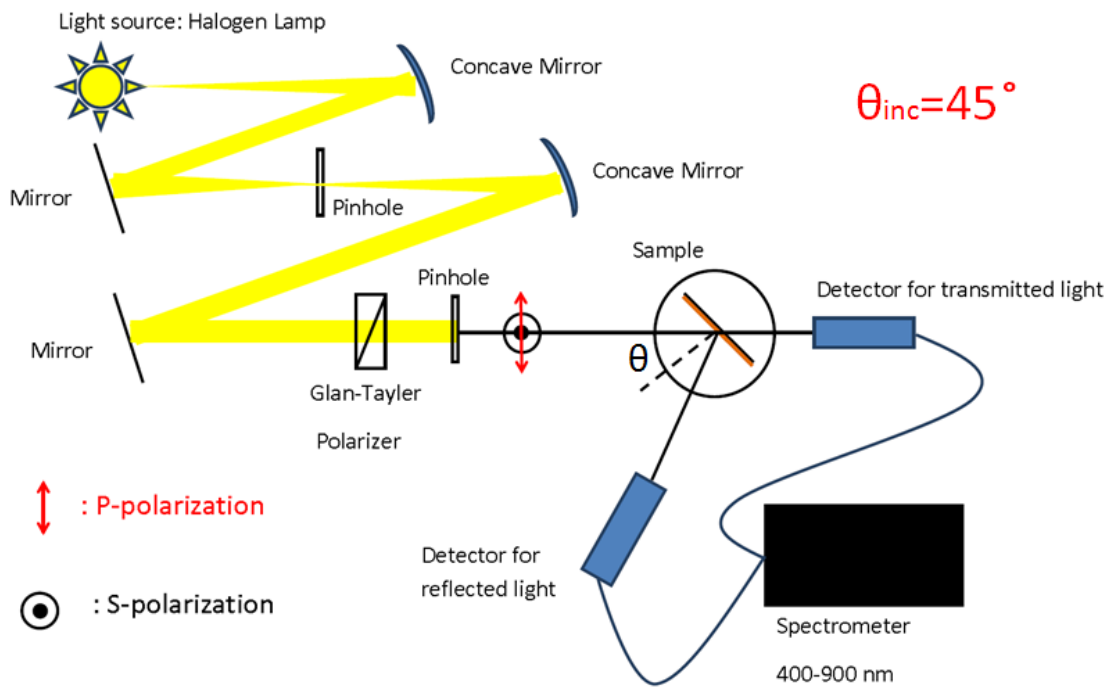
Figure 2.3: Schematic of experimental setup for transmission and reflection measurements for $\theta = 45°$.

was used around the film on the stage to reduce the electromagnetic noise of the environment.

The beam size was chosen so that it covers the sample at the normal incidence. Area around the film was masked with black paper so that light does not impinge on the electrodes for larger incidence angles which guarantee that the voltage is generated only by the porous area. For reducing pulse to pulse fluctuations, they were averaged for 32 pulses. Settings for wavelength, incidence angle and polarization measurements and data acquisition were controlled with a LabVIEW program. Figure. 2.2, right shows the measured incidence angle dependence PIV in the screen on Labview program after completing the measurement for angles between $-85°$ and $+85°$.
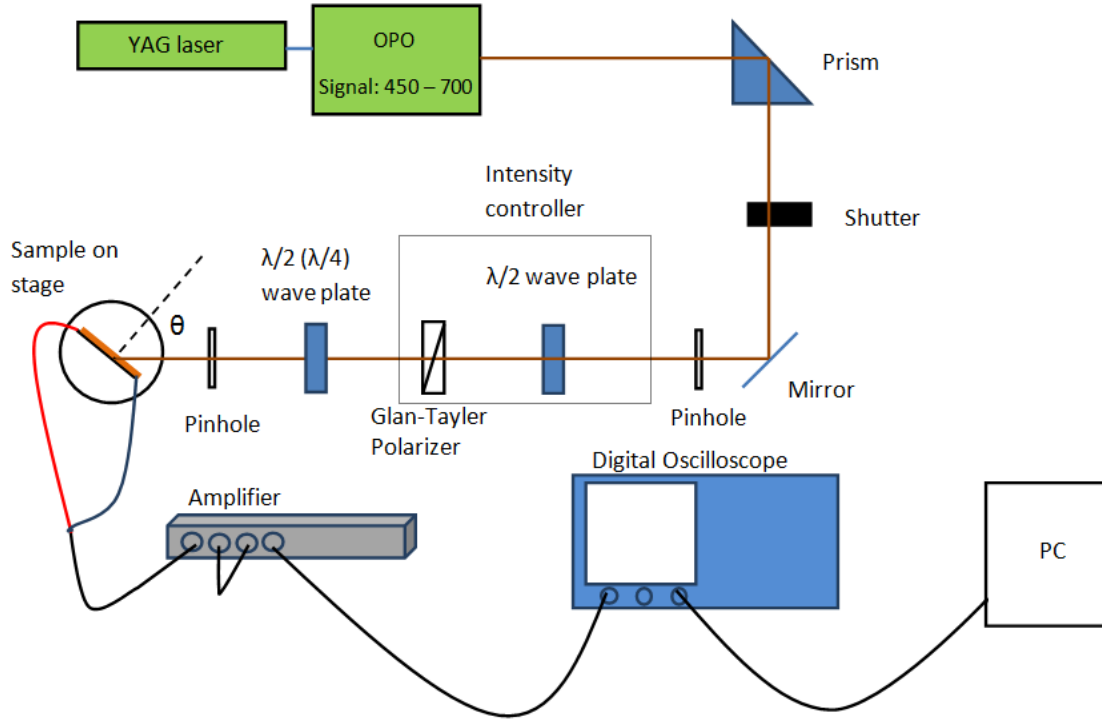
Figure 2.4: Schematic of experimental setup for wavelength resolved and incidence angle resolved measurement of PIV.

Setup for transmission and reflection measurement:

Experimental setup for transmission and reflection measurements is schematically shown in Fig. 2.3. Reflection and transmission spectra were measured at 45° and 0° incidence angle, respectively. A halogen lamp was used as a light source and concave mirrors and iris were employed to collimate light to the entrance of the detector. A Glan-Tayler prism provided incident light with s- and p-polarization. Glass was used as the reference and the spectra show the transmission and reflection with respect to it. From the wavelengths 450 nm to 600 nm, spectrometer (ACTON SpectraPro 2300i) with a liquid-nitrogen-cooled CCD camera (Roper Scientific) was used.

Setup for incidence angle and wavelength resolved measurement :

Wavelength resolved LPIV and TPIV were measured for different polarizations in the setup. Light from 450 nm to 600 nm provided by YAG laser and OPO was guided to the sample mounted on the stage at incidence angle of +50°. As intensity of laser light depends on wavelength, a half wave plate mounted on the first rotary stage combined with a polarizer is used to provide constant intensity for all the wavelengths in visible range. Combination of Glan-Tayler prism and half wave plate and quarter wave plate were applied to make incident light with linear and circular polarizations, respectively. In two configurations, wavelength resolved LPIV (with s-, p-, ±45° linear and circular) and TPIV (with ±45° linear and circular) polarized incident light were measured. By
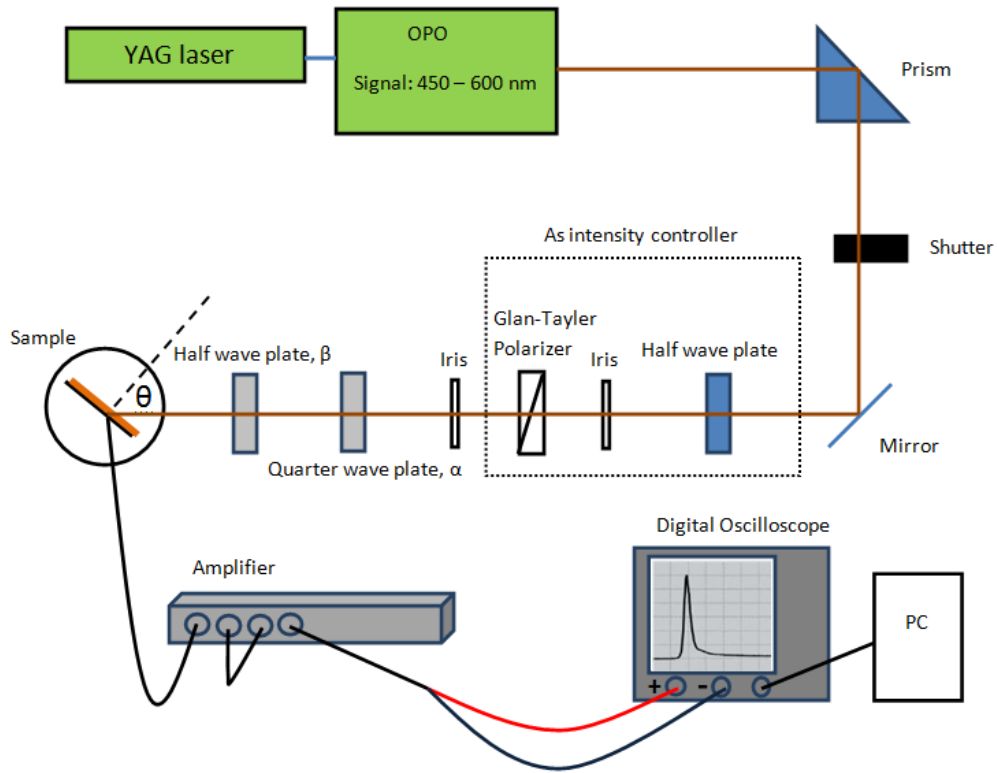
Figure 2.5: Schematic of experimental setup for polarization resolved measurement of PIV.

applying light with different wavelengths, peak of the generated signal was measured as positive or negative voltages for a fixed incidence angle and polarization of light. For incidence angle resolved measurement, wavelength and polarization of the light were fixed and incidence angle was changed by a rotary stage (Fig. 2.4).

Setup for polarization resolved measurement:

By some modifications in the setup for measuring wavelength or incidence angle resolved PIV, we can measure TPIV as a function of orientation of the incident light. For this purpose a polarizer fixed to produce p- polarization (horizontally polarized light) and a quarter wave plate with fast axis vertical for $\alpha = 90°$ are used. This quarter wave plate is employed to allow us to produce linear, circular or elliptically polarized light from the incoming p- polarized light by changing the position of its fast axis. Then this light passes through the half wave plate after the quarter wave plate. Depending on the position of the fast axis of this half wave plate (we define this position by angle β) we are able to change the orientation of the light and therefore measure TPIVas a function of this orientations. Another half wave plate before the polarizer is utilized to keep intensity of the incident light fixed for all the wavelengths (Fig.2.5). We measured polarization resolved photo-

induced voltage with 450 nm and 550 nm while incidence angle is fixed at $+50°$. Note that the sense of rotation of elliptically polarized light is inverted by insertion of a half wave plate.

CHAPTER 3

Spongy Nanoporous gold thin film

3.1 Overview

In this thesis linear and nonlinear response of nanoporous thin film of metals are studied. There are several methods to prepare nanoporous metal films with various shapes and sizes of nanopores which are simple compared to the methods for preparing periodic nanostructures, for example, Focused Ion Beam (FIB) and Electron Beam (EB) lithographies. Moreover they do not take so much time to complete. One method which we utilized to provide spongy nanoporous gold thin film is to etch an alloy film of gold and silver. The other method to prepare thin films with simple nanoholes is Nano Sphere Lithography (NSL) technique, which will be explained in the next chapter. Fabrication method and experimental results of PIV in spongy nanoporous gold thin film will be discussed in this chapter.

3.2 Sample preparation

We adopted glass substrate with 20 mm × 20 mm in size. Substrate should be transparent to make it possible to measure transmission spectrum of the nanostructure.
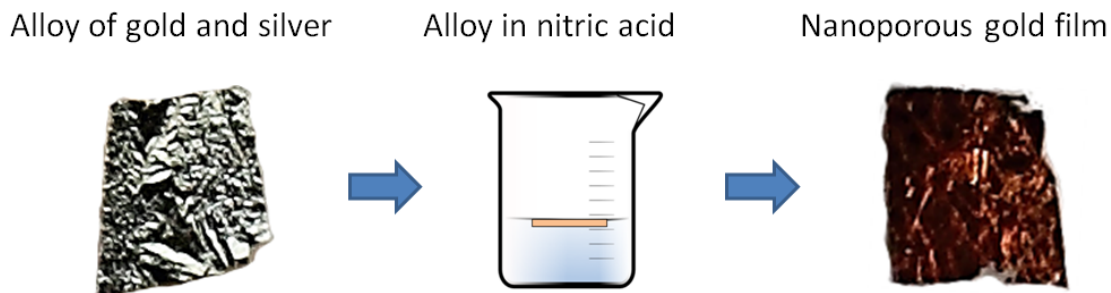
Figure 3.1: Etching process of an alloy of Au and Ag for providing spongy nanoporous gold film.

3.2.1 Cleaning substrate

Substrates are cleaned with acetone to remove the organic substances which are possible to be attached to the glass in the process of cutting glasses into desired size.

3.2.2 Etching alloy of gold and silver

Spongy nanoporous gold film can be generated by dealloying of some suitable alloys of gold like Au-Ag, Au-Cu and Au-Ni. In this process, the less noble component is removed and the more noble metal in the alloy, here gold, remains and forms an interconnected nanostructure of gold with pores. We dissolved silver from a 100 nm thick alloy of 50% gold and 50% silver, which is commercially available from Imai Kimpaku with 100 nm thickness, by exposuring to 65% concentrate Nitric acid (HNO_3) for 30 minutes. The color of the alloy before etching is white and after removing the silver the result is a film with brown color (Fig. 3.1). Because Ag is removed with the acid, the reflection above 500nm is significantly reduced which is the reason for the brown color of the film. This film is very fragile and it must be taken out from acid using a paper filter carefully and rinsed in distilled water to remove the residual acid. After rinsing, the glass substrate with electrodes is immersed in distilled water beneath the floating film to mount it across the gap between the electrodes (Fig. 3.2, c). Then the film is left for one day to evaporate the extra water.

The Atomic Force Microscope (AFM) image of the film shows nanostructure of gold ligaments and pores with the size about 30 nm. This interconnected conductive structure consists of pores of air and ligaments of gold make a homogenous composite and its mechanical, chemical and optical properties are different from the pure gold (Fig. 3.3, left).
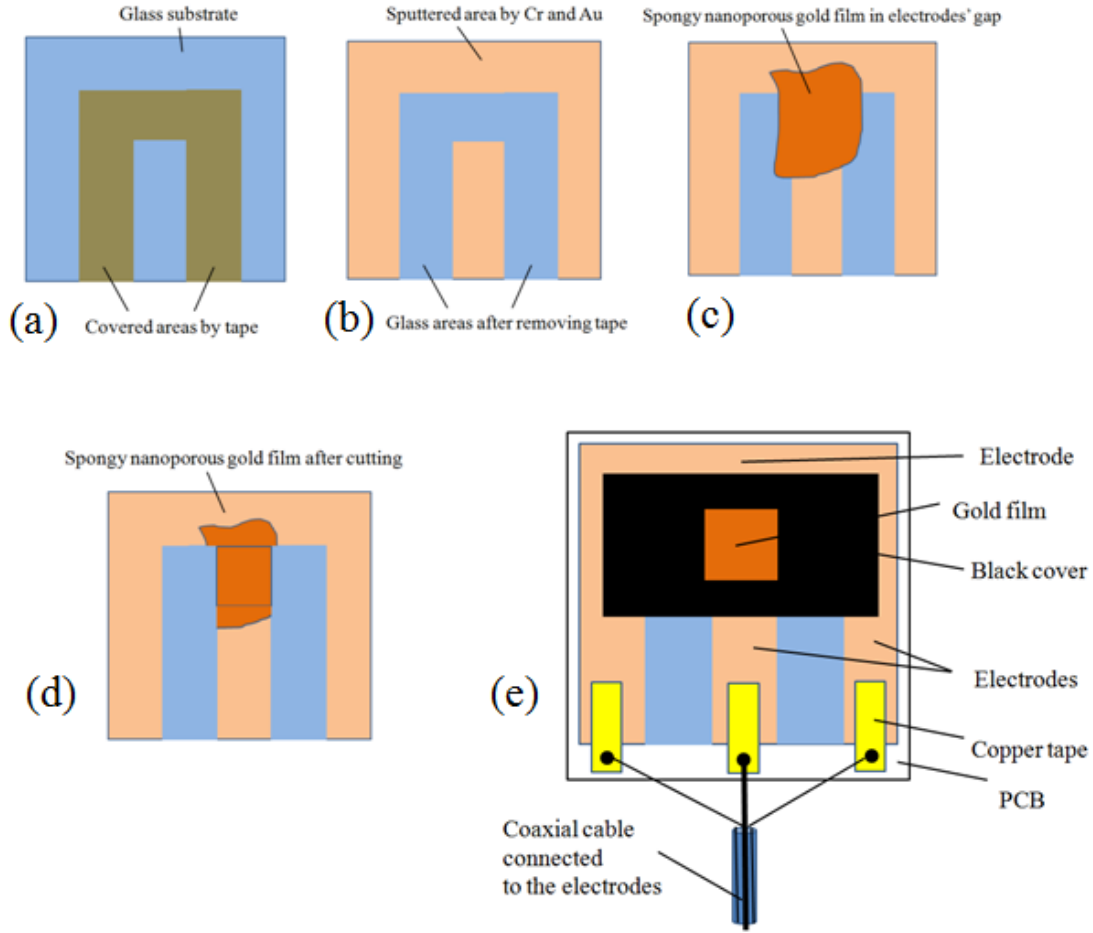
Figure 3.2: a) Glass substrate with tape, b) Removed tape after gold deposition, c) etched gold film across the gap, d) trimmed film in appropriate size, e) connected coaxial cable to the electrodes.

3.2.3 Preparation of electrodes

For attaching the electrodes to the film, we employed sputtering method to deposit Au. Ion beam sputtering machine (EIS-230S, ELIONIX) was used which has two ion guns and a chamber. The vacuum system can achieve the degree of vacuum 5×10^{-5} Pa. In the chamber there is a target holder which can contain three sputtering targets. For our purpose, we choose Au and Cr as targets. Before sputtering, a tape was used to cover the area of the glass which later the etched film will be placed on its gap (Fig. 3.2, a). After attaching the tape, a 3 nm thick intermediate layer of Cr was deposited on the substrate for better adhesion. Then a 40 nm layer of Au was deposited as electrodes. When deposition is finished, the tape is removed to open the gap across which the etched film is placed (Fig. 3.2, b).
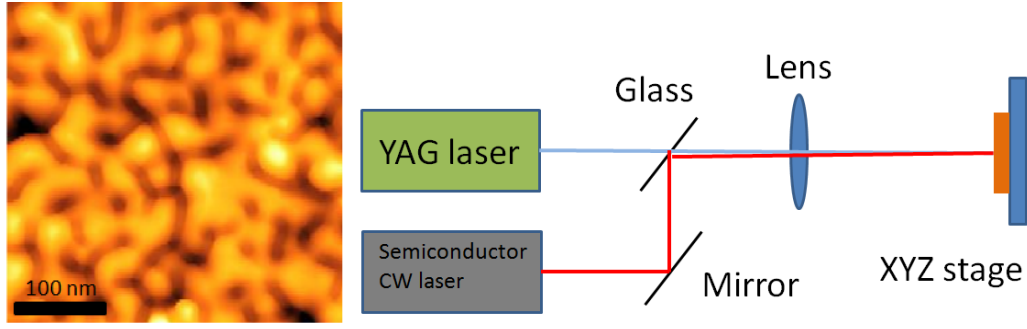
Figure 3.3: Left: AFM image of spongy nanoporous gold film, right: Schematic of the setup of laser cutting process.

3.2.4 Laser cutting of the sample

We employed the laser cutting technique for cutting the extra metallic area to have a regular shape of the sample with 5 mm × 5 mm size. Third harmonic generation (THG) light of Nd:YAG laser (fundamental wavelength: 1064 nm) was focused at the surface of the film. The focused THG laser pulses cut the metals and semiconductor CW laser (λ= 672 nm) was adopted collinearly with the THG laser as a guide since we cannot see the THG laser pulses (Fig. 3.3, right).

3.2.5 Attachment of electrodes on the sample

Each sample was provided with two parallel electrodes. For connecting the electrodes to the spongy nanoporous gold film to measure the photo-induced voltage, as mentioned above, we used sputtering technique to make a 40 nm layer of gold on the glass substrate with a gap for attaching the spongy nanoporous gold film across it. When spongy nanoporous gold film was mounted across the gap, pieces of copper tapes were connected on the deposited gold to make connection between connector pins and electrodes. Finally, two pins were soldered to the copper tapes. After the attachment of the electrodes, the substrate was fixed on a 25 mm × 25 mm printed circuit board (PCB). The areas between the film and electrodes were covered to avoid of generating voltage in these metallic parts around the film area and also in the electrodes at large incidence angles. As we see in Fig. (3.2, e) to measure the voltage a coaxial cable is attached to the electrodes with three points of connection. The two symmetric connections on right and left sides are designed to prevent the electrodes to work as an antenna and reduce the electromagnetic noise. Typical Ohmic resistivity is 25 Ω.
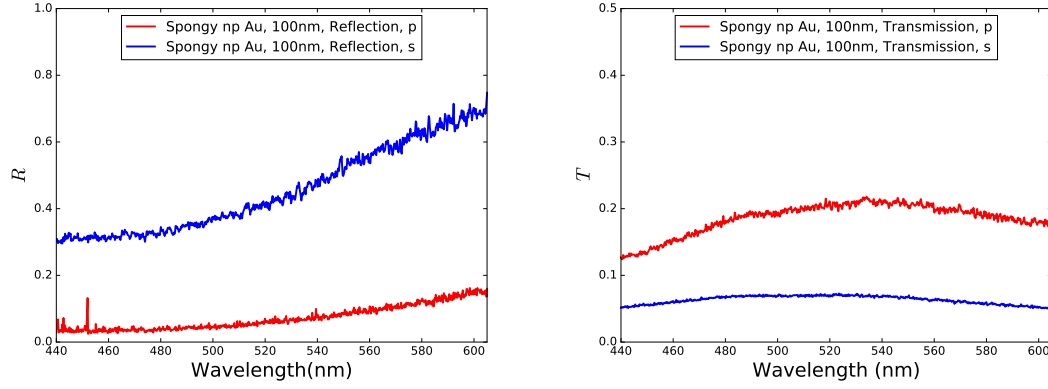
Figure 3.4: Transmission and reflection spectra of spongy nanoporous gold film for s- and p- polarization with $\theta = +45°$.
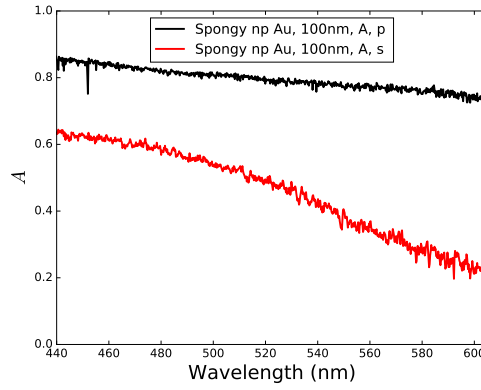
Figure 3.5: Absorption spectra of spongy nanoporous gold film for s- and p- polarization.

3.3   Results and discussions

In order to compare the linear optical properties (transmission and reflection) and LPIV and TPIV generated in spongy nanoporous thin films of Au with smooth thin film of Au with the same thicknesses as control film, smooth film of gold with 100 nm thickness was produced using deposition of Au on a 3 nm layer of Cr.

3.3.1   Linear optical properties of sample

Transmission and reflection spectra of the spongy nanoporous Au film and smooth film of Au with the same thickness for p- polarization are shown in Fig. 3.4. The Transmission of the nanoporous film is larger than that of the smooth film due to penetration of light in nanoholes. But the reflection exhibits an obvious decrease when compared with that of the smooth film for the wavelength larger than 500 nm. As a result, the absorption, A of the nanoporous film is much larger than smooth Au film. From $A = 1 - R - T$ we estimate A for visible range (Fig. 3.5).
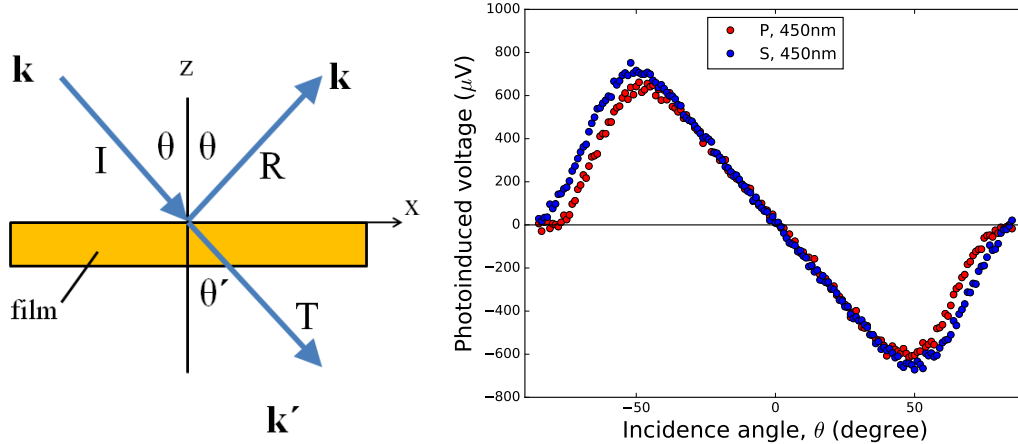
Figure 3.6: Left: Linear momentum conservation in the system without diffraction, right: Incidence angle resolved measurement of the LPIV for p- and s- with 450 nm incident light.

3.3.2 Incidence angle resolved measurement

For incidence angle resolved photo-voltage the maximum intensity of laser was 1 MW/cm^2. Light at a fixed wavelength was incident obliquely on the sample in two configurations which is mounted on the rotary stage. Laser beam is fixed in the xz plane and film rotates on a rotational stage around y-axis of the film. By rotating the stage, angle of incident light changed between $-85°$ to $85°$ at the interval of $1°$. Polarization of light was controlled by combinations of a half wave plate, a quarter wave plate and a polarizer. Peak of the signal was measured using the amplifier and oscilloscope. The raw voltage before amplifier is given in the data.

1. Incidence angle resolved measurement for 450 nm:

Longitudinal PIV:

Incidence angle resolved photo-induced voltage at the wavelength of 450 nm in the longitudinal configuration with s- and p- polarized light are shown in the Fig. 3.6, right. For both s- and p-polarized light the sign is negative for positive angles.

Lateral momentum conservation model :

For periodic case, incident light is reflected, transmitted, diffracted and absorbed in the structure and for conservation of momentum in the x-direction (Fig. 3.6, left) we have [10]:

$$k\hbar \sin \theta = Rk'\hbar \sin \theta + Tk'\hbar \sin \theta' + \sum_{g,j} \hbar D_g^j (k'\hbar \sin \theta' + G_g) + K\hbar \tag{3.1}$$

Here k is wave vector of incident light at the air, θ is the incident and reflection angle, R and T are reflection and transmission coefficients, k' the wave vector in the substrate. $K\hbar$ is transferred lateral momentum from one photon to the film along x-direction. Considering that for our random structure there is no diffracted light:

$$\sum_{g,j} \hbar D_g^j (k'\hbar sin\theta' + G_g) = 0 \tag{3.2}$$

Figure 3.6 left shows that incident, reflected and transmitted light in such system. By applying Snell's law as: $k \sin\theta = k' \sin\theta'$ and by arranging the relation we have:

$$K\hbar = (1 - R - T)k\hbar \sin\theta \tag{3.3}$$

or

$$K\hbar = Ak\hbar \sin\theta \tag{3.4}$$

A shows the absorbed light by the film.

$\hbar K$ is transferred lateral momentum from one photon and we need to calculate the momentum transferred from one pulse by evaluating the number of photons in one pulse using intensity of incident light, I_o (MW/cm^2), which is energy per unit area per unit time. Having $\hbar\omega$ as energy of one photon, for number of photons per unit area per unit time is $I_o/\hbar\omega$. So, momentum per unit area per unit time; momentum flux (P_{flux}) can be estimated by multiplying momentum of one photon and number of photons per unit area per unit time:

$$P_{\text{flux}} = K\hbar \frac{I_o}{\hbar\omega} = Ak \sin\theta \frac{I_o}{\omega} = A \sin\theta \frac{I_o}{c} \tag{3.5}$$

This momentum flux is equal to the force on the free electrons in the films due to the incident light. In the equilibrium state, electric field induced by the free electrons, E and force from incident light are balanced. So, in a film with length L and W along x and y direction, free electron density n and thickness d:

$$P_{\text{flux}}WL + neWLEd = 0 \tag{3.6}$$

thus, induced electric field in the structure is:

$$E = -\frac{P_{\text{flux}}}{ned} \tag{3.7}$$

Then produced voltage along the x direction is:

$$V_x = \int_0^L E dx = -\frac{L P_{\text{flux}}}{ned} \tag{3.8}$$

e is elementary charge.

Using this relation for V_x and parameter for spongy nanoporous gold film (λ=450 nm, I_o=1 MW/cm^2, $\theta = +50°$, $A_{450\text{nm}}$= 0.85, $d = 50$ nm (typical thickness of film) for p- polarization we have:

$$V_x = -560\mu\text{V} \tag{3.9}$$

Compared to the measurement (Fig. 3.6) that shows $V_x = -600\mu\text{V}$, we see they are in good agreement. For $\theta = -50°$ calculation gives $+560\mu\text{V}$. So, similar [10] with asymmetric structure conservation of lateral momentum could produce the observed voltage in our random structure. But in contrast to [10] we cannot use components of Lorentz force on a hole and we can estimate this voltage using the total transferred lateral linear momentum to the whole film by the incident light.

Since voltage depends on intensity of flux of light; $I_0 \cos(\theta)$, and lateral k vector; $k \sin(\theta)$ we can say that

$$V \propto I_0 \cos(\theta) k \sin(\theta) \propto \sin(2\theta) \tag{3.10}$$

When $2\theta = 90°$ voltage is maximum. So, as is clear in Fig. 3.6 at $\theta = 45°$ there is maximum values for the voltages. Due to lower absorption (due to for smooth Au film compare to the spongy nanoporous gold film, P_{flux} is smaller that explains weak voltage for smooth Au film as we see fro 450 nm in Fig. 3.7.

Although here we estimated the voltage only by total transferred momentum, but sometimes we need to consider microscopic calculation as well [45].

Angle dependence of photo-induced voltage in longitudinal configuration with circular and $\pm 45°$ linear polarized light are shown in Fig. 3.8. Sign and intensity of the voltage for RCP and LCP light is the same. The same tendency is observed for $\pm 45°$ linear polarized light. These voltages are generated by s- and p- components of circular and $\pm 45°$ linear polarized light.
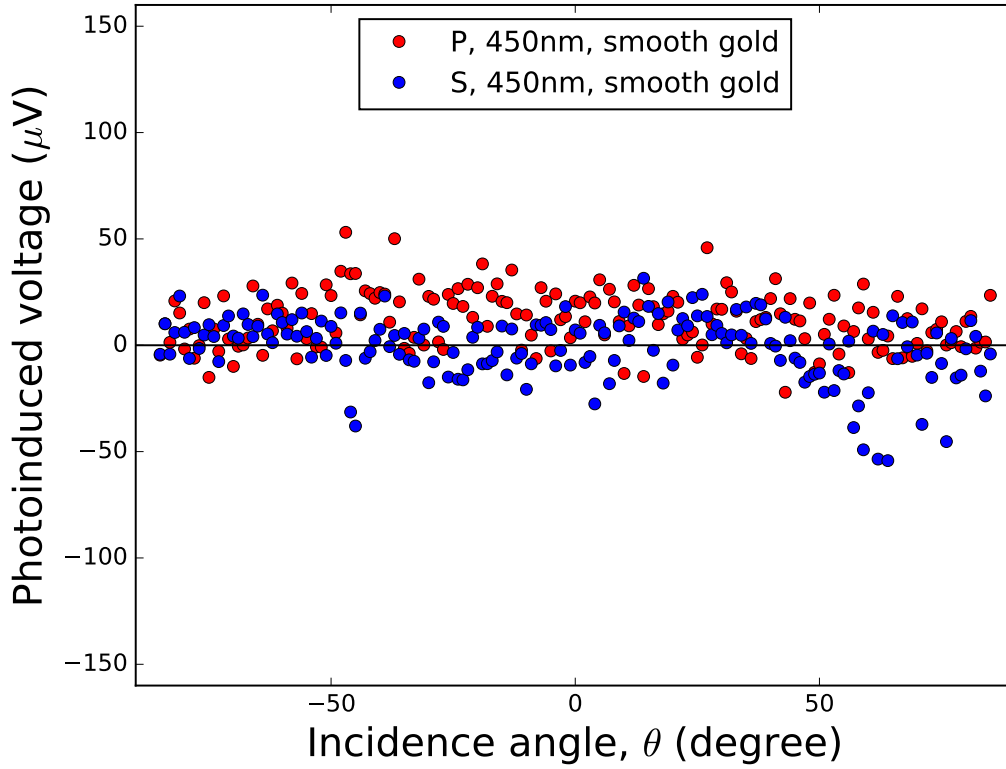
Figure 3.7: Incidence angle resolved measurement of the LPIV with 450 nm incident light for p- and s- polarization for smooth film.

We can show circular polarized light with s- and p- components as:

$$\mathbf{E}_{\text{circ}}^{\pm} = \frac{1}{\sqrt{2}}(\mathbf{E}_{\text{p}} \pm i\mathbf{E}_{\text{s}}) \tag{3.11}$$

Here + sign is for right hand and − is for left hand circular polarized. We can show ±45° linear polarized light in the same way by their s- and p- components:

$$\mathbf{E}_{45}^{\pm} = \frac{1}{\sqrt{2}}(\mathbf{E}_{\text{p}} \pm \mathbf{E}_{\text{s}}) \tag{3.12}$$

So, for these polarizations both s- and p- components of light are present and have role to produce the voltage by transferring their lateral linear momentum as we see in Fig. 3.9.

In Fig. 3.10 wavelength dependence LPIV with circular and ±45° linear polarized light are combination of averaged wavelength dependence LPIV of s- and p- polarized lights, separately. Top graphs in Fig. 3.10 show wavelength dependence LPIV with circular polarized and ±45° linear light which have a sign change around 540 nm. On the other hand down graphs show $\frac{1}{2}(V_{\text{LPIV}}^{\text{p}} + V_{\text{LPIV}}^{\text{s}})$ which is consistent with LPIV with RCP and LCP lights and have a sign change in the same wave-

Figure 3.8: Left: Incidence angle resolved measurement of the LPIV for circular polarized light with 450nm incident light, right: ±45° linear polarized light.

$$\boldsymbol{E}_{\text{cir}}^{\pm}(\text{r}) = {}^{1}\!/\!{\sqrt{2}} \left(\boldsymbol{E}_{\text{p}} \pm i\boldsymbol{E}_{\text{s}}\right)$$

Figure 3.9: Components of circular polarized light.

length.

Figure 3.10: Top: Wavelength resolved measurement of the LPIV for circular incident light and $\pm 45°$ linear polarized light with $\theta = 50°$, down: Average of the wavelength resolved measurement of the LPIV for s- and p-polarized light.
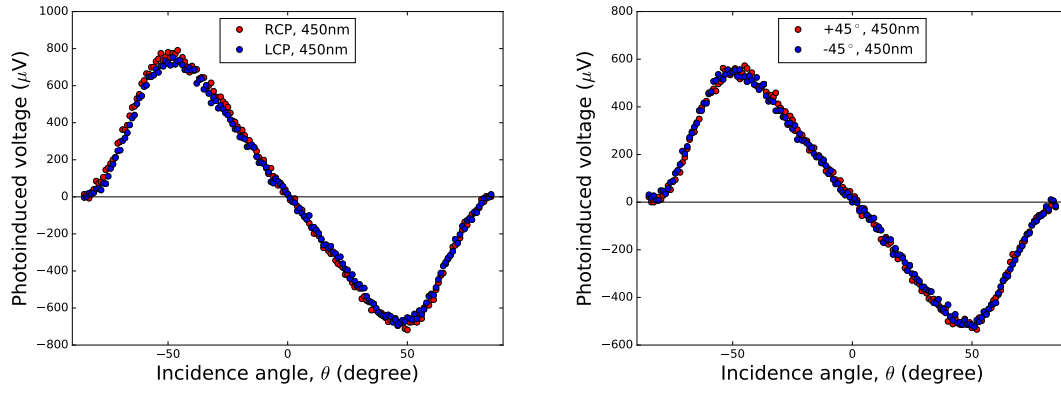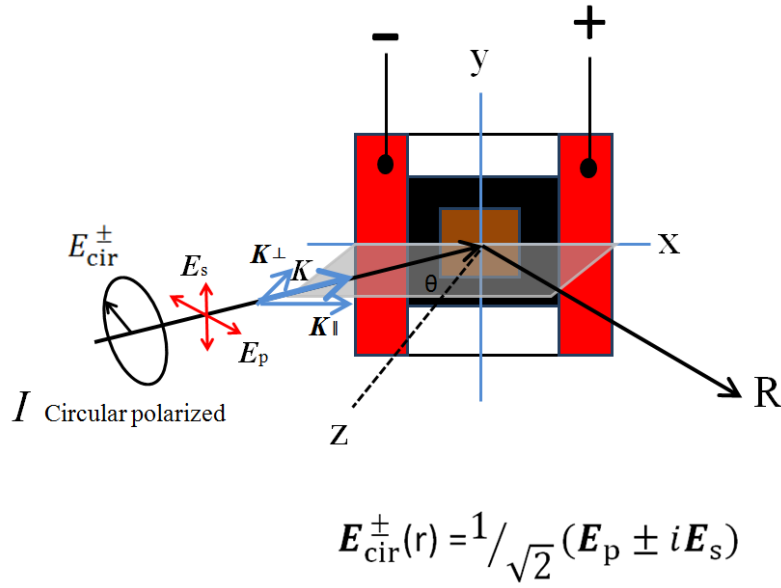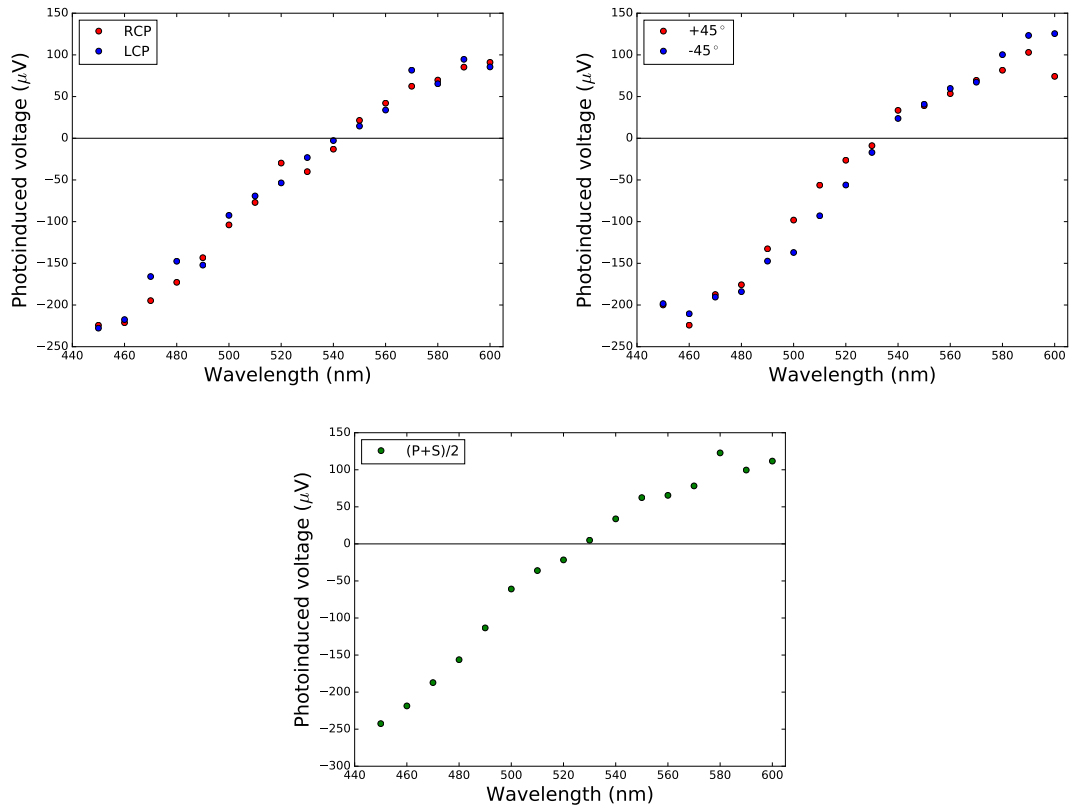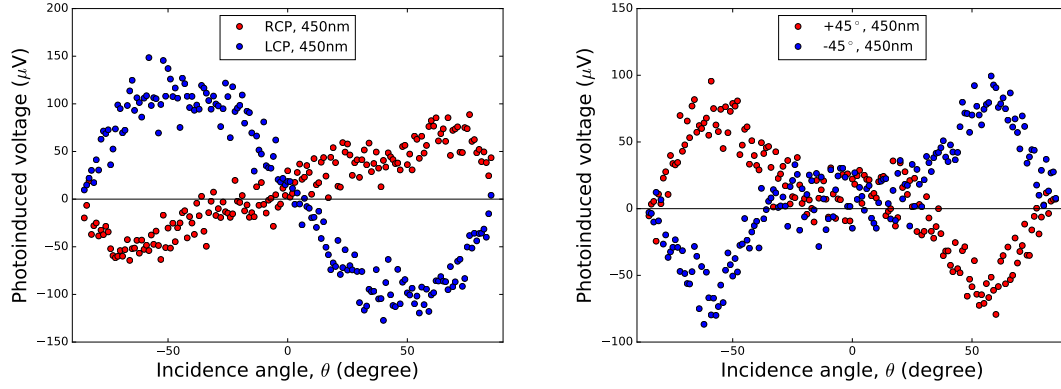
Figure 3.11: Left: Incidence angle resolved measurement of the TPIV for circular polarized light with 450nm incident light, right: ±45° linear polarized light.

Transverse PIV:

Figure 3.11 left, presents the experimental dependence of the photo-induced voltage on the incidence angle, θ, for transverse configuration with circular polarized light. At normal incidence light voltage is zero and they have $\sin(2\theta)$ tendency. For the same incidence angle, sign of the voltage for RCP is opposite of voltage for LCP. So, polarity of the voltage changes as the sense of polarization rotation changes from right to left.

By increasing incidence angle from zero to larger angles, voltage increases for both negative and positive directions. At about $\theta = +50°$, for RCP there is a maximum positive voltage. For LCP, we have a maximum negative voltage at this angle. For angles larger than $\theta = +50°$ voltage decreases and at $\theta = \pm85°$ voltage is almost zero.

Figure 3.11 right, shows dependence of the photo-induced voltage on the angle of incidence for transverse configuration with ±45° linear polarized light. By increasing incidence angle from zero to larger angles, voltage increases for both negative and positive directions. Sign of the voltage for +45° linear polarization is opposite of the −45° linear polarization. So, polarity of the voltage changes as the sense of polarization changes from positive to negative. At about $\theta = +60°$, for −45° linear polarization, there is a maximum positive voltage. For +45°, we have a maximum negative voltage at this angle. For angles larger than $\theta = +60°$ voltage decreases and at $\theta = \pm85°$ voltage vanishes.

The difference between results from the spongy nanoporous gold and smooth gold film is the amplitudes of the voltages. For 450 nm applied light TPIV of the spongy nanoporous gold is twice larger than smooth film but for 550 nm they are four times larger. For TPIV with smooth film as we can see in Fig. 3.12, with 450 nm incident light, tendency of voltages for RCP are similar
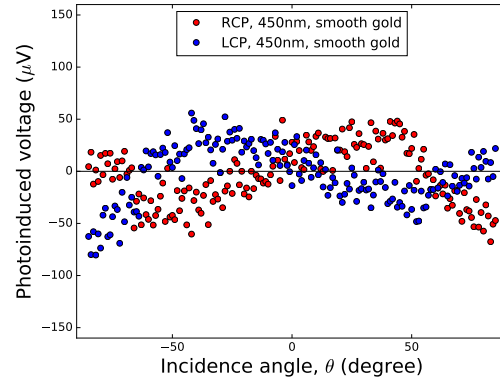
Figure 3.12: Incidence angle resolved measurement of the TPIV with 450nm incident light for circular polarization for smooth film.

and also similar to that of spongy nanoporous gold film. With the same explanation of the mirror symmetry it is possible to explain these voltages. This comparison between smooth thin film and spongy nanoporous thin film with the same thickness show clearly the role of the nanoholes in larger absorption in nanoporous film.
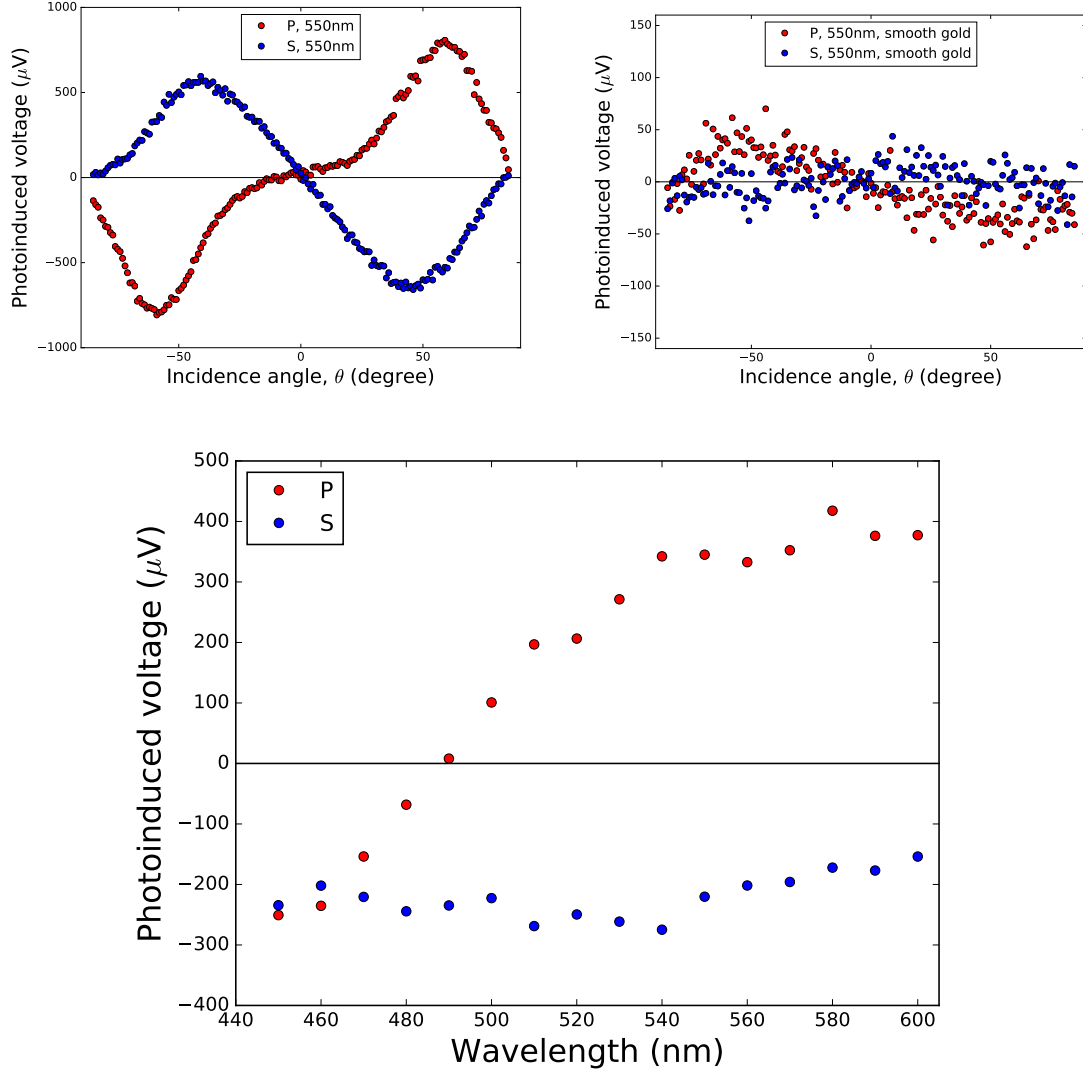
Figure 3.13: Top: Incidence angle resolved measurement of the LPIV for p- and s- polarization with 550nm incident light for spongy nanoporous gold film and smooth gold film, down: Wavelength resolved measurement of the LPIV for p- and s- polarization with $\theta = 50°$.

2. Incidence angle resolved measurement for 550 nm:

Longitudinal PIV:

Incidence angle resolved photo-induced voltage at the wavelength of 550 nm in longitudinal configuration with s- and p- polarized light are shown in the Fig. 3.13. For s-polarized light it follows $\sin(2\theta)$ dependence and the sign is negative for positive angles. It is reasonable as electron has negative charge, which is pushed by light momentum. At about $\theta = +45°$, for s- polarization there is a maximum negative voltage. Surprisingly for p-polarization, photo-induced voltage is positive for positive incidence angle. This voltage does not follow $\sin(2\theta)$ behavior and at about $\theta = +60°$ there is a maximum positive voltage. LPIV in smooth gold film with 550 nm fro s- and p-polarizations show in the smooth film voltages are much smaller than spongy nanoporous gold film
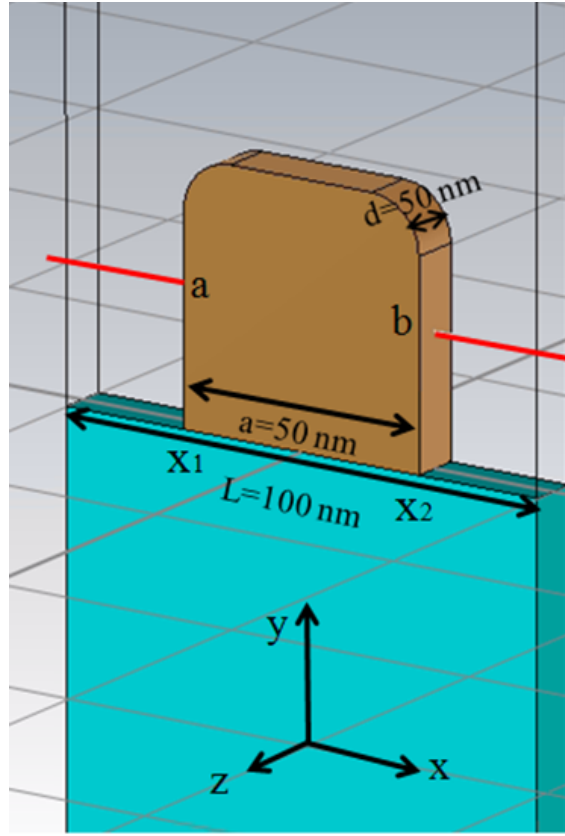
Figure 3.14: Microwave studio CST model for calculation of electric fields on points at sides of the unit cell (thickness, d=50, length, a=50nm and period, L=100nm).

due to smaller absorption due to lack of nanoholes. Wavelength resolved photo-induced voltage in longitudinal configuration with p- and s- polarized light show for s- polarization, voltage is always negative for positive incident angles, while for p- polarization sign changes at 490 nm.

To investigate the origin of sign change by wavelength for p- polarization we model spongy nanoporous gold as a 1-dimentional gating structure with 50% gold (ligaments) and 50% air (holes) as in Fig. 3.14. A microwave studio CST software package is used to do numerical simulation for this grating. **E** fields for s- and p- polarization with incidence angle +50° were calculated to estimate Lorentz force as

$$\mathbf{F} = -|\alpha||\nabla|\mathbf{E}||^2 \tag{3.13}$$

and

$$|\alpha| = \frac{e^2}{4m(\omega^2 + \gamma^2)} \tag{3.14}$$

is polarizibility of the gold. we can show

$$\alpha \propto \frac{\omega_p{}^2}{\omega^2} \propto \lambda^2 \tag{3.15}$$

Along x-axis

$$F_x = -|\alpha|\frac{\partial |E|^2}{\partial x} \tag{3.16}$$

for one unit cell with length L

$$F_x^{\text{unit}} = \int_0^L F_x dx = -|\alpha| \int_{x_1}^{x_2} \frac{\partial |E|^2}{\partial x} dx \tag{3.17}$$

or

$$F_x^{\text{unit}} = -|\alpha|(|E|^2|_{x_2} - |E|^2|_{x_1}) \tag{3.18}$$

For p- polarization from Fig. 3.15 for $x_1 = a$ and $x_2 = b$ (two sides of the ligament) we have

$$|E|^2|_{x_2} - |E|^2|_{x_1} < 0 \tag{3.19}$$

So

$$F_x^{\text{unit}} = -|\alpha|(|E|^2|_{x_2} - |E|^2|_{x_1}) > 0 \tag{3.20}$$

and inside the ligament force direction of force is from point a to point b for all wavelengths (Fig. 3.16). This charge distribution results in a positive potential along x-axis that we can consider them as small batteries. Summation of these positive potentials along $+x$ makes a positive voltage for p- polarization.

For s- polarization from Fig. 3.17 for $x_1 = a$ and $x_2 = b$ (two sides of the ligament) we have

$$|E|^2|_{x_2} - |E|^2|_{x_1} \leq 0 \tag{3.21}$$

So

$$F_x^{\text{unit}} = -|\alpha|(|E|^2|_{x_2} - |E|^2|_{x_1}) \leq 0 \tag{3.22}$$

and inside the ligament force direction of force is from point b to point a for all wavelengths (Fig. 3.18). This charge distribution results in a negative potential along x-axis that we can consider them as small batteries. Summation of these negative potentials along $+x$ makes a negative voltage for s- polarization.
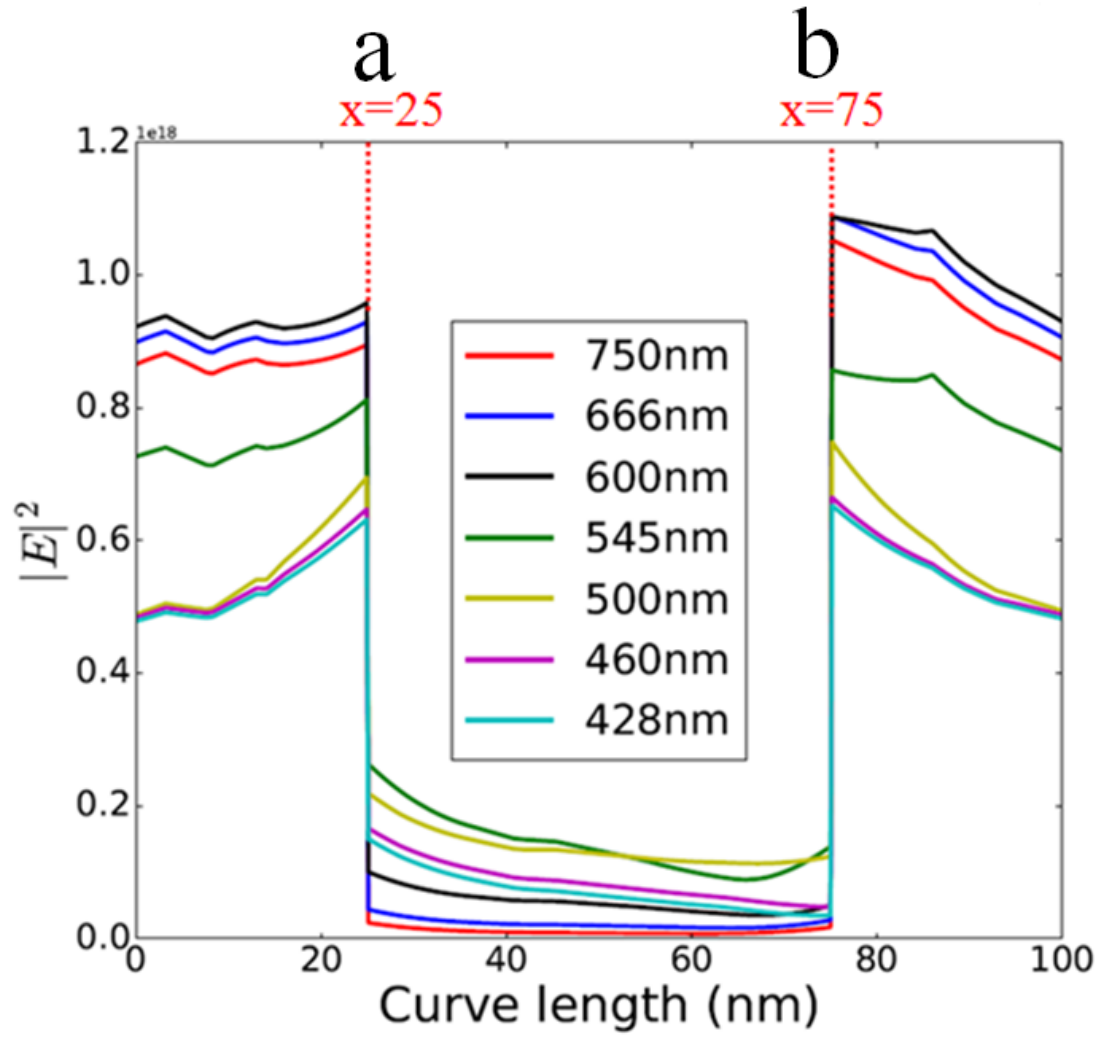
Figure 3.15: $|E|^2$ along one unit cell for different wavelengths with p- polarization.
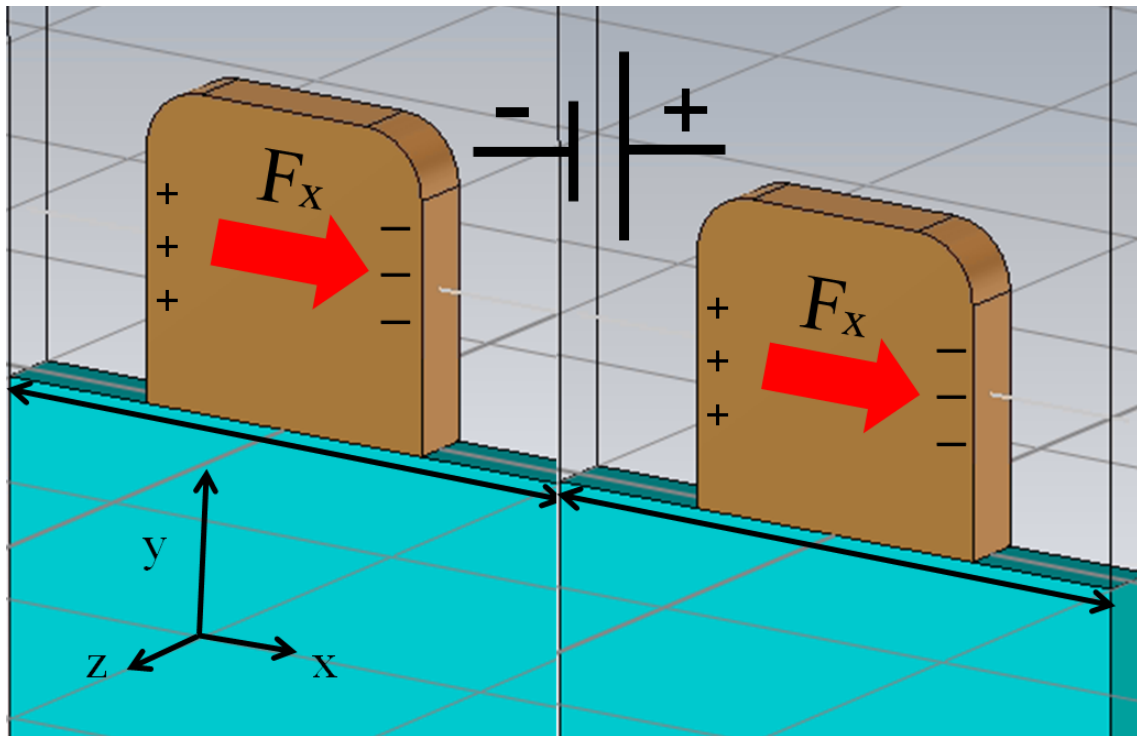
Figure 3.16: Force in each unit cell and induced battery in the hole for p- polarization.
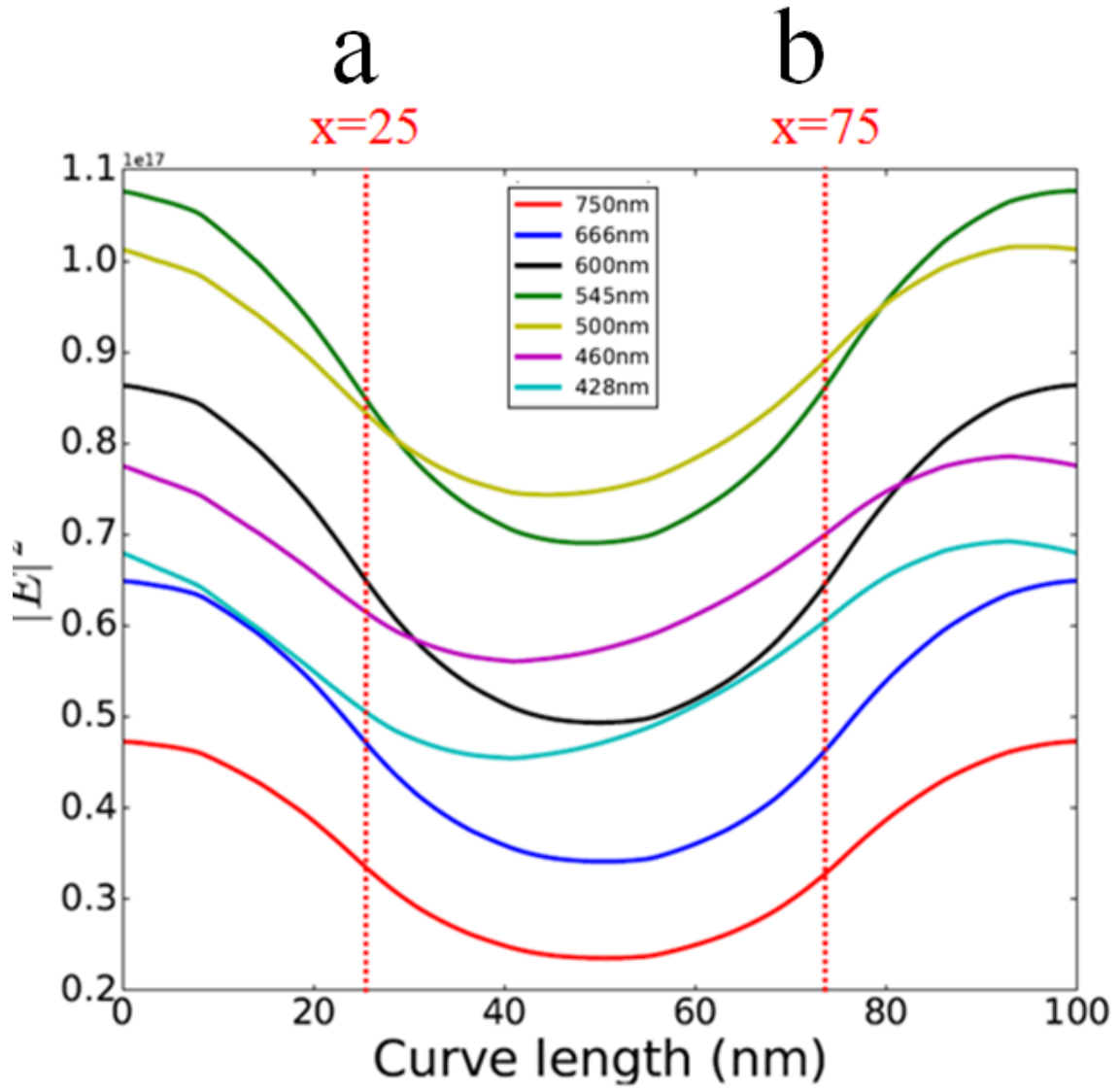
Figure 3.17: $|E|^2$ along one unit cell for different wavelengths with s- polarization.
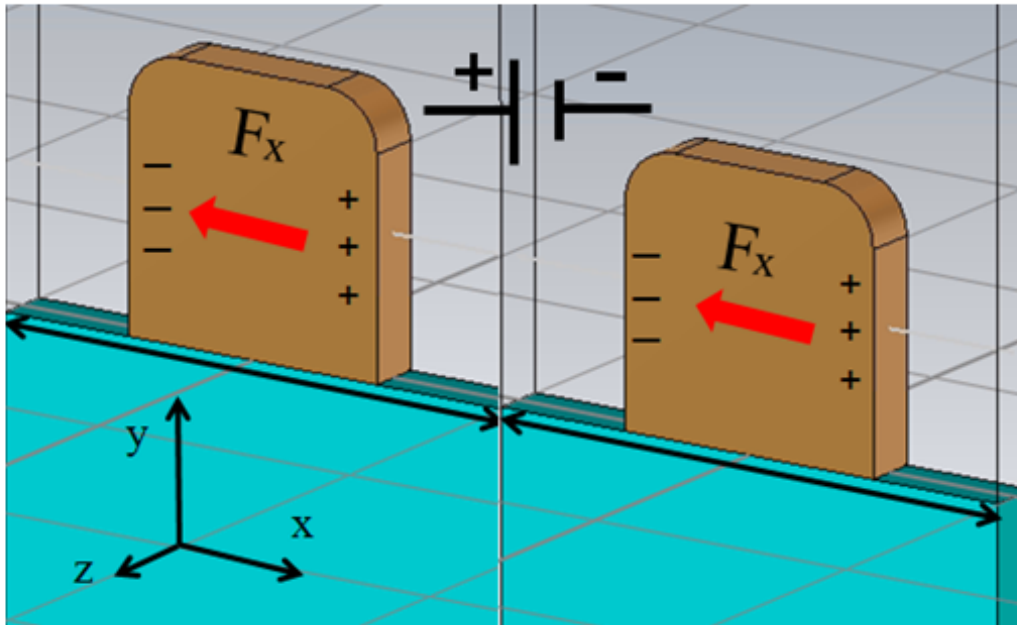
Figure 3.18: Force in each unit cell and induced battery in the hole for s- polarization.
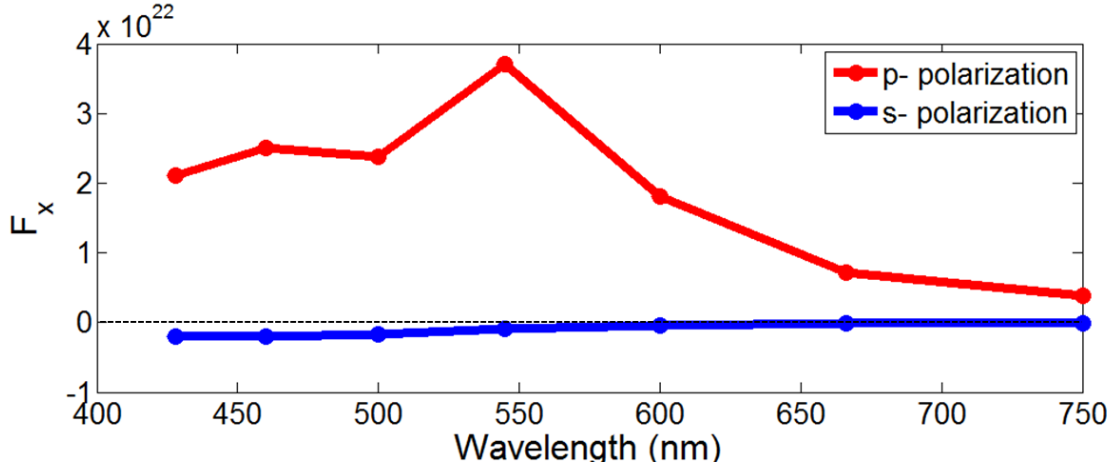
Figure 3.19: Wavelength dependence force along one unit cell for s- polarization and p- polarization.
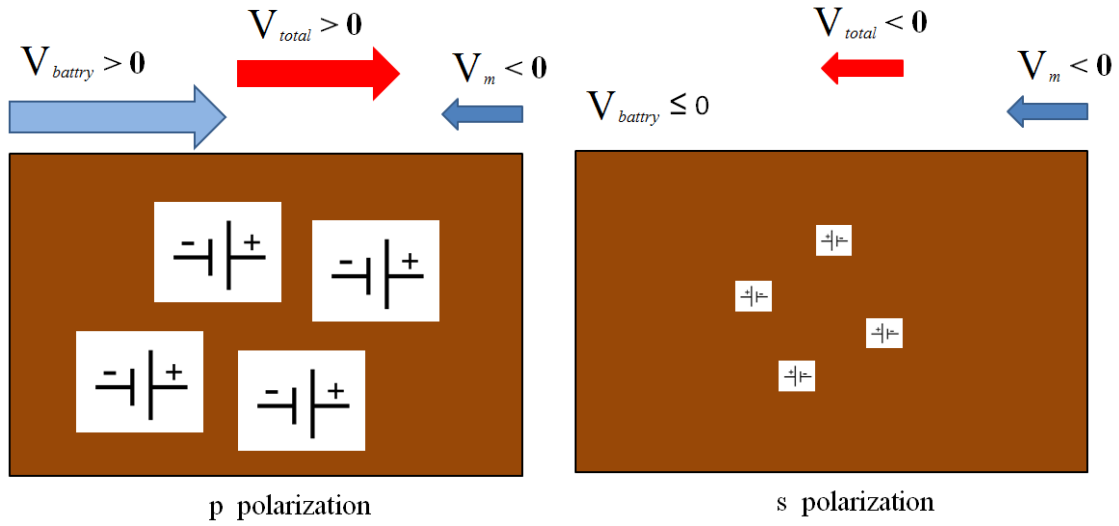
Figure 3.20: Voltage in spongy nanoporous gold film due to momentum flux and induced batteries for s- and p-polarization.

In Fig. 3.19 we have calculated these force due to discontinuity at the barriers for s- and p-polarization for visible range. As we can see, for s- polarization, this force is much smaller than p-polarization.

If we show these induced small batteries in the sample for s- and p- polarization as in Fig. 3.20, to combination of positive voltage from batteries and voltage from momentum flux result is a positive voltage for p- polarization. But for s- polarization the effect of batteries is much smaller than voltage from momentum flux and gives a negative voltage for s- polarization for all wavelengths.

Fig. 3.21 shows the measured $-A(\theta)\sin\theta\cos\theta$ for s- polarization for with 530 nm incident light. As we saw in the linear momentum model this value is proportional to the voltage and it is consistent with the measurement of LPIV for s- polarization. So, we can conclude that for s-
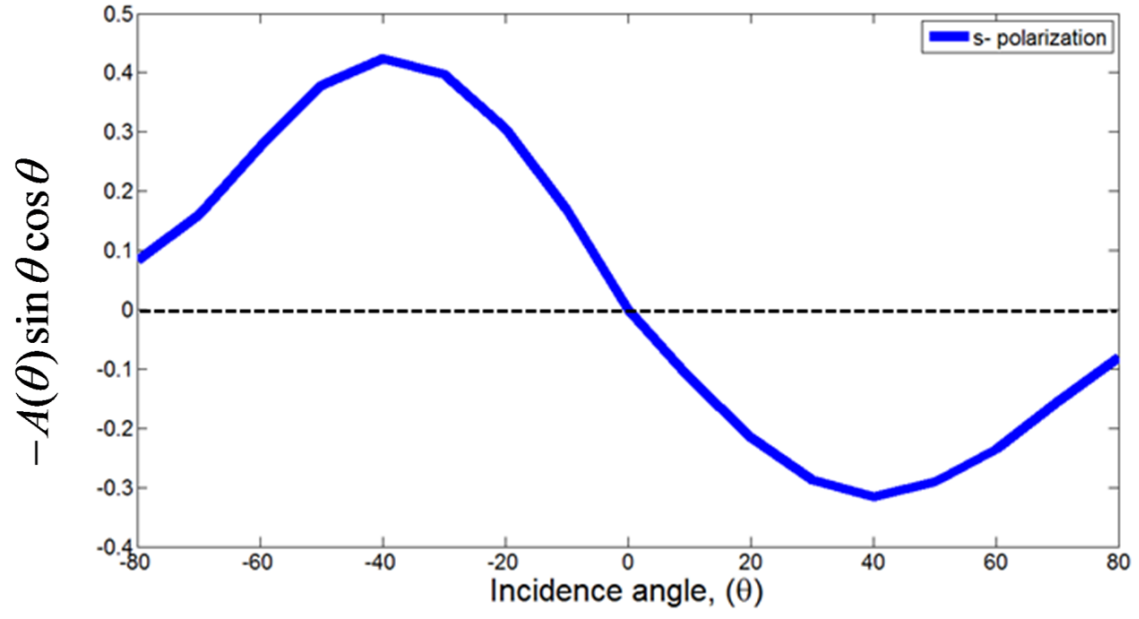
Figure 3.21: Incidence angle dependence linear momentum flux for s- polarization with λ=530 nm.

polarization voltage is generated due to linear momentum flux transferred from light to film for all range.
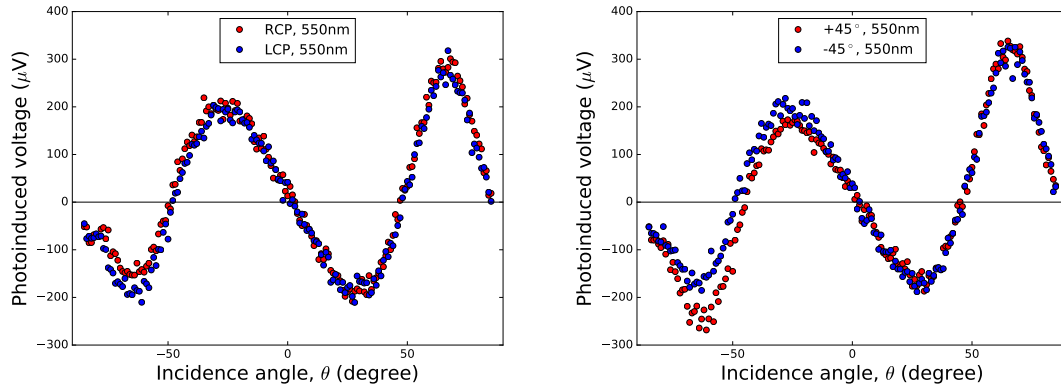
Figure 3.22: Incidence angle resolved measurement of the LPIV for circular polarized and $\pm 45°$ linear polarized light with 550nm incident light.

Angle dependence of photo-induced voltage in longitudinal configuration for 550 nm with circular and $\pm 45°$ linear polarized light are shown in Fig. 3.22. For these polarization, p- component generates a positive signal as we explained above and combinations of s- and p- components of these polarization result in these complicated tendencies.
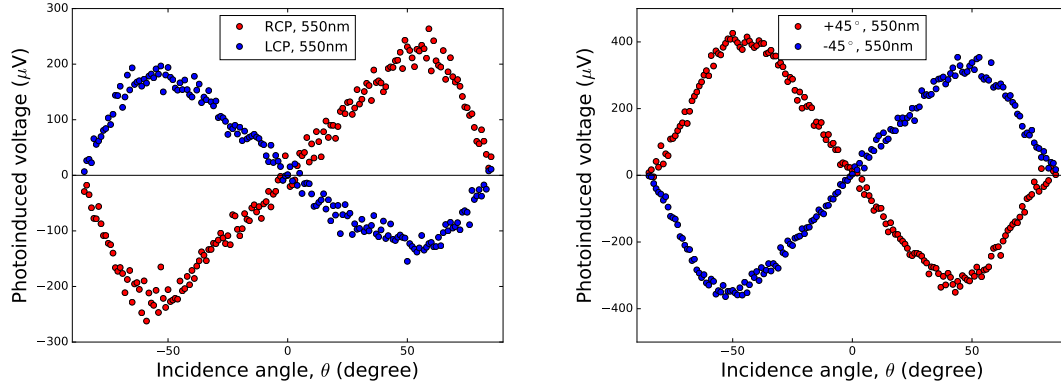
Figure 3.23: Incidence angle resolved measurement of the TPIV for circular polarized and $\pm45°$ linear polarized light with 550nm incident light.

Transverse PIV:

Figure 3.23 left, presents the experimental dependence of the photo-induced voltage on the incidence angle, θ, for transverse configuration with circular polarized light. For the same incidence angle, sign of the voltage for RCP is opposite of voltage for LCP. So, polarity of the voltage changes as the sense of polarization rotation changes from right to left.

By increasing incidence angle from zero to larger angles, voltage increases for both negative and positive directions. At about $\theta = +50°$, for RCP there is a maximum positive voltage. For LCP, we have a maximum negative voltage at this angle. For angles larger than $\theta = +50°$ voltage decreases and at $\theta = \pm85°$ voltage is almost zero. So, angle dependence of amplitude of the voltage can be proportional to $\sin(2\theta)$ for both senses of rotation. These results similar to that of 450 nm TPIV.

Figure 3.23 right, shows dependence of the photo-induced voltage on the angle of incidence for transverse configuration with $\pm45°$ linear polarized light. By increasing incidence angle from zero to larger angles, voltage increases for both negative and positive directions. Sign of the voltage for $+45°$ linear polarization is opposite of the $-45°$ linear polarization. So, polarity of the voltage changes as the sense of polarization changes from positive to negative. At about $\theta = +50°$, for $-45°$ linear polarization, there is a maximum positive voltage. For $+45°$, we have a maximum negative voltage at this angle. For angles larger than $\theta = +50°$ voltage decreases and at $\theta = \pm85°$ voltage vanishes.

For TPIV with smooth film as we can see in Fig. 3.24, with 550 nm incident light, the main difference between results from the spongy nanoporous gold and smooth gold film is the amplitudes of the voltages. This comparison between smooth thin film and spongy nanoporous thin film show
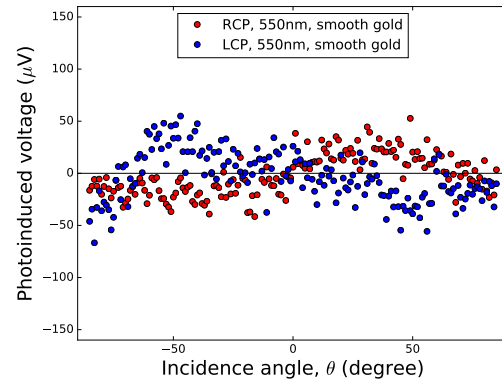
Figure 3.24: Incidence angle resolved measurement of the TPIV with 550nm incident light for circular polarization for smooth film.

clearly the role of the nanoholes in larger absorption in nanoporous film.
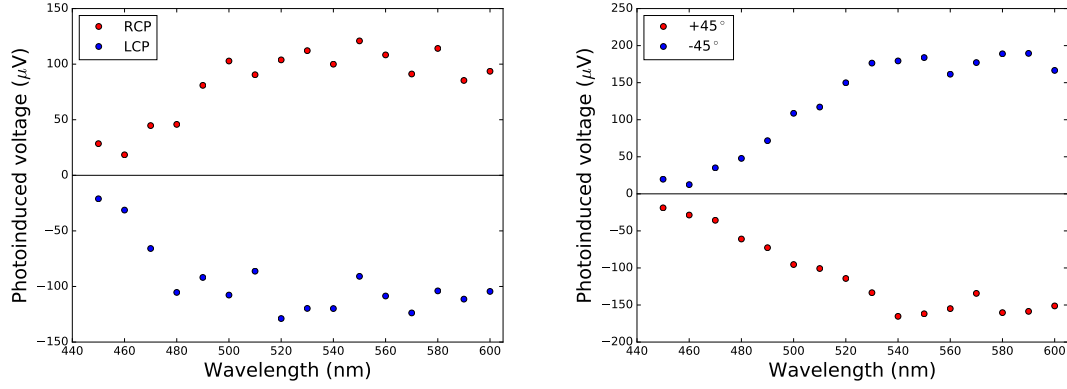
Figure 3.25: Wavelength resolved measurement of the TPIV for circular incident and ±45° linear polarized light with $\theta = 50°$.

Figure 3.25 left, shows dependence of the photo-induced voltage on the wavelength for transverse configuration with circular and diagonal polarized light at fixed incidence angle, +50° and fixed intensity (0.35 MW/cm^2). Sign of the TPIV does not change by changing wavelength in this wavelength range, forRCP it is always positive and for LCP always negative. Figure 3.25, right, shows incidence angle dependence of the photo-induced voltage on the angle of incidence for transverse configuration with ±45° linear polarized light.

When we apply light with linear polarization (expect for p- and s- polarizations) and circular polarization on the film the reflected light is elliptical polarized and angular momentum from light to the electrons can be transferred. This angular momentum depends on the handedness (helicities) of the light and could be positive or negative. As it was mentioned before, TPIV will be explained in term of transferred angular momentum to film.

Mirror inversion for explaining sing change by sense of rotation:

Here we use mirror inversion of film with respect to $y = 0$ plane to explain the sign reversal of TPIV for circular and $\pm 45°$ linear polarized incident lights. In the chapter 6 we will develop a model to estimate TPIV using conservation of angular momentum and helicities of incident, reflected and transmitted lights. For TPIV, it is a characteristic feature that the voltage change its sign by changing the sense of circular polarization or $\pm 45°$ linear polarization. In case of plasmonic crystal slabs, it is possible to explain these responses by means of the symmetry of field in a unit cell [16]. In order to explain the polarization dependence of photo-induced voltage in such a random structure as spongy nanoporous gold film, we need more general reasoning. For this purpose, we consider the mirror transformation $(y \leftrightarrow -y)$ of the whole system including incident beam with respect to the incident $y = 0$ plane as Fig.3.26 for TPIV. If we introduce the response function of photo-induced voltage as

$$\mathbf{V}\left(\mathbf{E}\right) \quad = \quad \begin{pmatrix} V_x\left(\mathbf{E}\right) \\ V_y\left(\mathbf{E}\right) \end{pmatrix} \tag{3.23}$$

for electromagnetic wave with electric field $\mathbf{E}$. Through the transformation depicted in Fig.3.26, we can easily see that the following relation exactly holds between the response of the original system and that of its mirror image, $\mathbf{V}^{\mathrm{m}}$,

$$\mathbf{V}^{\mathrm{m}}\left(\mathbf{E}^{\mathrm{m}}\right) \quad = \quad \begin{pmatrix} 1 & 0 \\ 0 & -1 \end{pmatrix} \mathbf{V}\left(\mathbf{E}\right) = \begin{pmatrix} V_x\left(\mathbf{E}\right) \\ -V_y\left(\mathbf{E}\right) \end{pmatrix} \tag{3.24}$$

where $\mathbf{E}^{\mathrm{m}}$ is the mirror image of $\mathbf{E}$.

On the other hand, when a spongy nanoporous gold film is too random to be macroscopically distinguished from its mirror image, the relation $\mathbf{V}\left(\mathbf{E}\right) \cong \mathbf{V}^{\mathrm{m}}\left(\mathbf{E}\right)$ should be approximately satisfied and leads to the phenomenological consequence. Being microscopically random allow us to consider it as an macroscopically isotropic film. So, applying oblique incident light we can break symmetry of the sample for electric fields which later we use it to calculate the voltage using Lorentz force in the film.
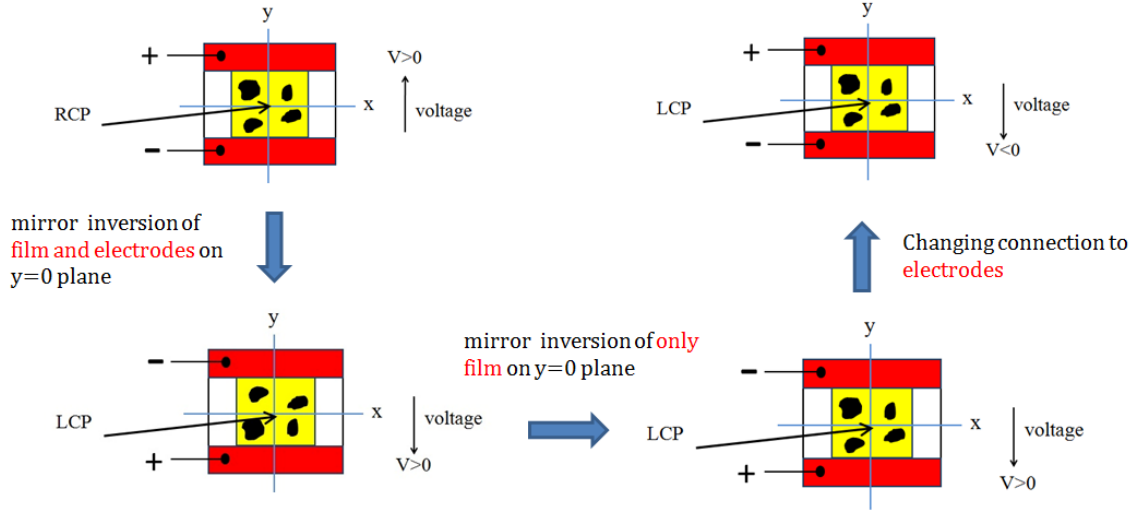
Figure 3.26: (a) Mirror inversion and sign change by change in sense of rotation.

$$
\begin{pmatrix} V_x\left(\mathbf{E}^{\mathrm{m}}\right) \\ V_y\left(\mathbf{E}^{\mathrm{m}}\right) \end{pmatrix} \cong \begin{pmatrix} V_x\left(\mathbf{E}\right) \\ -V_y\left(\mathbf{E}\right) \end{pmatrix}
\tag{3.25}
$$

For a random structure, we cannot define a unit cell. But for a perfect random structure that is macroscopically isotropic

$$
u(r) = (u(x, y, z) + u(-x, y, z) + u(x, -y, z) + u(-x, -y, z))/4
\tag{3.26}
$$

And voltage still can be shown as

$$
V_y = -\frac{1}{Ne} \int_0^{Ly} f_{\mathrm{DC},y} dy \int_0^{Lx} dx \int_0^{Lz} dz
\tag{3.27}
$$

for this isotropic material by oblique incident light we can break the symmetry and generate this voltage

This argument explains the polarity with respect to the polarization state of incident beam for every incidence angle resolved measurement in for spongy nanoporous gold film.

General response of film:

The above discussion can explain PIV for all polarizations.

The proposal for the general response of the film is summarized as follows,

$$
\mathbf{V}\left(\mathbf{E}\right) \;=\; \begin{pmatrix} V_x\left(\mathbf{E}\right) \\ V_y\left(\mathbf{E}\right) \end{pmatrix} = \begin{pmatrix} |z_\mathrm{p}|^2\, V_\mathrm{p}\left(|\mathbf{E}|,\theta\right) + |z_\mathrm{s}|^2\, V_\mathrm{s}\left(|\mathbf{E}|,\theta\right) \\ 2\left[\mathrm{Re}\left(z_\mathrm{p}^* z_\mathrm{s}\right) V_{45}\left(|\mathbf{E}|,\theta\right) + \mathrm{Im}\left(z_\mathrm{p}^* z_\mathrm{s}\right) V_\mathrm{c}\left(|\mathbf{E}|,\theta\right)\right] \end{pmatrix} \tag{3.28}
$$

where $\mathbf{E} = |\mathbf{E}|\left(z_\mathrm{p}\mathbf{e}_\mathrm{p} + z_\mathrm{s}\mathbf{e}_\mathrm{s}\right)$

and z_p and z_s are complex coefficients satisfying $|\vec{z}|^2 = |z_\mathrm{p}|^2 + |z_\mathrm{s}|^2 = 1$ and representing the polarization state of incident beam, $\mathbf{e}_\mathrm{p(s)}$ is the polarization vector of p(s)- polarization, and θ is the angle of incidence.

1. for p- polarization:

$z_\mathrm{p} = 1$ and $z_\mathrm{s} = 0$, so:

$$
\mathbf{V}\left(\mathbf{E}\right) \;=\; \begin{pmatrix} V_x\left(\mathbf{E}\right) \\ V_y\left(\mathbf{E}\right) \end{pmatrix} = \begin{pmatrix} |z_\mathrm{p}|^2\, V_\mathrm{p}\left(|\mathbf{E}|,\theta\right) \\ 0 \end{pmatrix} \tag{3.29}
$$

2.. for s- polarization:

$z_\mathrm{s} = 1$ and $z_\mathrm{p} = 0$, so:

$$
\mathbf{V}\left(\mathbf{E}\right) \;=\; \begin{pmatrix} V_x\left(\mathbf{E}\right) \\ V_y\left(\mathbf{E}\right) \end{pmatrix} = \begin{pmatrix} |z_\mathrm{s}|^2\, V_\mathrm{s}\left(|\mathbf{E}|,\theta\right) \\ 0 \end{pmatrix} \tag{3.30}
$$

3. for circular polarization:

$z_\mathrm{p} = \frac{1}{\sqrt{2}}$ and $z_\mathrm{p} = \pm\frac{1}{\sqrt{2}}i$, so: $\mathrm{Im}(z_\mathrm{p}^* z_\mathrm{s}) = \pm\frac{1}{2}$ and $\mathrm{Re}(z_\mathrm{p}^* z_\mathrm{s}) = 0$, so:

$$
\mathbf{V}\left(\mathbf{E}\right) \;=\; \begin{pmatrix} V_x\left(\mathbf{E}\right) \\ V_y\left(\mathbf{E}\right) \end{pmatrix} = \begin{pmatrix} 0 \\ \pm V_\mathrm{c}\left(|\mathbf{E}|,\theta\right) \end{pmatrix} \tag{3.31}
$$

4. for diagonal polarization:

$z_\mathrm{p} = \frac{1}{\sqrt{2}}$ and $z_\mathrm{p} = \pm\frac{1}{\sqrt{2}}$, so: $\mathrm{Im}(z_\mathrm{p}^* z_\mathrm{s}) = 0$ and $\mathrm{Re}(z_\mathrm{p}^* z_s) = \pm\frac{1}{\sqrt{2}}$, so:

$$\mathbf{V}(\mathbf{E}) \quad = \quad \begin{pmatrix} V_x(\mathbf{E}) \\ V_y(\mathbf{E}) \end{pmatrix} = \begin{pmatrix} 0 \\ \pm V_{45}(|\mathbf{E}|, \theta) \end{pmatrix} \tag{3.32}$$

As we see this general response can predict both LPIV and TPIV for different polarized lights with sign of these voltages correctly.

3.3.3 Summary

We successfully fabricated spongy nanoporous gold thin film and measured LPIV and TPIV in this film. Linear momentum model is able to explain the LPIV. Simulation with Microwave studio CST software was used to explain the sign change for p- polarization for longer wavelengths. In chapter 6 we will develop a model to calculate transferred angular momentum to the film and estimate the TPIV.

3.3.4 Conclusion

We have investigated LPIV and TPIV in spongy nanoporous gold thin film. Comparison of PIV in spongy nanoporous gold with that of the smooth gold film shows that large signal is due to higher absorption in nanoporous gold film due to the penetration of light to the nanoholes. While we estimated LPIV for s- polarization with conservation of linear momentum similar to that of for p- polarization with shorter wavelengths, for p- polarization with longer wavelengths excitation of LSPR in the ligaments generates opposite force inside the ligaments which results to positive voltage. LPIV generated by circular and diagonal polarized light is due to combination voltage of s- and p- components of light. For longer wavelengths for p- polarization effect of LSPR is larger than the linear momentum and make a complicated incidence angle dependence behavior for LPIV for circular and diagonal polarized light. For TPIV we can explain the sign change by sense of rotation using mirror inversion. This symmetry works because spongy nanoporous gold is too random that can be considered as an isotropic material.

CHAPTER 4

Gold thin film with random nanoholes

4.1 Overview

In order to fully understand to origin of the sign change of LPIV in spongy nanoporous gold film as discussed in pervious chapter, here we investigate these voltages in a thin film of gold with simple nanoholes with 25 nm thickness to study effect of size and shape of the holes and thickness of the film on the generated voltages. Gold thin film with random nanoholes can be produced with nanosphere lithography. In this method nano sized spheres of polymers, for example, polystyrene (PS) is applied as mask which after removing them nanoholes of almost with the same size of the PS spheres are produced.

4.2 Sample Preparation

Gold thin film with random nanoholes were provided in the following process:

4.2.1   Cleaning substrate

Cleaning process of the substrates has 3 steps as follows:

1. Ultrasonic cleaning process with the substrate soaked in acetone for 5 minutes .

2. Ultrasonic cleaning process with the substrate soaked in ethanol for 5 minutes.

3. Ultrasonic cleaning process with the substrate soaked in distilled water for 5 minutes.

By this cleaning process, first organic substances are removed by acetone and then acetone is removed by ethanol. Finally, ethanol is removed by distilled water. The substrate is kept in distilled water after the cleaning process.

4.2.2   Preparing and adding $AlCl_3.6H_2O$

For attachment of the PS spheres to the substrate a solution of Aluminum Chloride Hydroxide ($AlCl_3.6H_2O$) [46] was deposited on the substrate by sonication process for 5 min. This solution provides a hydrophilic surface that PS spheres attach to it. For preparing this solution, a mixture of 95 wt.% of distilled water and 5 wt.% of $AlCl_3.6H_2O$ was provided.

4.2.3   Polystyrene coating

Substrate was removed from $AlCl_3.6H_2O$ and rinsed in distilled water for 2 min. Then it was blow dried with N_2 gas. One drop of PS spheres of 100 nm diameter was mixed with 8 drops of distilled water to dilute the solution and reduce number of the spheres per volume to be able to have an appropriate number of spheres per area of glass substrate and prevent from accumulation of the spheres (Fig. 4.1, a). Fig. 4.1, b shows 3D image of polystyrene sphyeres on the substrate. One drop of this diluted solution of PS spheres was coated on the glass (Fig. 4.3, a) by putting it for 40 second on the prepared glass with $AlCl_3.6H_2O$ and followed by distilled water rinse to remove extra PS spheres. Then wet glass was immersed in the 130° C hot ethylene glycol to fix the PS spheres to the surface by baking process. Then substrate was rinsed with distilled water and obliquely blow dried with N_2 gas. AFM images show PS spheres and their random position on the glass. Cross section of the AFM image of thePS spheres shows that height of the spheres on the glass is about 100 nm in average (Fig. 4.1, c).
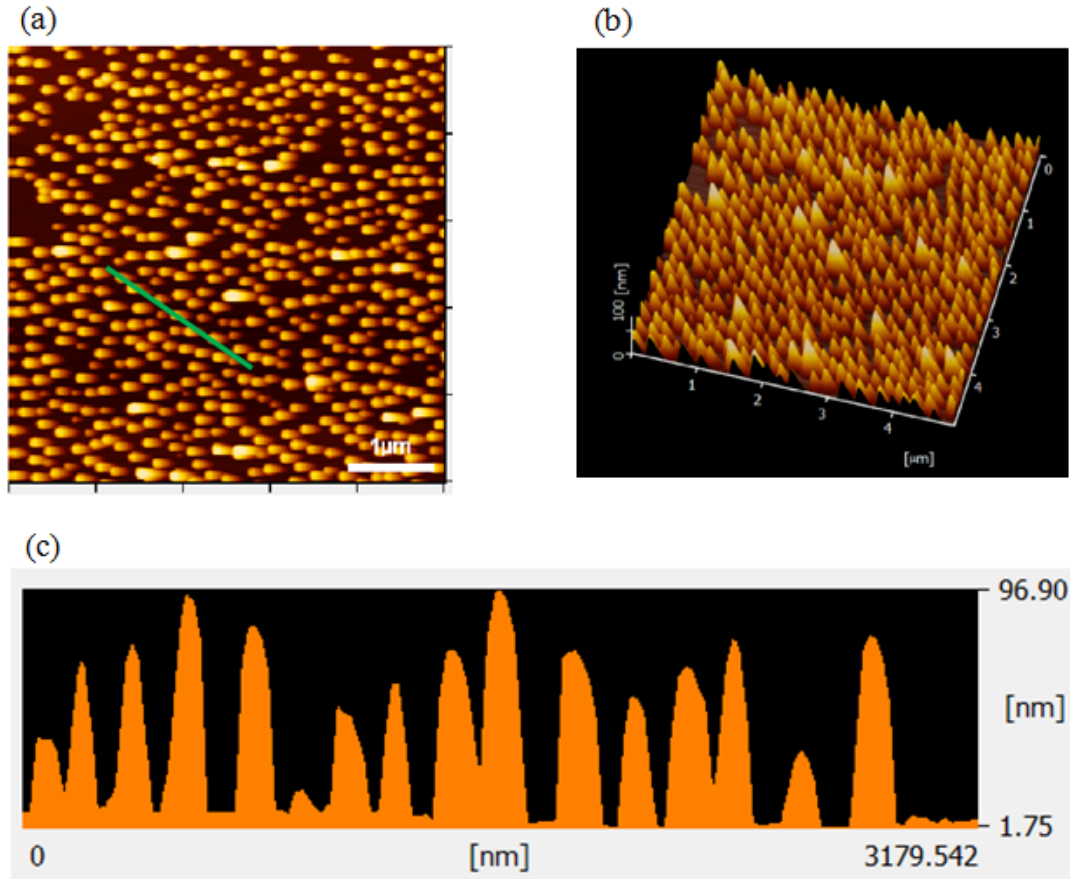
Figure 4.1: a)PS spheres on the glass substrate, b) 3D image of PS spheres, c) Cross section image of PS Spheres on the glass.

4.2.4 Sputtering Cr and Au

On the substrate coated with PS spheres as a mask, a 25 nm layer of gold was deposited by sputtering after deposition of a 3 nm layer of Cr as adhesion layer (Fig. 4.3, b). Metal on the PS area will make the film with nanoholes after tape stripping and the rest of it will work as parts of the connected electrodes to the sides of the trimmed film.

4.2.5 Tape stripping of polystyrene

To remove PS spheres tape stripping technique was performed with a adhesive tape. One piece of the tape was cut in the same size of the PS coated area. This piece was placed on the deposited gold to cover the PS coated area. Tape was positioned on top of the area and by applying small pressure using a small piece of cotton without damaging it; we make sure that the tape is attached to that area perfectly. Then we left the tape for 2 days before striping it. By fast striping, it is possible to remove almost all the PS spheres and provide nanoholes in the deposited film (Fig.
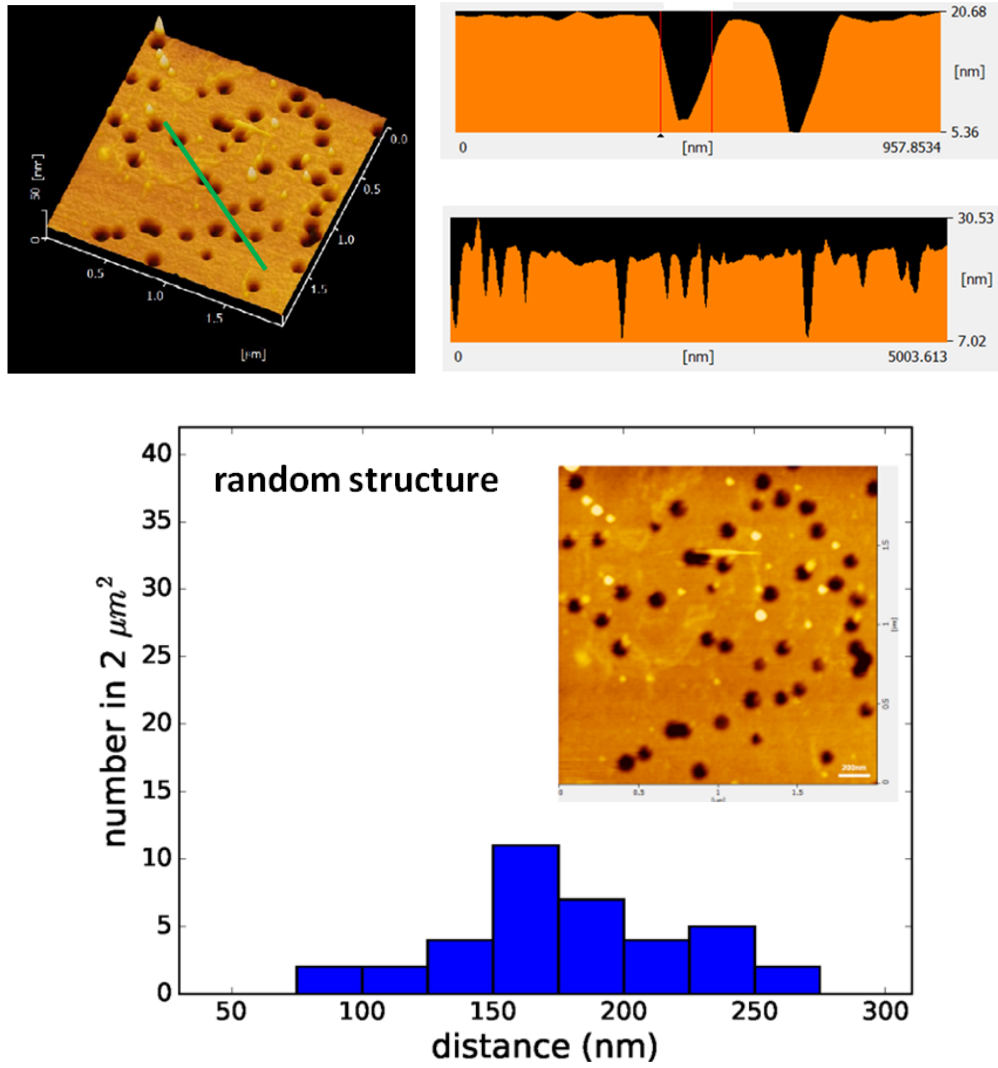
Figure 4.2: Top: 3D image of nanoholes in gold film provided by tape striping of PS spheres and Cross section image of nanoholes in thin film, down: hole distribution for gold thin film with simple holes in $2\mu m^2$ of the film.

4.3, c). Figure 4.2 shows the 3 dimensional AFM image of nanohole randomly positioned in the thin film. Cross section of films shows shape, size and depth of the holes in film with different thicknesses. Density of holes is 20 holes per μm^2.

4.2.6   Laser cutting of the sample

Similar to spongy nanoporous gold, the film was trimmed by a THG laser. Extra area of gold connected to the nanohole area was cut and the rest was shaped by cutting laser to provide two connected conductive area for attaching the electrodes (Fig. 4.3, d). By this trimming we make a symmetric shape for sample that for normal incident light cannot generate voltage.
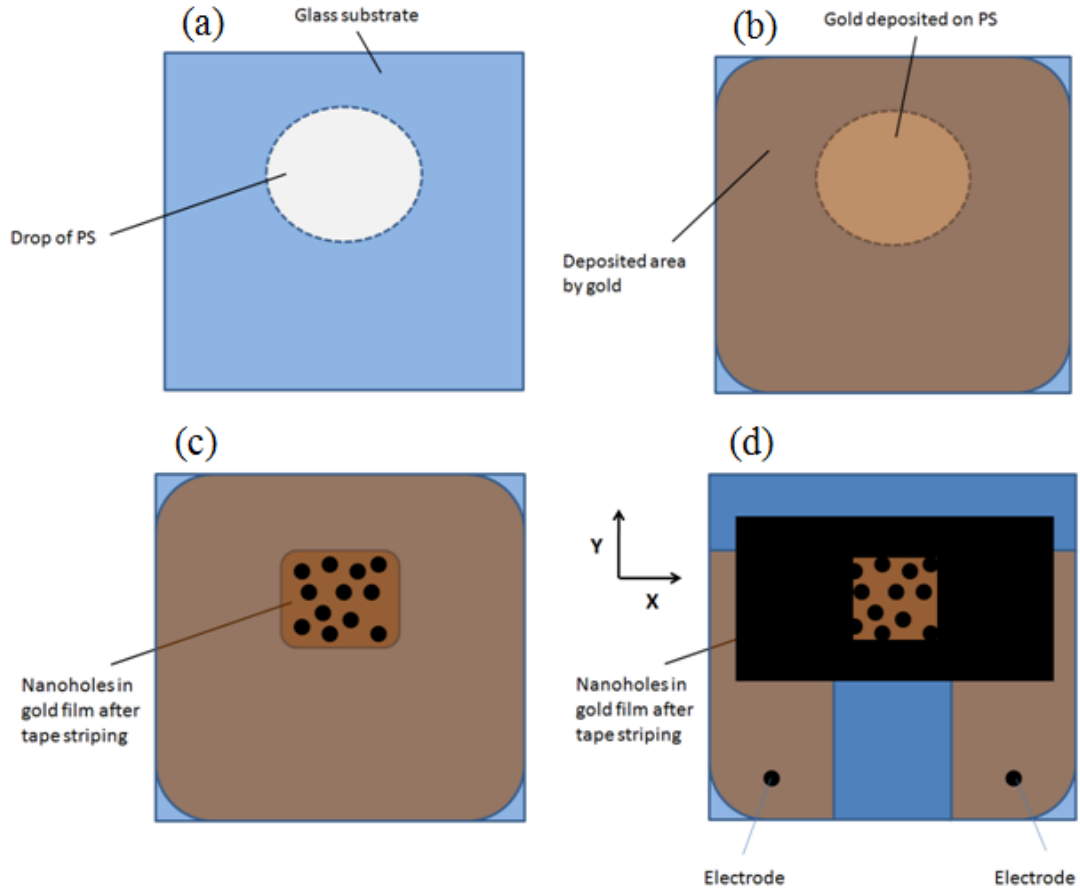
Figure 4.3: a) Drop of PS on glass substrate, b) Deposition of Cr and Au, c) Tape striping for removing PS spheres, d) Trimmed film in appropriate size and connected electrodes.

4.2.7   Attachment of electrodes on the sample

As we see in Fig. 4.3 film was trimmed with a focused laser beam into dimensions of 5 mm × 5 mm. After the placement of the sample on electrodes, the substrate was fixed on a 20 mm × 20 mm printed circuit board (PCB). Typical Ohmic resistivity is about 70 Ω for 25 nm thick and 90 Ω for 15 nm thick.
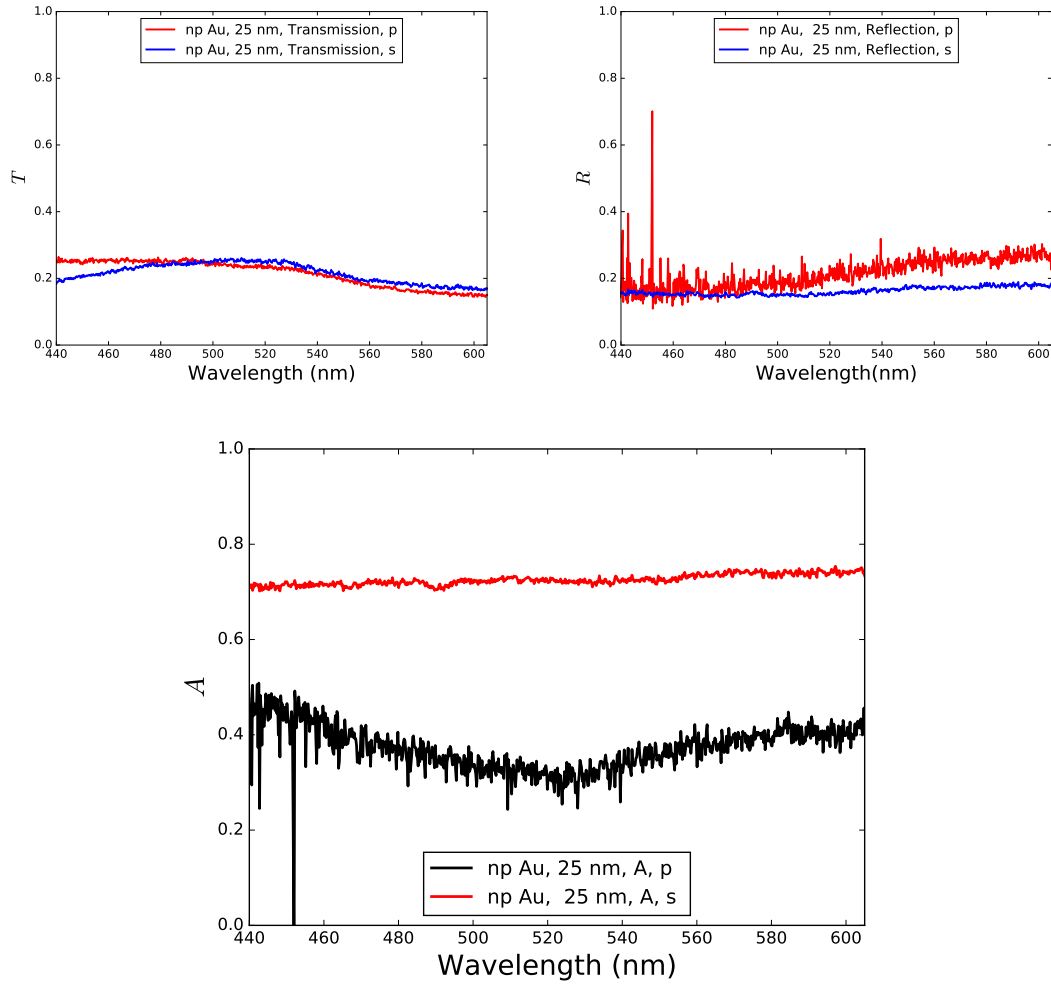
Figure 4.4: Top: Transmission and reflection spectra of 25 nm thick gold films with nanoholes for s- and p-polarization, down: absorption spectrum of 25 nm thick gold films with nanoholes for s- and p- polarization..

4.3 Results and discussions

4.3.1 Linear Optical Properties

Transmission and reflection spectra of 25 nm thick gold films with nanoholes were measured for s- and p- polarization in Fig. 4.4. Similar ot spongy nanoporous gold film, in these spectra there is not any resonant feature related to the excitation of surface plasmon modes.

4.3.2 Incidence angle resolved measurement

1. Incidence angle resolved measurement for 450 nm:

Longitudinal PIV:

Incidence angle resolved photo-induced voltage for 450 nm in longitudinal configuration with s- and p- polarized light are shown in the Fig. 4.5. For both s- and p- polarized light it follows

$\sin(2\theta)$ dependence and the sign is negative for positive angles. Similar to the spongy nanoporous gold using lateral momentum flux and parameter for gold thin film with simple holes ($\lambda = 450$ nm, I_I=1 MW/cm^2, $\theta = +45°$, $A_{450\text{n}m}$= 0.5, d=25 nm (thickness of the film)) for p- polarization we can estimate $V_x = -310\mu$V which is consistent with the measurement that is about -280μ V for 25 nm thick film.

Angle dependence of photo-induced voltage in longitudinal configuration with circular and $\pm45°$ linear polarized light are also shown in this figure. Sign and intensity of the voltage for RCP and LCP circular polarized light is the same. The same tendency is observed for $\pm45°$ voltages. Similar to spongy nanoporous gold film these voltages are combination of s- and p- components of these polarized lights.
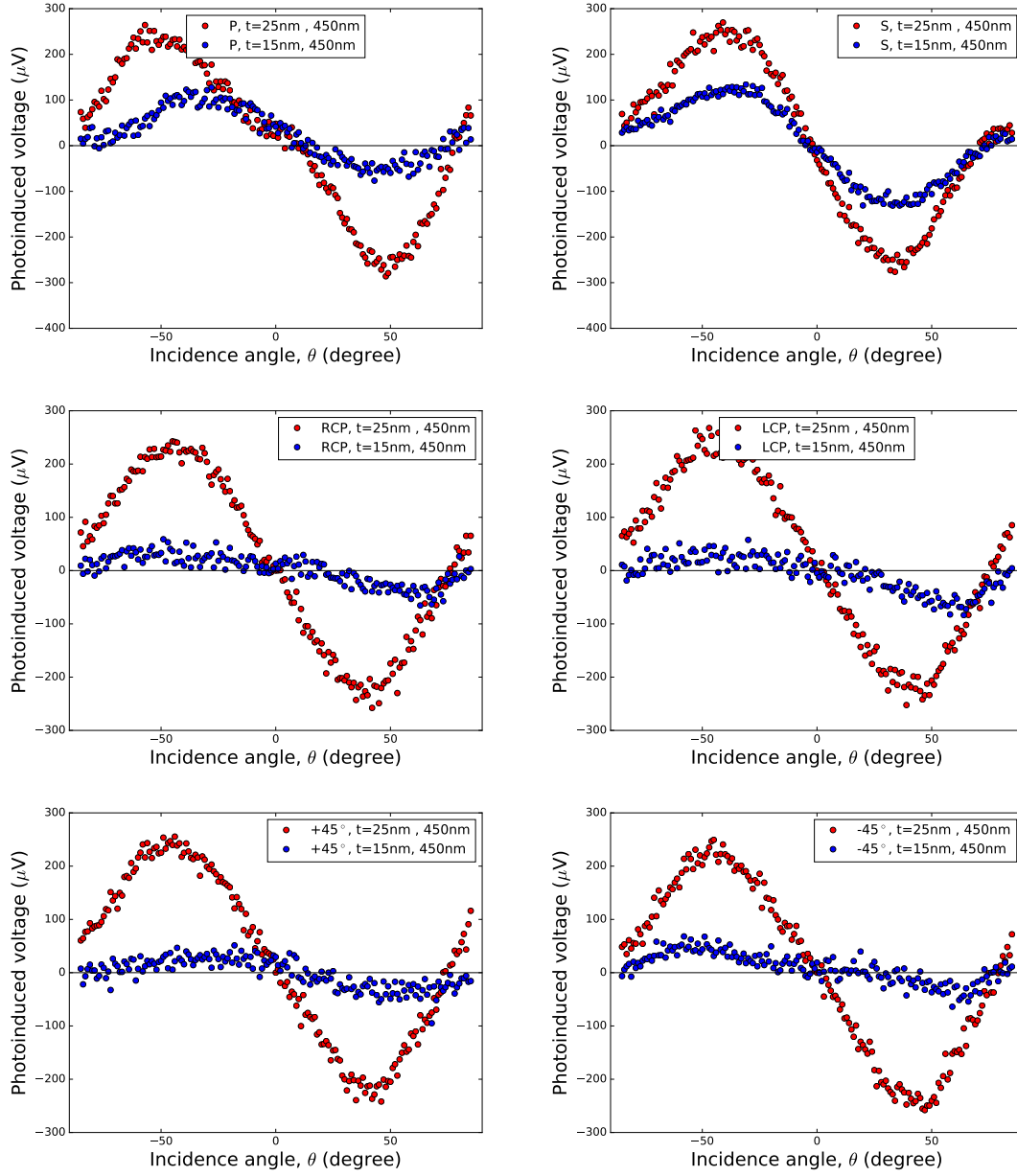
Figure 4.5: Incidence angle resolved measurement of the LPIV for p- and s- polarized light, circular polarized light and ±45° linear polarized light with 450nm incident light.
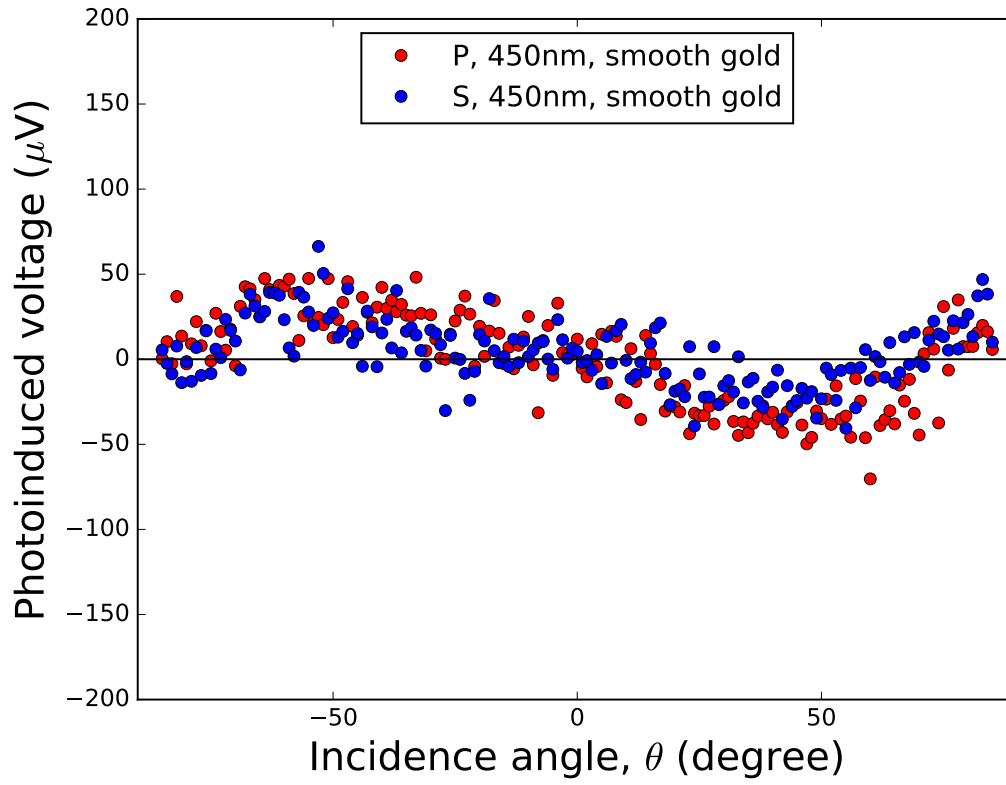
Figure 4.6: Incidence angle resolved measurement of the LPIV for p- and s- polarized light with 450 nm incident light for smooth film.

For smooth thin film with 25 nm LPIV generated by s- and p- polarizations with 450 nm incident light shows that these voltages are almost zero due to small absorption (Fig. 4.6).
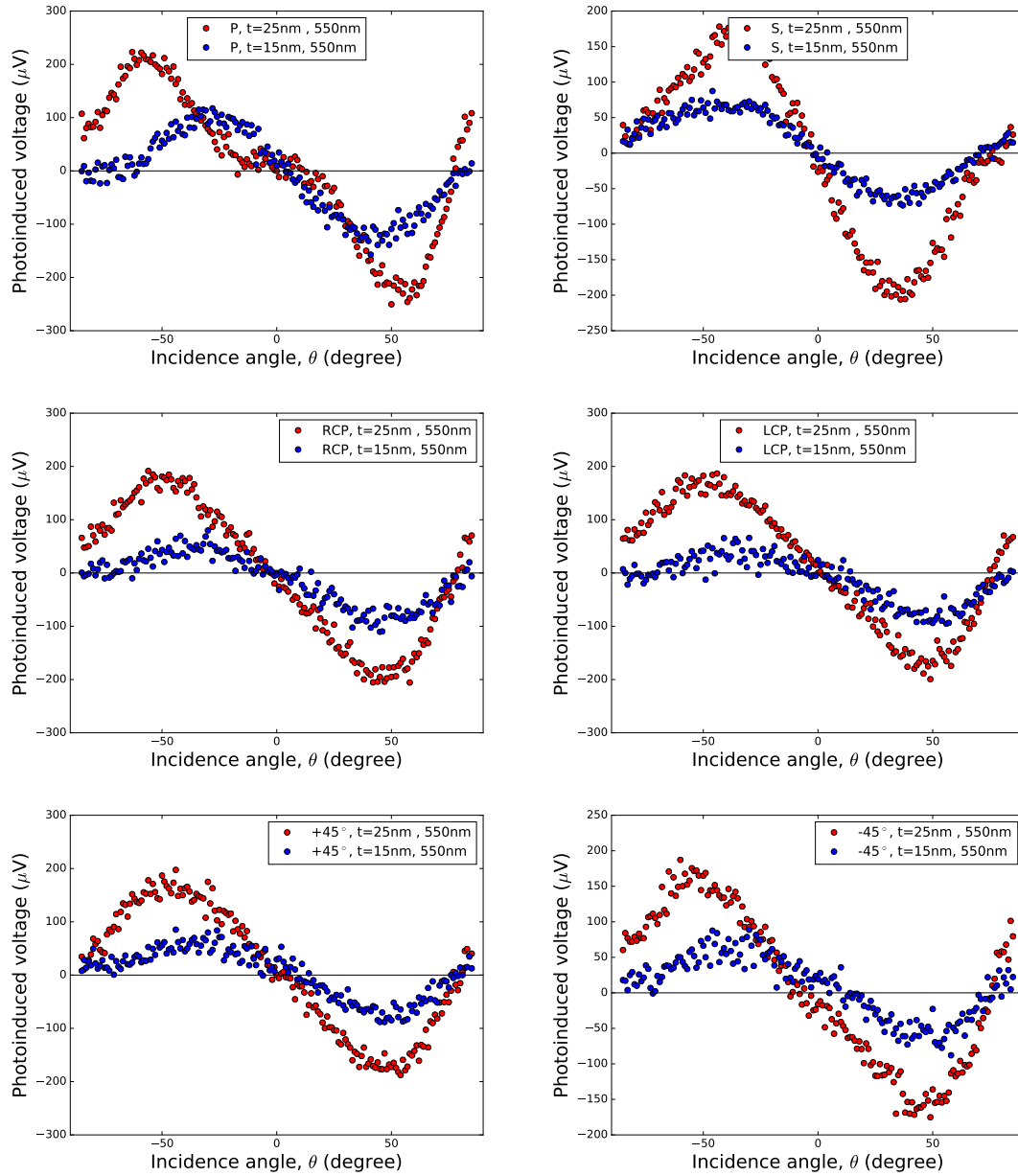
Figure 4.7: Incidence angle resolved measurement of the LPIV for p- and s- polarized light, circular polarized light and $\pm 45°$ linear polarized light with 550nm incident light.

2. Incidence angle resolved measurement for 550 nm:

Longitudinal PIV:

Incidence angle resolved photo-induced voltage at the wavelength of 550 nm in longitudinal configuration with s- and p- polarized light is shown in the Fig. 4.7. For s-polarized light it follows $\sin(2\theta)$ dependence and the sign is negative for positive angles. It is reasonable as electron has negative charge, which is pushed by light momentum. As for p- polarization there is not any sign change for 550 nm for p- polarization we can conclude that the effect of LSPR is this type of nanoporous is small due to different structure compared to the spongy nanoporous gold. In spongy

nanoporous gold film volume ratio of gold and holes is 50%-50% and for this sample is 85%-15%. So, smaller volume of nanoholes in the whole volume of the film results in smaller voltage due to positive voltages of the batteries (Fig. 4.8) . So, for p- polarization similar to s- polarization linear momentum transferred to the film makes a negative voltage for positive incidence angles for p- polarization. Higher concentration of holes is difficult to achieve because by increasing the number of PS spheres in the solution, spheres start to accumulate and we cannot produce simple holes in the film.

Angle dependence of photo-induced voltage in longitudinal configuration with circular and $\pm45°$ linear polarized light are also shown in Fig. 4.7. These voltages could be combinations of s- and p- components of circular and $\pm45°$ linear polarized light similar to the 450 nm voltages.

$$V_{total} > 0$$

$$V_{battry} > 0 \qquad\qquad\qquad\qquad\qquad V_m < 0$$

Gold thin film with simple holes

$$V_{total} > 0$$

$$V_{battry} > 0 \qquad\qquad\qquad\qquad\qquad V_m < 0$$

Spongy nanoporous gold
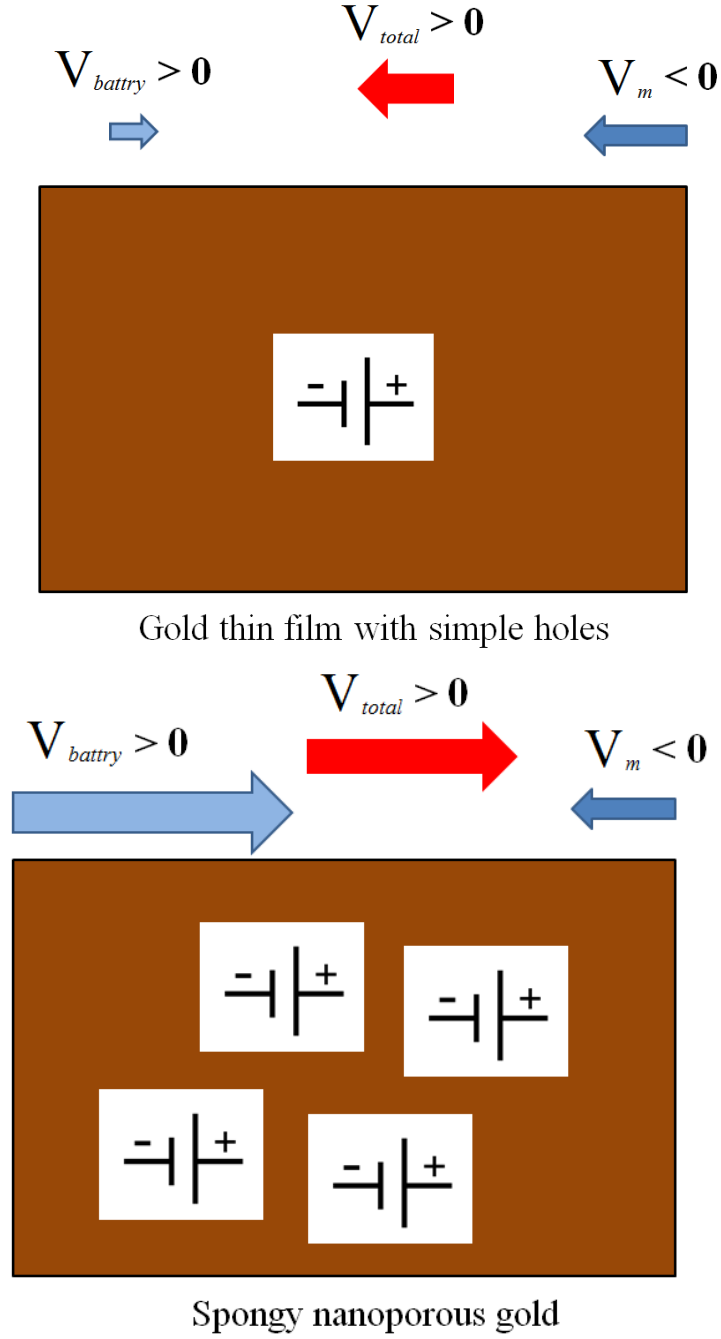
Figure 4.8: Voltage in gold film with simple holes due to momentum flux and induced batteries for p- polarization compred to spongy nanoporous gold film.
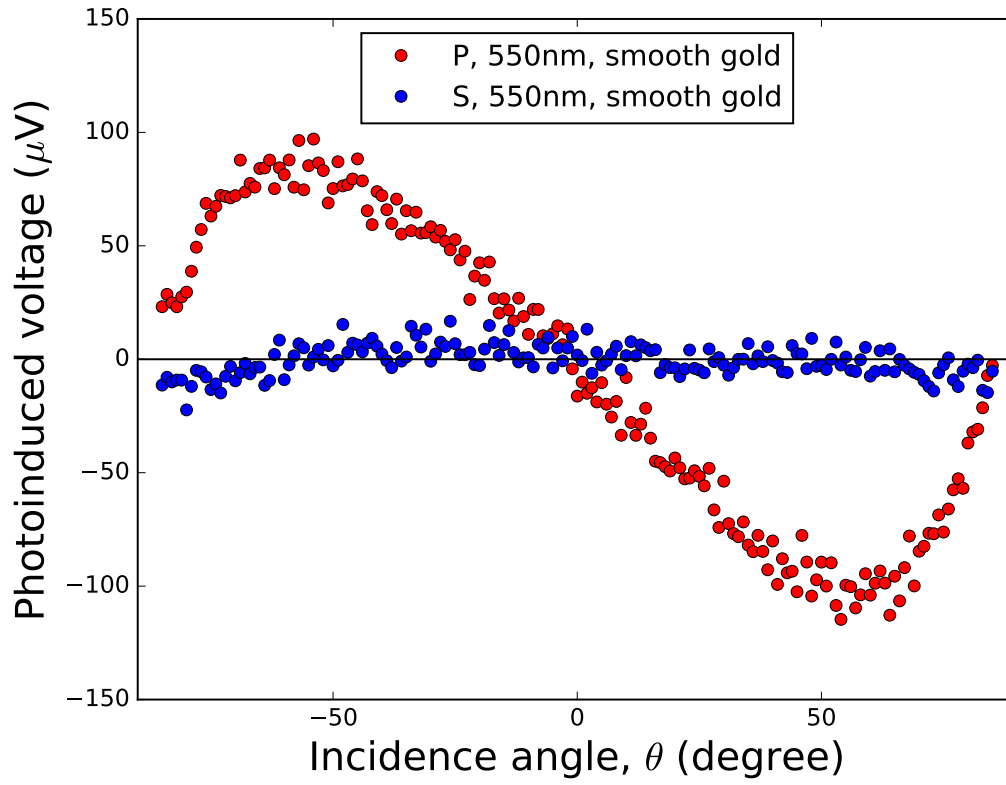
Figure 4.9: Incidence angle resolved measurement of the LPIV for p- and s- polarized light with 550nm for 25 nm thick smooth gold film.

For smooth thin film with 25 nm LPIV generated by s- and p- polarizations with 550 nm incident light (Fig. 4.9) shows that these voltages are smaller due to small absorption.

4.3.3   Wavelength resolved measurement

Longitudinal PIV:

Wavelength resolved photo-induced voltage for films of 25 nm and 15 nm in thickness in the longitudinal configuration with p- and s- polarized light are shown in Fig. 4.10. For s- polarization, voltage is always negative for positive incidence angle. On the other hand, we found that in contrast to spongy nanoporous gold film for p- polarization the sign of the voltage does not change with wavelength for both thicknesses and is always negative. While for 25 nm thick film there is a stronger voltage for smaller wavelengths, for 15 nm thick is almost the same for all wavelengths and also smaller than the voltage of the film with 25 nm thickness (Fig. 4.10). For the s- polarization we have the same tendency for voltages generated in both 25nm and 15 nm thick films which similar to spongy nanoporous gold film are always negative (Fig. 4.10).

For $\pm 45°$ linear and circular polarized light there are negative voltages for all wavelengths and sign of the voltages do not change by degree of polarization for $\pm 45°$ linear and sense of rotation for circular polarized light. Similar to spongy nanoporous voltages, they are combinations of s- and p- polarized light components of these polarizations (Fig. 4.10).
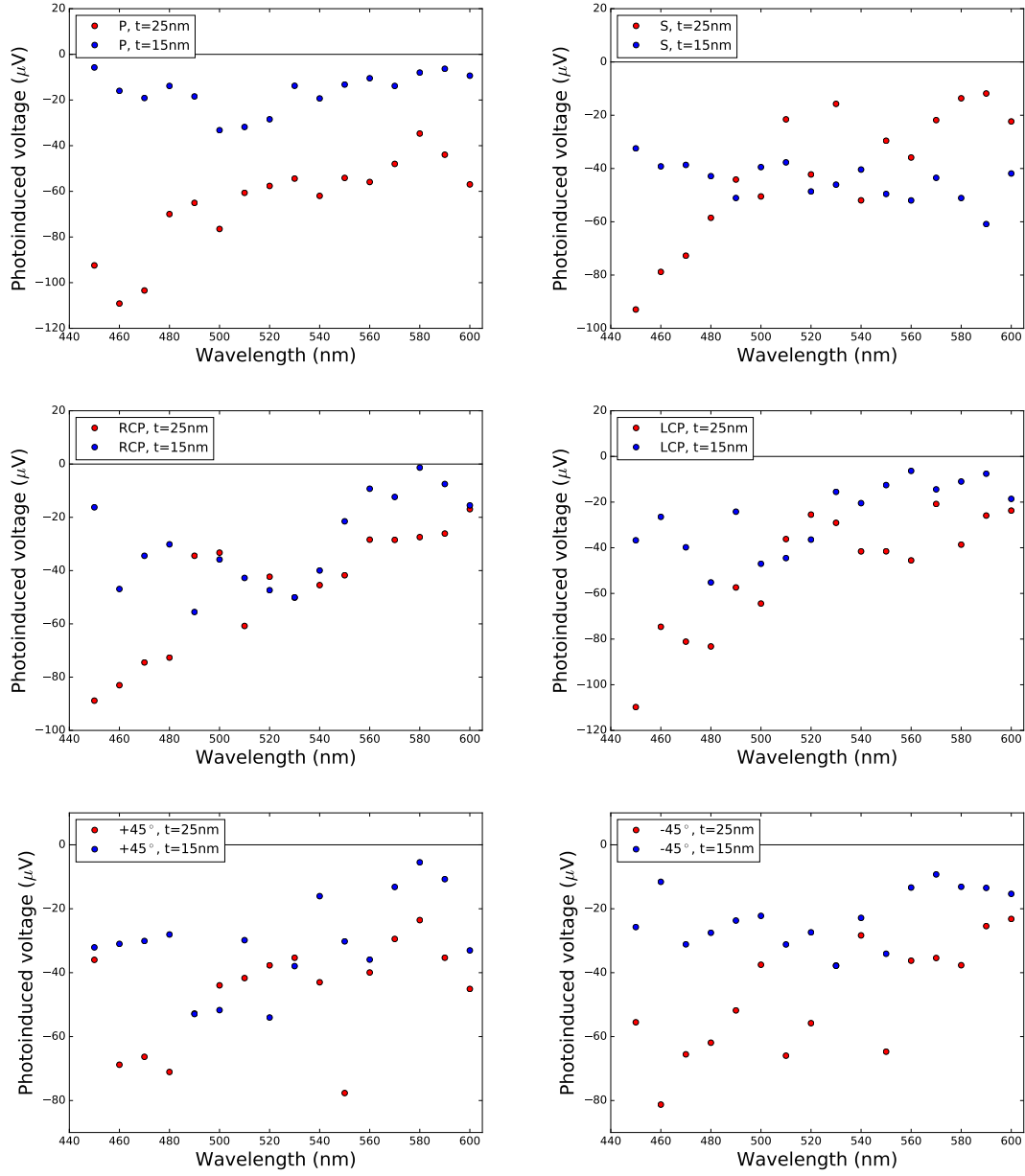
Figure 4.10: Wavelength resolved measurement of the LPIV for p- and s- polarized light, circular polarized light and $\pm45°$ polarized light with $\theta = +50°$ incidence angle of 25 nm and 15 nm thick films.

Table 4.1: Geometrical comparison of two gold samples

Samples	density of pores	hole size (nm)	shape	thickness (nm)
Spongy nanoporous gold	50% gold-50% hole	50	bicontinous	100
Gold thin film with simple holes	85% gold-15% hole	100	isolated	25

4.3.4 Summary

We successfully fabricated gold thin film with simple holes and measured LPIV and TPIV in this film. In contrast to spongy nanoporous gold film linear momentum model could explain the LPIV for s- and p- polarization similar to the spongy nanoporous gold and there is not any sign change for longer wavelengths for p- polarization.

4.3.5 Conclusions

We have investigated LPIV and TPIV in gold thin film with simple holes. In contrast to spongy nanoporous gold we estimated LPIV for s- and p- polarization with conservation of linear momentum and there is not any sign change for p- polarization due to small LSPR in this film. Different hole volume ratio, size, shape and thickness of these two films (table 4.1) are responsible to these different behaviors for these two metallic gold nanostructures. So, we can consider spongy nanoporous gold as metamaterial that shows that anomalous sign change for p- polarization in LPIV.

CHAPTER 5

Silver thin film with simple nanoholes

5.1 Overview

By now we have investigated LPIV in two types of gold thin films which have different fabrication methods and also different ratio, shape and size of holes. Here to study the effect of the material on the generated voltage, we show experimental results of silver thin film with simple nanoholes.

5.2 Sample preparation

Preparation of thin film of silver with nanoholes is similar to gold film. One difference is that for silver film we do not need an adhesive layer of Cr. The other is that by increasing the thickness of the deposited layer of silver it is more difficult to remove the PS spheres by tape striping. So, we employed another method for this purpose. In this method after deposition of 25 nm of silver on PS spheres, we soaked it in Xylene for three days. Then ultrasonic cleaning process was done with the film soaked in Xylene for one hour. By this method it is possible to provide a thin film of silver with nanoholes that is almost perfectly clean of the PS spheres. Typical Ohmic resistivity of the sample is 50 Ω.
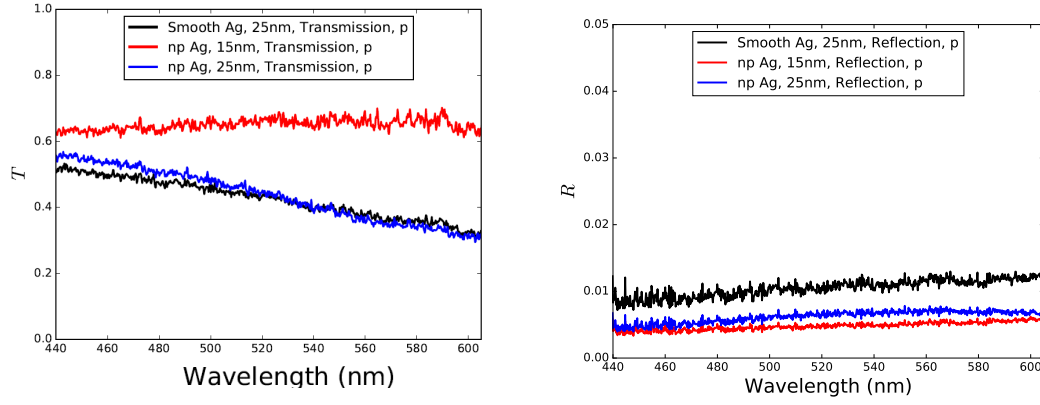
Figure 5.1: Transmission and reflection spectra of 25 nm and 5 nm thick nanoholes silver thin film compared to 25 nm thick smooth film of silver for p- polarization.

5.3 Results and discussions

5.3.1 Linear Optical Properties

Transmission and reflection spectra of 25 nm and 15 nm thick silver films with nanoholes are compared to the smooth silver film of 25 nm for p- polarization in Fig. 5.1. As we see in Fig. 5.1 transmission of nanoporous thin film with 15 nm thickness is larger than 25 nm thick nanoporous film and 25 nm thick smooth film. As transmissions of 25 nm thick nanoporous film and 25 nm thick smooth film are almost the same so number of holes does not change the total volume of the silver as calculation shows that the these thin films with simple nanoholes consist of 15% hole and 85% silver. For reflection of 15 nm thick nanoporous silver film is larger than that of 25 nm nanoporous silver film, so, absorption of 25 nm thick nanoporous silver film is larger than 15 nm thick nanoporous silver film.
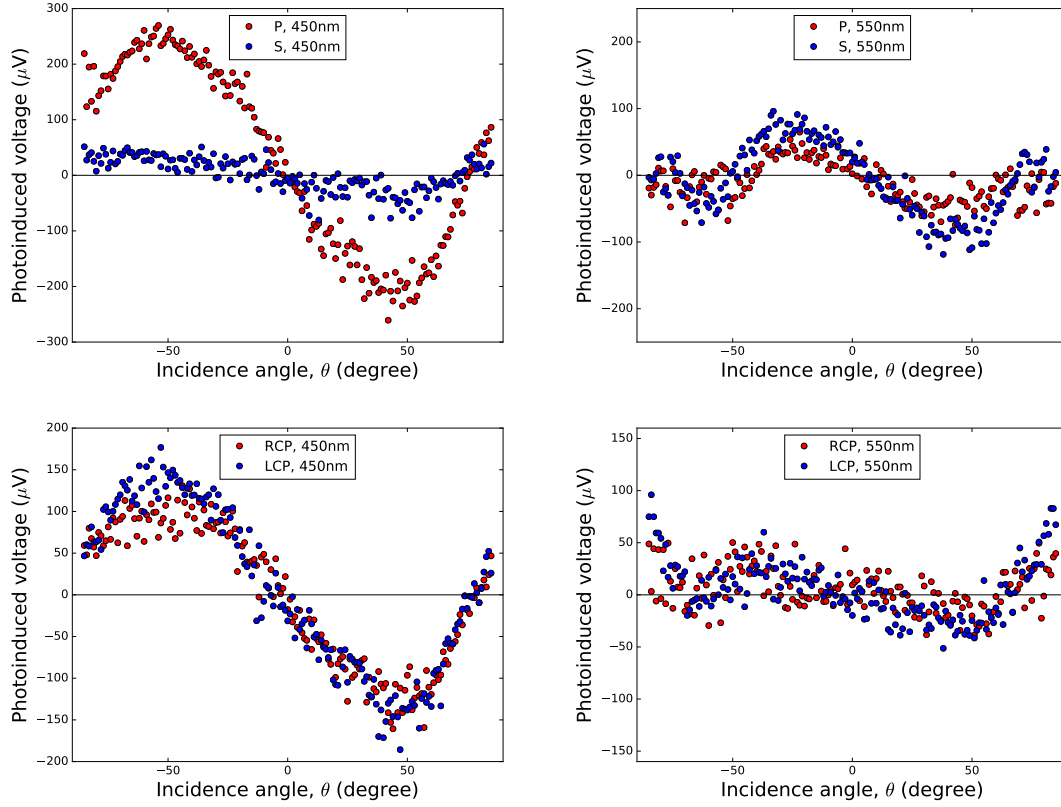
Figure 5.2: Incidence angle resolved of the LPIV for p- polarization, s- polarization and circular polarization with 450nm and 550 nm.

Incidence angle resolved measurement:

Longitudinal PIV:

Incidence angle resolved LPIV with p- and s- polarization for nanohole silver film of 25 nm thickness show that for 450 nm voltage for s- polarized is small and could be explained by transfer of momentum from photons to the electrons (Fig. 5.2). For p- polarization the tendency is similar to the s- polarization but amplitude is larger. For 550 nm amplitude of the voltages for s- and p- polarized light are almost the same. So, at this wavelength the same mechanism happens for s- polarization. For p- polarized light the role of localized surface plasmon are not as significant as the 450 nm. It may be due to the stronger excitation of localized surface plasmon for smaller wavelengths for nanohole silver thin film [47]. For circular polarized light for these two wavelengths the measurements are consistent with the gold thin film results which showed that they are produced by combination of s- and p- components of the circular polarized light.

Measurements of smooth thin silver with the 25 nm thickness compared to that of the nanohole silver film with the same thickness show that for LPIV with s- polarization the voltage is almost zero but for p- signal is nonzero but smaller that the nanohole silver film. In this case we can say even the film does not have nanoholes but still roughness of the film could generate localized
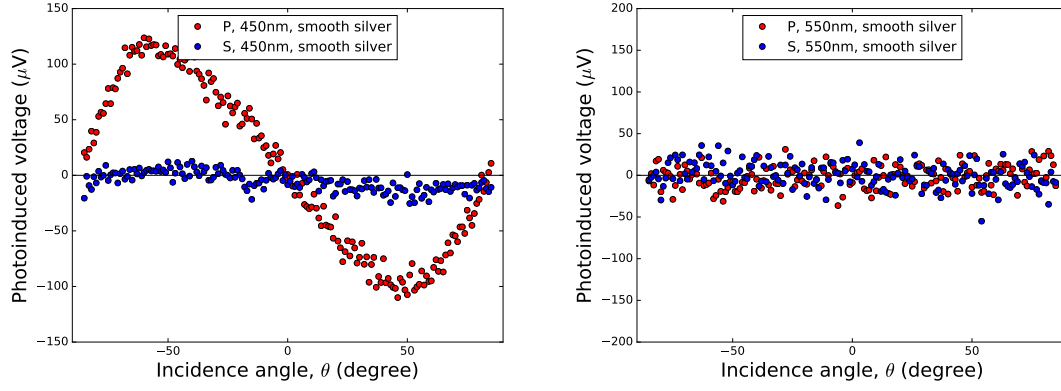
Figure 5.3: Incidence angle resolved of the LPIV for p- and s- polarization with 450nm and 550 nm for 25 nm thick smooth silver film.

surface plasmon for shorter wavelengths similar to the nanohole silver film and this excitation is very small for 550 nm (Fig. 5.3).

5.3.2 Conclusions

We have investigated LPIV and TPIV in silver thin film with simple holes. As we see by changing the material from gold to silver that behavior of the voltage does not change, so, we can conclude that these voltage do not depend on the electronic structure and interband transitions in these materials in visible range. So, we can consider these materials as metamaterials.

CHAPTER 6

Polarization resolved measurement

As we conclude before, spongy nanoporous gold film is macroscopically isotropic in the xy-plane. So, by rotating the film around the z-axis, symmetry of the film does not break, so along this axis angular momentum of the applied light is conserved. Here we utilize this conservation to understand the origin of the TPIV and try to estimate the voltage by calculation of angular momentum using helicities of the incident, reflected and transmitted lights. In order to compare our calculation with the measurement here we show experimental results for TPIV as a function of half wave plate angle β, as explained in experimental methods before.

6.1 Experimental results

a) Transverse PIV with linearly polarized light

First we set the QWP fast axis angle α to be 90°, while the incident beam is p- polarized. In order to investigate orientation dependence of TPIV, we inserted HWP before the sample. By rotating the HWP, direction of the fast axis rotates, therefore the orientation of the $\boldsymbol{E}$ field of the passing light changes and as we can see in the Fig. 6.1 all orientations of linear polarization are generated which includes s- polarization (vertical $\boldsymbol{E}$ field), p- polarization (horizontal $\boldsymbol{E}$ field) and other angles of orientation between vertical and horizontal polarizations. Figure 6.1 show TPIV as a function of the half wave plate angle, β, for 450 nm and 550 nm. Because by adding 180° to β the same polarization is produced there is a periodic tendency for the voltages with period of 180°.

Figure 6.1: Top: Polarization resolved measurement of theTPIV for 450nm linear polarized incident light with $\theta = 50°$, down: Polarization resolved measurement of the TPIV for 550nm linear polarized incident light with $\theta = 50°$.

Figure 6.2: Top: Polarization resolved measurement of the TPIV for 450nm circular polarized incident light with $\theta = 50°$, down: Polarization resolved measurement of theTPIV for 550nm circular polarized incident light with $\theta = 50°$

b) Transverse PIV with circularly polarized light

First we set the QWP fast axis angle α to be 135° and 45°, while the incident beam is p- polarized in order to produce RCP and LCP circular polarized light, respectively. By rotating the HWP, direction of the fast axis rotates, therefore the orientation of the $\boldsymbol{E}$ field of light changes and as we can see in the Fig. 6.2 circular polarization are generated. Figure 6.2 shows TPIV as a function of the half wave plate angle, β, for 450 nm and 550 nm. As we see the graphs are almost straight lines because for all β incident light is circular and must generate the same amplitude for the voltages.

c) Transverse PIV with elliptically polarized light

First we set the QWP fast axis angle α to be 120° and 60°, while the incident beam is p- polarized in order to produce RCP and LCP elliptical polarized light, respectively. By rotating the HWP,
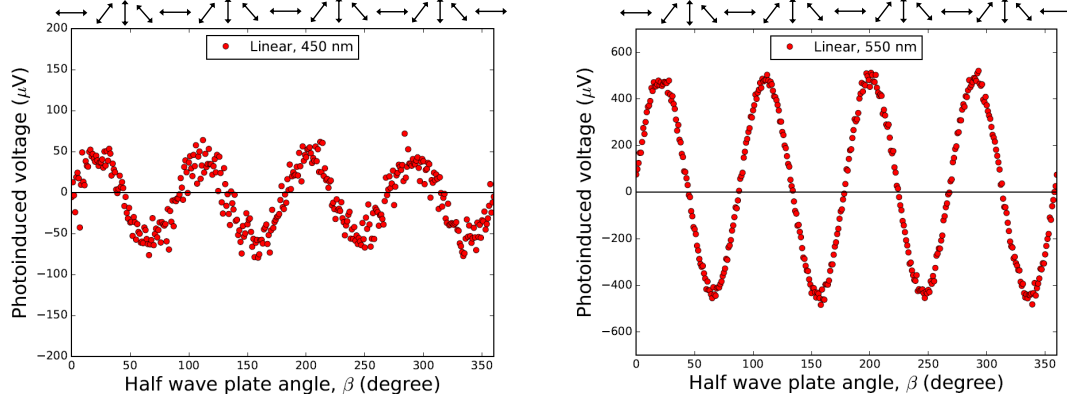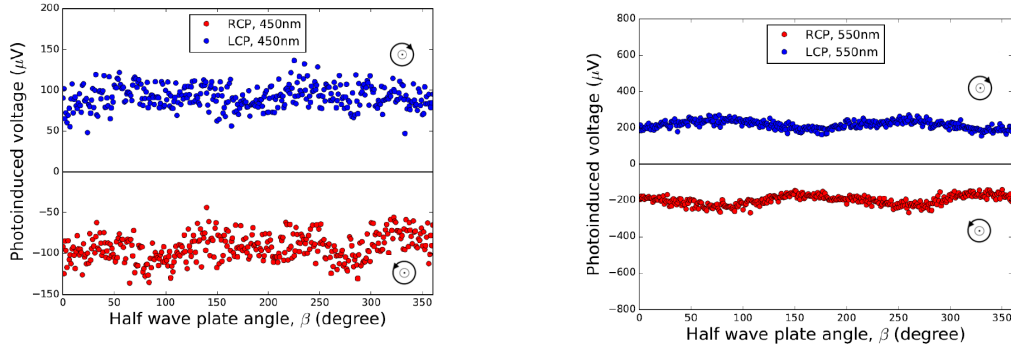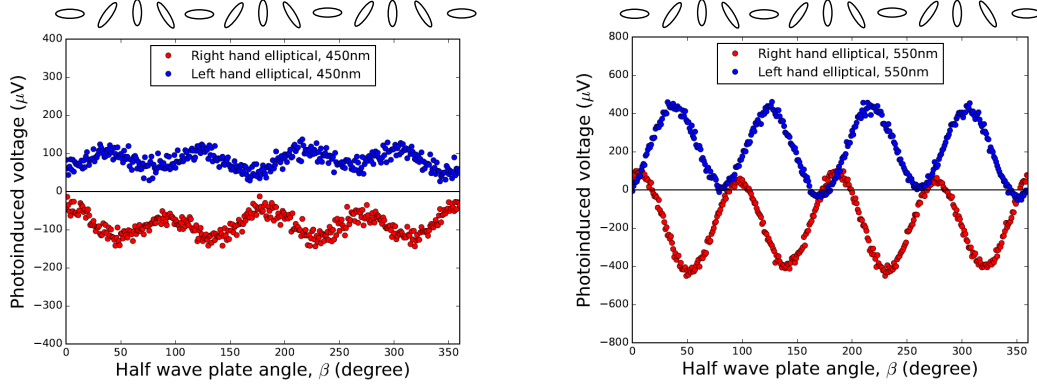
Figure 6.3: Top: Polarization resolved measurement of the TPIV for 450nm elliptical polarized incident light with $\theta = 50°$, down: Polarization resolved measurement of the TPIV for 550nm elliptical polarized incident light with $\theta = 50°$.
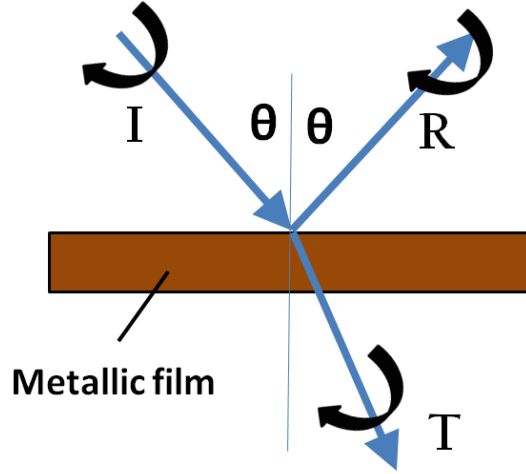
Figure 6.4: Incident, reflected and transmitted light of the film.

direction of the fast axis rotates, therefore the orientation of the E field of the passing light through it changes and as we can see in top of the Fig. 6.3 all orientations of elliptical polarization are generated which includes vertical and horizontal ellipses as well and other ellipses between vertical and horizontal. Figure 6.3 shows TPIV as a function of the half wave plate angle, β, for 450 nm and 550 nm. These TPIV generated by elliptical polarized light are between TPIV of linear polarized light in Fig.6.1 and TPIV of circular polarized light in Fig.6.2.

6.2 Angular momentum transfer calculation

In order to understand origin of the TPIV, we have calculated angular momentum transfer to the sample. Calculations were carried out by estimating of the transferred angular momentum from photon to the film upon reflection and transmission.

When light impinges on a material, depending on the polarization of the incident light, polarization of the reflected and transmitted light (Fig.6.4) is linear polarized or elliptical polarized; that is when incident light is vertical or horizontally polarized (p- or s- polarized) polarization of the reflected and transmitted light is also linearly polarized. In this case helicities of this incident, reflected and transmitted lights are zero and from conservation of the angular momentum the total transferred angular momentum to the sample is zero. But in the case of linearly polarized incident light with other degrees of polarization and also for circularly and elliptically polarized incident lights the reflected and transmitted lights are also elliptical polarized. In these cases the total transferred angular momentum from light to the sample is not zero and using helicities of the incident, reflected and transmitted lights we can calculated the amount of transferred angular momentum to the sample.

Here we explain the method to calculate the transferred angular momentum for spongy nanoporous gold with 450 nm and 550 nm wavelengths. Using Jones matrices for p- polarized input light and QWP we calculated output of the QWP (incident light on the film) and its ellipticity, η_I. After the QWP, this light passes through the HWP. Using measured reflection coefficients, $\tilde{r}_p = r_p e^{i\delta_{r_P}}$, $\tilde{r}_s = r_s e^{i\delta_{rs}}$, $\tilde{t}_p = t_p e^{i\delta_{t_p}}$ and $\tilde{t}_s = t_s e^{i\delta_{ts}}$ in Jones matrix for Fresnel equation, ellipticity of the reflected light, η_R, and the transmitted light, η_T, from the sample was measured. Considering conservation of angular momentum in the system along sample normal:

$$
\begin{aligned}
\Delta L_{\text{Sample}} &= L_I \cos\theta - (L_T \cos\theta + L_R \cos(\pi - \theta)) \\
&= L_I \cos\theta - L_T \cos\theta + L_R \cos\theta \\
&= (L_I - L_T + L_R)\cos\theta \\
&= \hbar \frac{I_o}{\hbar\omega} S_{area} \Delta t (\eta_I - T\eta_T + R\eta_R)\cos\theta
\end{aligned}
\tag{6.1}
$$

So, for flux of angular momentum we have

$$
L_{\text{flux}} = \frac{\Delta L_{\text{Sample}}}{S_{area}\Delta t} = \hbar \frac{I_o}{\hbar\omega}(\eta_I - T\eta_T + R\eta_R)\cos\theta
\tag{6.2}
$$

If we show $(\eta_I - T\eta_T + R\eta_R)$ as Y

$$
L_{\text{flux}} = \frac{I_o}{\omega}Y\cos\theta
\tag{6.3}
$$

So, by calculating Y we are able to find L_{flux} and in a way similar to lateral momentum we can calculate the V_y.

L_I, L_T, L_R and η_I, η_T, η_R are angular momenta and ellipticity for incident, transmitted and

reflected light beams, respectively. R, T and θ are reflection, transmission coefficients and incidence angle of the incident beam, respectively. I is intensity of the incident light. Helicity of light can be calculated by:

$$\eta_{\mathrm{J}} = \frac{i\boldsymbol{E}_{\mathrm{J}} \times \boldsymbol{E}_{\mathrm{J}}^{*}}{|\boldsymbol{E}_{\mathrm{J}}|^2}, \qquad \mathrm{J = I,\ R,\ T} \tag{6.4}$$

For calculating the transferred angular momentum we show p- polarized input light by vector as:

$$\boldsymbol{E}_0 \quad = \quad \begin{pmatrix} 1 \\ 0 \end{pmatrix} \tag{6.5}$$

Here we want to calculate $\Delta L_{\mathrm{Sample}}$ from helicities and reflection, transmission coefficients for different polarizations of light. Because helicity of the light is fixed by rotating orientation of the linearly, circularly and elliptically polarized light, we employed a quarter wave plate to produce different polarizations from p- polarized input light. After quarter wave plate a half wave plate rotates orientation of the light between $0°$ and $360°$ and the produced light apply on the sample. So, for calculations we show the effect of a quarter wave plate and a half wave plate using Jones Matrices:

$$\boldsymbol{Q}(\alpha) \quad = \quad \begin{pmatrix} \cos\alpha & -\sin\alpha \\ \sin\alpha & \cos\alpha \end{pmatrix} \begin{pmatrix} i & 0 \\ 0 & 1 \end{pmatrix} \begin{pmatrix} \cos\alpha & \sin\alpha \\ -\sin\alpha & \cos\alpha \end{pmatrix} \tag{6.6}$$

α is the angle that fast axis of quarter wave plate makes with x-axis which determines right handedness and left-handedness of the output of the quarter wave plate. For example, when $\alpha = 45$ as we defined it in chapter 2 it is a LCP and so on.

$$\boldsymbol{H}(\beta) \quad = \quad \begin{pmatrix} \cos\beta & -\sin\beta \\ \sin\beta & \cos\beta \end{pmatrix} \begin{pmatrix} e^{i\delta_{HWP}} & 0 \\ 0 & 1 \end{pmatrix} \begin{pmatrix} \cos\beta & \sin\beta \\ -\sin\beta & \cos\beta \end{pmatrix} \tag{6.7}$$

β is the angle that fast axis of half wave plate makes with x-axis which determines the phase delay between input and put light. Then incident light can be shown by:

$$, \quad \boldsymbol{E}_{\mathrm{I}}(\alpha, \beta) = \boldsymbol{H}(\beta)\boldsymbol{Q}(\alpha)\boldsymbol{E}_0. \tag{6.8}$$

And effect of reflection and transmission on the incident light can be shown using Jones Matrices for Complex Fresnel coefficients as:

$$\boldsymbol{F}_{\mathrm{R}} \quad = \quad \begin{pmatrix} r_{\mathrm{p}}e^{i\delta_r} & 0 \\ 0 & r_{\mathrm{s}} \end{pmatrix} \tag{6.9}$$

and

$$\boldsymbol{F}_{\mathrm{T}} \quad = \quad \begin{pmatrix} t_{\mathrm{p}}e^{i\delta_t} & 0 \\ 0 & t_{\mathrm{s}} \end{pmatrix} \tag{6.10}$$

So, finally reflected light and transmitted light are:

$$\boldsymbol{E}_{\mathrm{R}}(\alpha, \beta) = \boldsymbol{F}_{\mathrm{R}}(\theta)\boldsymbol{E}_{\mathrm{I}}(\alpha, \beta) \qquad , \qquad \boldsymbol{E}_{\mathrm{T}}(\alpha, \beta) = \boldsymbol{F}_{\mathrm{T}}(\theta)\boldsymbol{E}_{\mathrm{I}}(\alpha, \beta). \tag{6.11}$$

For phase delays for s- and p- polarized lights we have:

$$\delta_r = \delta_{\mathrm{rp}} - \delta_{\mathrm{rs}} \qquad\qquad \delta_t = \delta_{\mathrm{tp}} - \delta_{\mathrm{ts}} \tag{6.12}$$

These phases are calculated using setups in the Fig. 6.5. For input $+45°$ linearly polarized input light we have sample at $+50°$ incidence angle and for transmission and reflection configurations try to find the angles on the QWP and second polarizer to vanish the light which are used to measured the phase delays for reflection and transmission.

Using setup in Fig. 6.6 we measured the power of the reflection and transmission lights using a power meter. The reflection and transmission coefficients can be calculated by squaring these amplitudes.
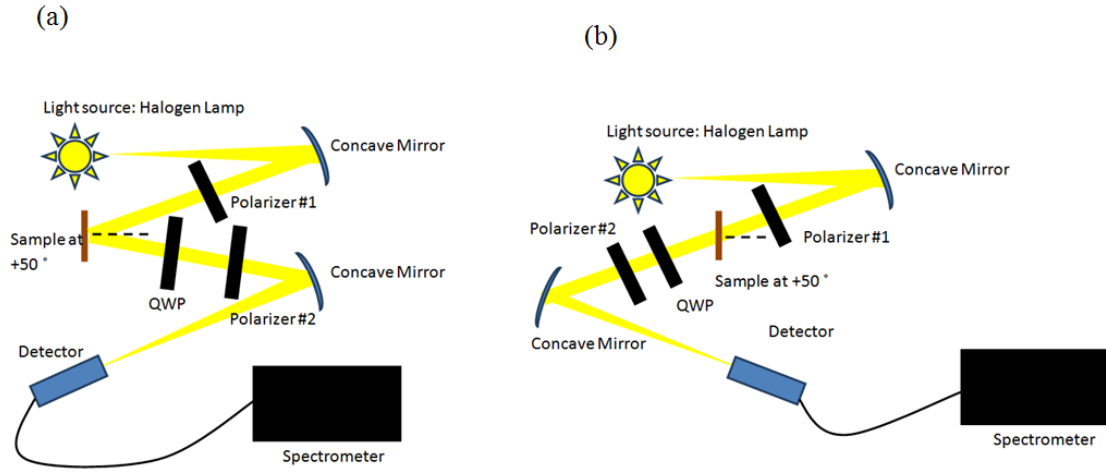
Figure 6.5: Schematic of experimental setup for finding polarizer and quarter wave plate angle for calculating phase delays, a) reflection setup, b) transmission setup.
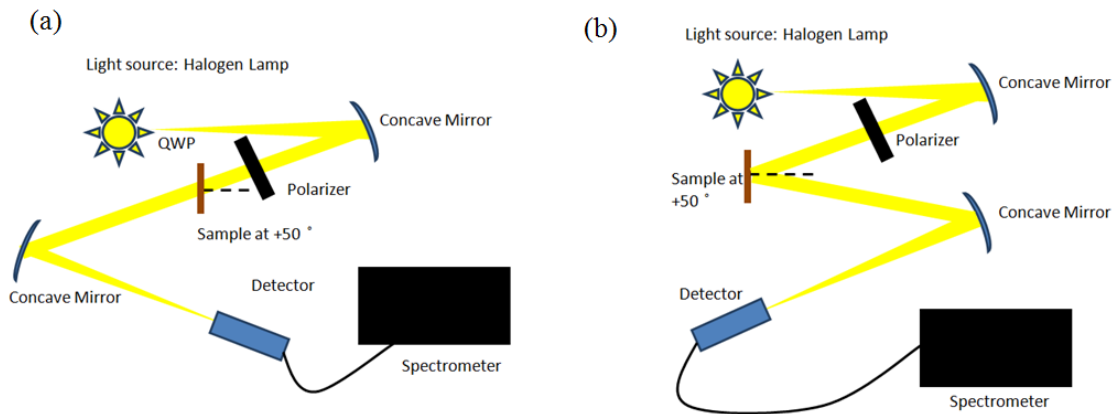
Figure 6.6: Schematic of experimental setup for finding reflection and transmission coefficients: a) reflection setup, b) transmission setup.
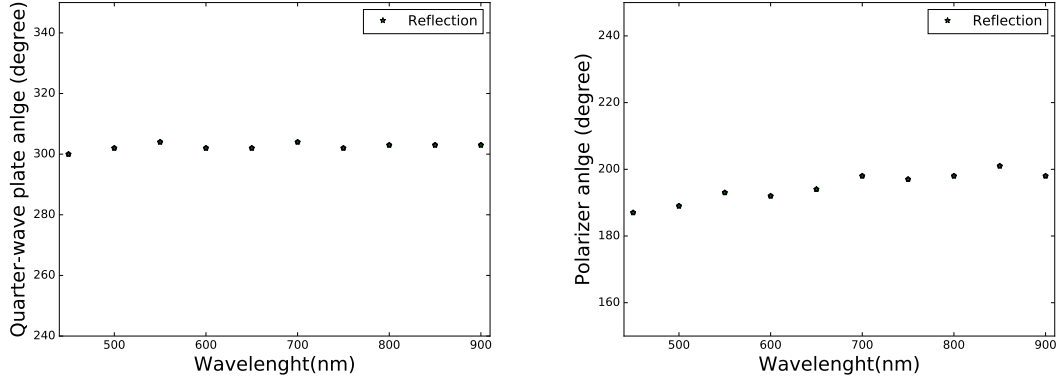
Figure 6.7: Polarizer and quarter wave plate angles for reflection ellipsometry for spongy nanoporous gold film.
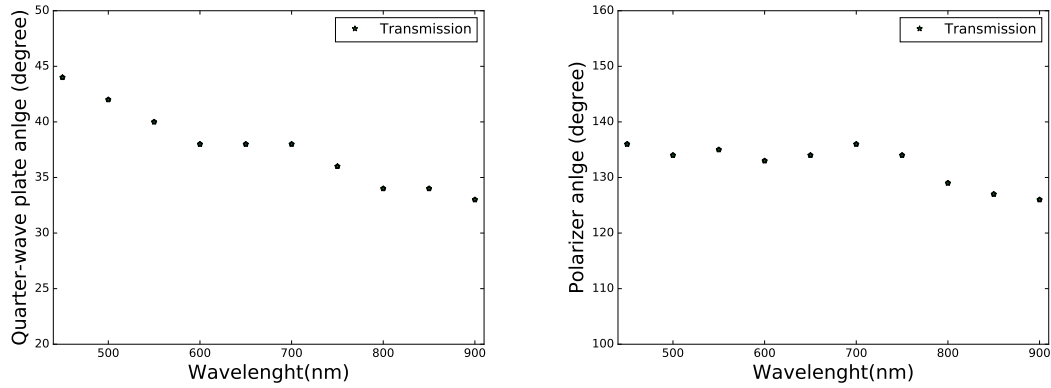
Figure 6.8: Polarizer and quarter wave plate angles for transmission ellipsometry for spongy nanoporous gold film.

6.3 Results and discussions

6.3.1 Spongy nanoporous gold thin film

For a proper HWP for all visible range, $\delta_{HWP} = \pi$. Complex Fresnel coefficients of our sample were determined from a separate experiment for visible wavelengths using the above conventional ellipsometry technique.

The angles for polarizer and quarter wave plate for all visible range for both films are shown in Fig. 6.7 and 6.8. Because our measurements for TPIV in the chapter 3 and 4 were performed for two wavelengths; 450 nm and 550 nm, here we have results of the phase delays and coefficients for these two wavelengths as below:

λ=450 nm:

$$r_{\mathrm{p}} = (0.065)^{1/2} \qquad , \qquad r_{\mathrm{s}} = (0.24)^{1/2} \qquad , \qquad \delta_r = -0.66\pi \qquad (6.13)$$

Figure 6.9: Polarization resolved measurement of the TPIV for 450nm and 550 nm linear polarized incident light with $\theta = 50°$ incidence angle.

$$t_{\mathrm{p}} = (0.02)^{1/2} \qquad , \qquad t_{\mathrm{s}} = (0.06)^{1/2} \qquad , \qquad \delta_t = 0 \tag{6.14}$$

λ=550 nm:

$$r_{\mathrm{p}} = (0.11)^{1/2} \qquad , \qquad r_{\mathrm{s}} = (0.34)^{1/2} \qquad , \qquad \delta_r = 0 \tag{6.15}$$

$$t_{\mathrm{p}} = (0.12)^{1/2} \qquad , \qquad t_{\mathrm{s}} = (0.09)^{1/2} \qquad , \qquad \delta_t = -1.76\pi \tag{6.16}$$

Using the above results for phase delays and coefficients and having fast axis of the quarter wave plate horizontal ($\alpha = 0$) which results in p- polarized light that then passes through the half wave plate and its rotation between $0°$ and $360°$ with $1°$ increment we could provide all orientations for the linear polarized light which are shown at top of the Fig. 6.9 for both 450 nm and 550 nm. In these two graphs β shows the angle of the half wave plate and we have plotted the transferred angular momentum as a function of β. For example, when $\beta = 0$ or $\beta = 45$ the results are p- and s- polarized light, respectively.
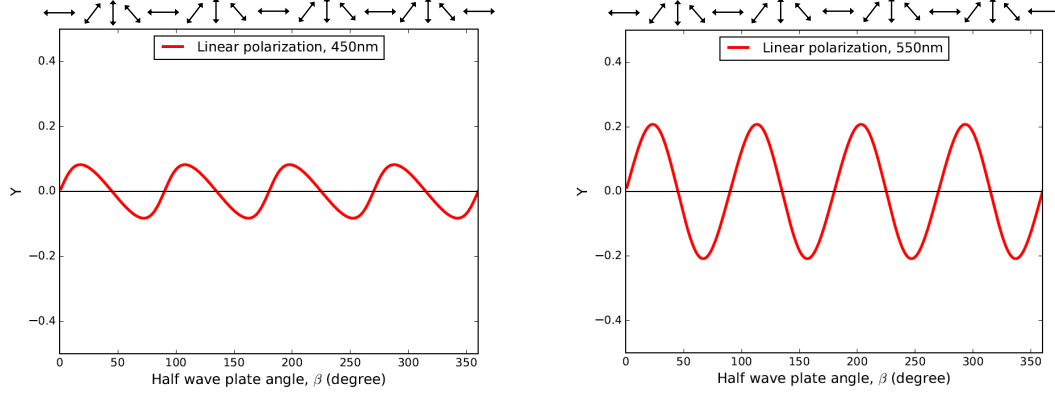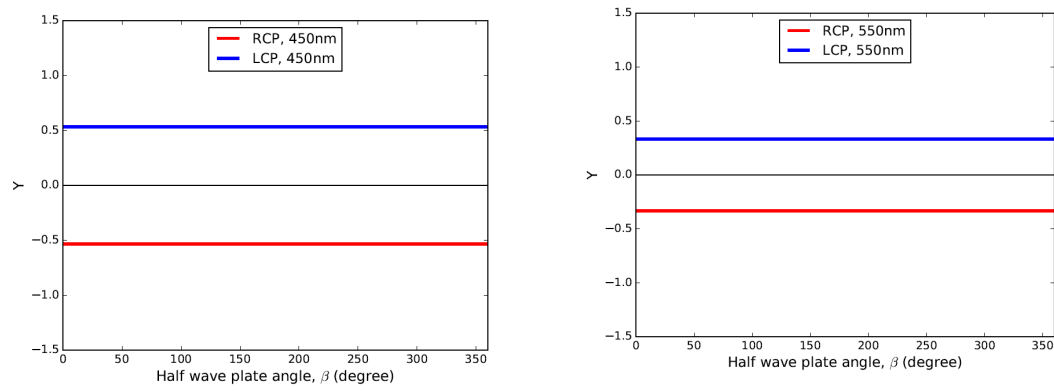
Figure 6.10: Polarization resolved measurement of the TPIV for 450nm and 550 nm circular polarized incident light with $\theta = +50°$ incidence angle.

Estimation of V_y using angular momentum flux:

For $\beta = 22.5°$ we can generate right hand circular polarized light. For this β for 450 nm calculation gives $Q = +0.1$.

Then produced voltage along the y direction is:

$$V_y = (\frac{LP_{\text{flux}}}{ned}) \tag{6.17}$$

and replacing P_{flux} with $L_{\text{flux}}k$ (k is wave vector of light) we have

Then produced voltage along the x direction is:

$$V_y = (\frac{L_{\text{flux}}kL}{ned}) \tag{6.18}$$

So, using I_I=1 MW/cm^2, L=5 mm, $n = 5.8 \times 10^{28}$ m^{-3}, $\theta = +45°$, $\lambda = 450$ nm and d=25 nm we have

$$L_{\text{flux}} = \frac{I_I}{\omega}Q\cos\theta = 8 \times 10^{-7}(\frac{J}{m^{-3}}) \tag{6.19}$$

and finally

$$V_y = (\frac{L_{\text{flux}}kL}{ned}) = +55\mu\text{V} \tag{6.20}$$

When sign of the Y is negative we will have a voltage with opposite sign. So, the voltage depends on the helicities of the lights.

Having $\alpha = 45°$ and $\alpha = 135°$, we produced RCP and LCP circular polarized light after the quarter wave plate. Fig. 6.10 show graphs for transferred angular momentum by these polarizations for both wavelengths. Fig. 6.11 show calculations for elliptical RCP and LCP produced with $\alpha = 120°$ and $\alpha = 60°$, respectively.

When our half wave plate is perfect half wave plate in visible range for all circular polarized lights we must have a straight line for both wavelengths, because there is not any effect on orientation of circular polarized light by rotating it through the half wave plate. But our measurements in the chapter 2 do not show the straight tendency. It means that our half wave plate is not perfect in this range. In our calculation we consider this imperfect work of the half wave plate and Fig. 6.11, down shows results for proper and improper half wave plates.

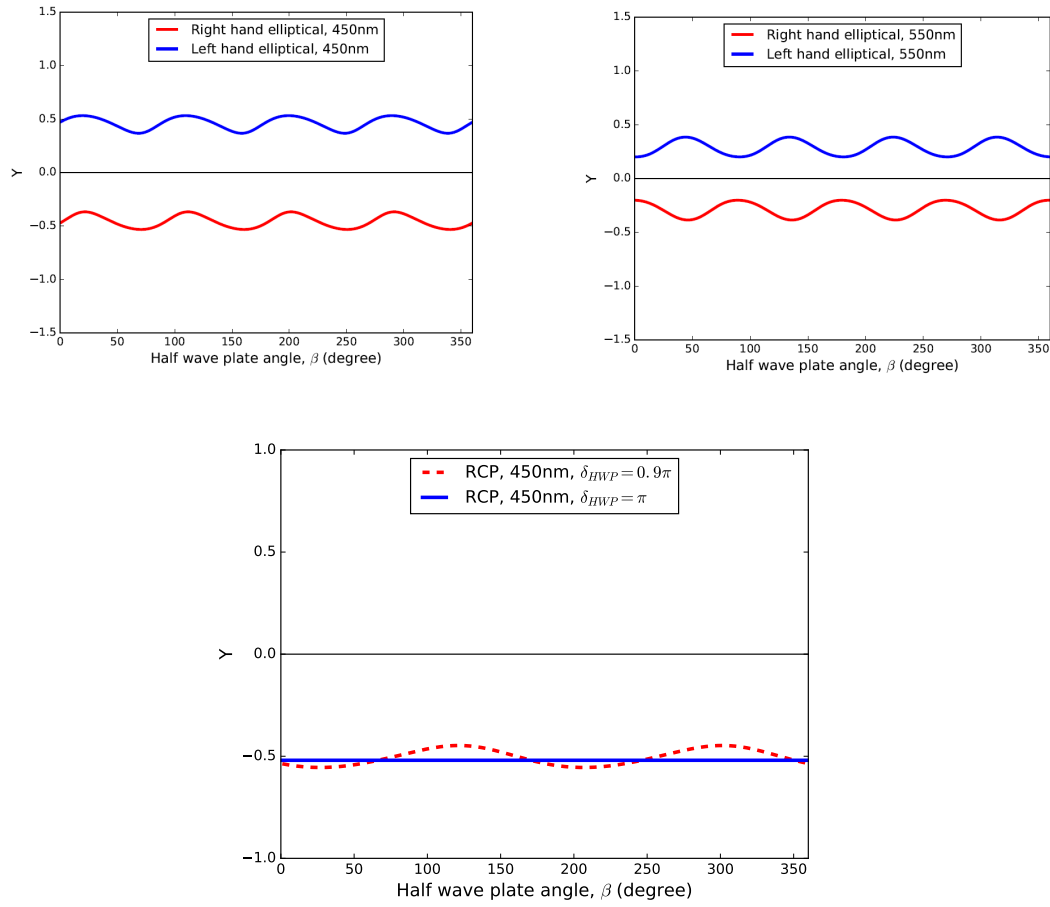**Figure 6.11:** Top: Polarization resolved measurement of the TPIV for 450nm and 550 nm elliptical polarized incident light with $\theta = +50°$ incidence angle, down: Polarization resolved measurement of the TPIV for 450nm RCP incident light with $\theta = +50°$ incidence angle for perfect ($\delta_{HWP} = \pi$) and imperfect ($\delta_{HWP} = 0.9\pi$) half wave plate for spongy nanoporous gold film.

6.4   Conclusions

Angular momentum transfer model was used to calculate TPIV in nanoporous gold films. Estimation of the voltages shows good agreement with the measurements. In the estimations we used parameter Y that could be negative or positive that gives the sign of the voltages.

6.5   Proposal for ellipcity-meter based on TPIV

6.6   Overview

Based on the observed TPIV in a 25 nm thin film of gold with simple nanoholes, we propose an ellipticity meter [48] . It is the first proposal of such a type of device to determine ellipticity. This device can be used to distinguish linearly, circularly and elliptically polarized light, can be fabricated from one 25 nm layer of this material compared to the linear polarization analyzer based on nanographite [49]. Among random and ordered nanostructures, two dimensional plasmonic nanostructures made by NSL are particularly suitable for commercialization. This method is an easy and low cost way to manufacture thin films [50]. Thin film of gold with random nanohole created by nanosphere lithography (NSL) is one of these random nanostructures and it has attracted interest to optical phenomena and applications of nanoholes in metal films [51]. This nanostructure has a good potential to serve as a plasmon nanohole photodetectors in visible range and various optoelectronic devices and applications in various fields such as optics, biological sensing and photovoltaic [52].

6.7   Mechanism

TPIV patterns for each polarized input light can be used in design of a ellipticity-meter to determine ellipticity of any unknown polarized light. In this case we can rotate the sample instead of rotating an achromatic HWP and we need not rely on the very accurate achromatic wave plate, which is a great advantage of the device. For this purpose we employ a design worked to determine ellipticity of the incident light on the film.

This ellipticity meter consists of a bushing cylinder and a slant on it for mounting the thin film with two electrodes. They are connected to an electrical measuring instrument and allow us to monitor the generated photo-voltage (Fig.6.12). As TPIV is proportional to the angular momentum transfer rather than the angular momentum carried by the incident beam, TPIV itself
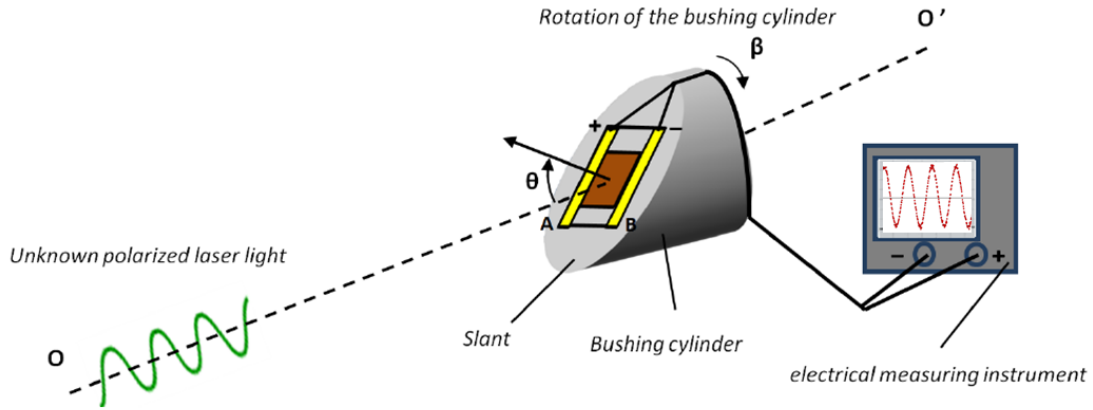
Figure 6.12: Bushing cylinder which rotates around axis OO' that coincides with propagation direction of the unknown light. For an unknown polarized light (green wave) by rotating the bushing, relative orientation of the incident light polarization to the electrodes is changed and TPIV is measured.

is not the measure of the ellipticity of the incident beam. As the bushing cylinder rotates, plane of incidence rotates while the two electrodes measure TPIV for different polarization orientation. It corresponds to having a fixed film and light with rotating orientation apply on the film. The β dependence shows specific pattern depending on the ellipticity carried by the incident beam. By comparing the pattern to the calculation, it is possible to determine the ellipticity of the incident beam. The ratio of average and amplitude gives an index that is related to the angular momentum. In order to make a quantitative determination of ellipticity, however, calibration due to wavelength dependence of Fresnel coefficients is necessary.

In contrast to polarization analyzer designed in [49] our ellipticity meter can be used to determine any linearly, circularly and elliptically polarized unknown light in visible wavelengths. Fabrication method of the thin film is simple compared to other materials used to fabricate such analyzers, for example, single wall carbon nanotube and nanographite. All electric semiconductor based detectors for Stokes parameter including helicity has been proposed since 2008 [53]. Using a CW laser with lock-in amplifier we can increase the sensitivity of the device. On the other hand by rotating the bushing cylinder we do not need to have half plate which may not be perfect for all range. So, this device does not depend on the wavelength.

In summary we have experimentally investigated transverse photo-induced voltage TPIV in 25 nm thick gold film with random nanoholes prepared by NSL technique. While TPIV is not generated by s- and p- polarized incident light, linearly, circularly and elliptically polarized light can generate TPIV. Sign and amplitudes of the voltage dependent on the sense of polarization, ellipticity and degree of polarization in circularly, elliptically and linearly polarized light. Calculation based on angular momentum transfer shows that transferred angular momentum from photon to

the film is responsible for this voltage. Based on this mechanism we have proposed a polarimeter that determines ellipticity.

CHAPTER 7

Summary

Nanoporous gold thin films are fabricated successfully using dealloying and nanosphere lithography techniques. For the first time photo-induced voltage is observed in these metallic random structures with irregular holes. For normal incidence angle both LPIV and TIV are zero. TPIV has a sign change by change the sense of rotation for circular and diagonal polarizations. Similar to periodic photonic crystals, LPIV with s- polarization can be estimated using linear momentum transfer to the film. For p- polarization only for spongy nanoporous gold, excitation of LSPR for longer wavelengths generate large positive voltage in nanoholes that depending on the density of pores. Considering this anomalous sign change only for spongy nanoporous gold, we can consider it as a metamaterial compared to the gold thin film with simple nanoholes.

CHAPTER 8

Conclusions

Longitudinal and transverse photo-induced voltage in periodic structures has been investigated and 2nd order Lorentz force can explain the voltages in these structures. In these structures there is enhancement of the voltages at the resonances at particular incidence angle and wavelength. In this thesis I have investigated photo-voltage in nanoporous gold films with randomly distributed holes in the structure. These films have free electrons with simple band structures and their subwavelength feature allows us to consider them as metamaterials if they provide structure dependent anomalous response. Because of the holes and their random distribution in the structure, electric fields inside the structure is complicated and it is not practical to calculate microscopic Lorentz force to obtain the voltage as was used in previous works.

Therefore I have tried another approach which is conservation of linear momentum in the film. By this approach we can estimate the LPIV for s- polarization for all wavelengths, while for p-polarization the positive sign for longer wavelength cannot be explained. Because our structure is random we do not expect specific resonance in wavelengths and to investigate the origin of this anomalous response we modeled spongy nanoporous gold by a simple grating and numerical calculation of electromagnetic fields. Simulation shows that gradient force due to discontinuity in the boundaries of hole and gold results in small batteries inside the holes, even in the non-resonant case and summation of these batteries makes the total positive LPIV with p- polarization for positive incidence angle.

For more understanding the reason for this response of spongy nanoporous gold, gold thin film

with simple holes was fabricated. In contrast to the spongy nanoporous gold film, LPIV with p- polarization does not show such anomalous response as observed for spongy nanoporous gold. Considering the ratio of holes in the total volume of two samples which is 50% and 15% for spongy nanoporous gold and gold thin film with simple holes, respectively, it seems that for the gold thin film with the simple holes, gradient force due to discontinuities makes holes to work as small batteries, but smaller volume ratio of holes in the second structure gives rise to lower effect of the batteries. So, by applying p- polarization, large negative voltage generated by linear momentum and small positive voltage due to batteries gives the total negative voltage for positive incidence angles which is opposite to the positive voltage for positive incidence angle for spongy nanoporous gold film. So, the volume ratio of the films has the role for the different response of this gold structure. For spongy nanoporous gold high density of pores is responsible for DC field that gives the anomalous response. Thus, spongy nanoporous gold can be considered as metamaterial in this case.

For TPIV sign of the voltage is found to depend on the sense on the rotation of the circular or diagonal polarized light which is similar to the TPIV in periodic structures. Estimation of TPIV using Lorentz force in the structure is complicated due to randomness. So, similar to the LPIV we use conservation of angular momentum to calculate the voltages.

Finally, PIV does not depend on irregularity of holes and their random distributions and presence of holes has the main role to generate large voltage. In structure with irregular holes, TPIV was explained by mirror symmetry. Lack of resonance due to randomness results in broadband response and observation fundamental behaviors of the structure (applications in broadband devices, for example, sensors).

CHAPTER 9

Future works

1. PIV can be measured in films with different size of holes and area density. By decreasing the size of holes and increasing the number of holes per area we expect to observe larger voltage due to larger effect of LSPR and increase surface to volume ratio of holes in the structure.

2. Nanoporous Aluminum is another plasmonic material that could generate PIV. As Hall measurement shows free carriers of Aluminum in room temperature are electrons and similar to gold and silver, we expect to observe similar behaviors for PIV voltage.

3. By infiltrating the nanoholes with appropriate polymers, it is possible to control the sign and amplitude of the PIV, which could have applications is optical sensing.

4. As we saw PIV does not depend on randomness, so periodic structures with small periods could be used to investigate more about fundamental nature of the sign change.

List of Publications

[1] **Akbari, M.**, Onoda, M., Ishihara, T. "Photo-induced Voltage in Nano-porous Gold Thin Film," Optics Express, Vol. 23, Issue 2, pp. 823-832, 2015.

[2] **Akbari, M.**, Ishihara, T. "Polarization dependence of transverse photo-induced voltage in gold thin film with random nanoholes," Optics Express, Vol. 25, Issue 3, pp. 2143-2152, 2017.

Bibliography

[1] G. M. Mikheev, V. M. Styapshin, P. A. Obraztsov, E. A. Khestanova, and S. V. Garnov. "Effect of laser light polarisation on the dc photovoltage response of nanographite films". *Quantum Electronics* 40 (2010), pp. 425–430.

[2] A. F. Gibson, M. F. Kimmitt, and A. C. Walker. "Photon Drag in Germanium". *Applied Physics Letters* 31 (1970).

[3] V. G. Agafonov, P. M. Valov, B. S. Ryvkin, I. D. Yaroshetski, and F. T. Poluprovodn. "Photon Drag in Germanium". *Sov. Phys. Semicond.,* 7 (1973).

[4] A. S. Vengurlekar and T. Ishihara. "Surface plasmon enhanced photon drag in metal films". *Applied Physics Letters* 87.9 (2005).

[5] G. M. Mikheev, A.G. Nasibulin, R.G. Zonov, A. Kaskela, and E. I. Kauppinen. "Photon-Drag Effect in Single-Walled Carbon Nanotube Films". *Nano Letters* 12 (2012), pp. 77–83.

[6] J. E. Goff and W. L. Schaich. "Hydrodynamic theory of photon drag". *Phys. Rev. B* 56 (1997), pp. 15421–15430.

[7] S. Luryi. "Photon-Drag Effect in Intersubband Absorption by a Two-Dimensional Electron Gas". *Phys. Rev. Lett.* 58 (1987), pp. 2263–2266.

[8] V. L. Gurevich and R. Laiho. "Photomagnetism of metals. first observation of dependence on polarization of light". *Physics of the Solid State* 42.10 (2000), pp. 1807–1812.

[9] T. Ishihara. "Optical response of semiconductor and metal-embedded photonic crystal slabs". *physica status solidi (a)* 201.3 (2004).

[10] T. Hatano, B. Nishikawa, M. Iwanaga, and T. Ishihara. "Optical rectification effect in 1D metallic photonic crystal slabs with asymmetric unit cell". *Opt. Express* 16 (2008), pp. 8236–8241.

[11]   T. Hatano, B. Nishikawa, H. Kurosawa, and T. Ishihara. "Transverse Photo Voltage Induced by Circularly Polarized Light in Metallic Photonic Crystal Slabs". *Conference on Lasers and Electro-Optics/Quantum Electronics and Laser Science Conference and Photonic Applications Systems Technologies* (2008).

[12]   T. Ishihara, T. Hatano, H. Kurosawa, Y. Kurami, and N. Nishimura. "Transverse Voltage Induced by Circularly Polarized Obliquely incident light in plasmonic Crystals". *Proceeding of SPIE Vol. 8461 846117-2* (2012).

[13]   H. Kurosawa and T. Ishihara. "Surface plasmon drag effect in a dielectrically modulated metallic thin film". *Opt. Express* 20.2 (2012), pp. 1561–1574.

[14]   E. L. Ivchenko and G. Pikus. "New photogalvanic effect in gyrotropic crystals". *JETP Lett* 27.11 (1978), pp. 604–608.

[15]   S. D. Ganichev, E. L. Ivchenko, S. N. Danilov, J. Eroms, W. Wegscheider, D. Weiss, and W. Prettl. "Conversion of Spin into Directed Electric Current in Quantum Wells". *Phys. Rev. Lett.* 86 (2001), pp. 4358–4361.

[16]   T. Hatano, T. Ishihara, S G. Tikhodeev, and N. A. Gippius. "Transverse Photovoltage Induced by Circularly Polarized Light". *Phys. Rev. Lett.* 103 (2009), p. 103906.

[17]   G. Mikheev, V. Aleksandrov, and A. Saushin. "Circular photogalvanic effct observed in silver-palladium film resistors". *Technical Physics Letters* 37 (2011), pp. 551–556.

[18]   K. G. Mikheev, A. S. Saushin, R.G. Zonov, A. G. Nasibulin, and G. M. Mikheev. "Photon-drag in single-walled carbon nanotube and silver-palladium films: the effect of polarization". *Journal of Nanophotonics* 10(1) (2015).

[19]   C. Jiang, V. A. Shalygin, V. Y. Panevin, S. N. Danilov, M. M. Glazov, R. Yakimova, S. Lara-Avila, S. Kubatkin, and S.D. Ganichev. "Helicity-dependent photocurrents in graphene layers excited by midinfrared radiation of a CO_2 laser". *Physical Review B* 84.12 (2011), p. 125429.

[20]   M. Akbari, M. Onoda, and T. Ishihara. "Photo-induced voltage in nano-porous gold thin film". *Optics express* 23.2 (2015), pp. 823–832.

[21]   N. Noginova, V. Rono, F.J. Bezares, and J. D.Caldwell. "Plasmon drag effect in metal nanostructures". *New Journal of Physics* 15.11 (2013), p. 113061.

[22] N. V. Proscia, M. Moocarme, R. Chang, I. Kretzschmar, V. M. Menon, and L. T. Vuong. "Control of photo-induced voltages in plasmonic crystals via spin-orbit interactions". *Optics express* 24.10 (2016), pp. 10402–10411.

[23] W. L. Barnes and W. Thomas. "Surface plasmon subwavelength optics". *Nature* 424 (2003).

[24] J. M. Pitarke, V. M. Silkin, E. V. Chulkov, and P. M. Echenique. "Theory of surface plasmons and surface-plasmon polaritons". *Reports on Progress in Physics* 70 (2007), pp. 1–87.

[25] S. Chang, S. K. Gray, and G. C. Schatz. "Surface plasmon generation and light transmission by isolated nanoholes and arrays of nanoholes in thin metal films". *Optics Express* 13.8 (2005), pp. 3150–3165.

[26] J. L. Hammond, N. Bhalla, S. D. Rafiee, and P. Estrela. "Localized surface plasmon resonance as a biosensing platform for developing countries". *Biosensors* 4.2 (2014), pp. 172–188.

[27] S. A. Maier. *Plasmonics: fundamentals and applications.* Springer Science & Business Media, (2007).

[28] J. D. Jackson. *Classical electrodynamics.* 3rd ed. New York, NY: Wiley, 1999. ISBN: 9780471309321.

[29] W. Cai and V. M. Shalaev. *Optical Metamaterials, Fundamental and Appliations.* Springer, (2009).

[30] W. Cai, U. K. Chettiar, H-K. Yuan, V. C. de Silva, A. V. Kildishev, V. P. Drachev, and V. M. Shalaev. "Metamagnetics with rainbow colors". *Opt. Express* 15.6 (2007), pp. 3333–3341.

[31] V. M. Shalaev, W. Cai, U. K. Chettiar, H-K. Yuan, A. K. Sarychev, V. P. Drachev, and A. V. Kildishev. "Negative index of refraction in optical metamaterials". *Opt. Lett.* 30.24 (2005), pp. 3356–3358.

[32] W. Wang, H. Xing, L. Fang, Y. Liu, J. Ma, L. Lin, C. Wang, and X. Luo. "Far-field imaging device: planar hyperlens with magnification using multi-layer metamaterial". *Opt. Express* 16.25 (2008), pp. 21142–21148.

[33] A. K. Popov and V. M. Shalaev. "Negative-index metamaterials: second-harmonic generation, Manley-Rowe relations and parametric amplification". *Applied Physics B* 84.1-2 (2006), pp. 131–137.

[34] G. H. B. Thompson. "Unusual Waveguide Characteristics associated with the Apparent Negative Permeability obtainable in Ferrites". *Nature* 175 (1955), pp. 1135–1136.

[35] J. Pendry. "Focus Issue: Negative Refraction and Metamaterials". *Opt. Express* 11.7 (2003), pp. 639–639.

[36] R. Singh, X. Lu, J. Gu, Z. Tian, and W. Zhang. "Random terahertz metamaterials". *Journal of Optics* 12.1 (2009), p. 015101.

[37] O. Hess, J. B. Pendry, S. A. Maier, R. F. Oulton, J. M. Hamm, and K. L. Tsakmakidis. "Active nanoplasmonic metamaterials". *Nature materials* 11.7 (2012), pp. 573–584.

[38] A. Wittstock, J. Biener, J. Erlebacher, and M. Baumer, eds. "Nanoporous Gold: From an Ancient Technology to a High-Tech Material". RSC Publishing, (2012).

[39] A. Wittstock, J. Biener, and M. Baumer. "Nanoporous gold: a new material for catalytic and sensor applications". *Phys. Chem. Chem. Phys.* 12 (2010), pp. 12919–12930.

[40] N. Sardana, F. Heyroth, and J. Schilling. "Propagating surface plasmons on nanoporous gold". *J. Opt. Soc. Am. B* 29.7 (2012).

[41] S. Hyun and E. Koo. "Scale-and shape-dependent transport property of nanoporous materials". *Journal of Applied Physics* 113.7 (2013), p. 074301.

[42] W. Li, J. O. Tegenfeldt, L. Chen, R. H. Austin, S. Y. Chou, P. A. Kohl, J. Krotine, and J. C. Sturm. "Sacrificial polymers for nanofluidic channels in biological applications". *Nanotechnology* 14.6 (2003), p. 578.

[43] L. S. Live, A. Dhawan, K. F. Gibson, H-P. Poirier-Richard, D. Graham, M. Canva, T. Vo-Dinh, and J-F. Masson. "Angle-dependent resonance of localized and propagating surface plasmons in microhole arrays for enhanced biosensing". *Analytical and bioanalytical chemistry* 404.10 (2012), pp. 2859–2868.

[44] T. Park, N. Mirin, J. B.Lassiter, C. L. Nehl, N. J. Halas, and P. Nordlander. "Optical properties of a nanosized hole in a thin metallic film". *Acs Nano* 2.1 (2008), pp. 25–32.

[45] H. Kurosawa, T. Ishihara, N. Ikeda, D. Tsuya, M. Ochiai, and Y. Sugimoto. "Optical rectification effect due to surface plasmon polaritons at normal incidence in a nondiffraction regime". *Opt. Lett.* 37.14 (2012), pp. 2793–2795.

[46] J. Junesch and T. Sannomiya. "Ultrathin suspended nanopores with surface plasmon resonance fabricated by combined colloidal lithography and film transfer". *ACS applied materials & interfaces* 6.9 (2014), pp. 6322–6331.

[47] F-H. Yeh, C-C. Tai, J-F. Huang, and I-W. Sun. "Formation of porous silver by electrochemical alloying/dealloying in a water-insensitive zinc chloride-1-ethyl-3-methyl imidazolium chloride ionic liquid". *The Journal of Physical Chemistry B* 110.11 (2006), pp. 5215–5222.

[48] M. Akbari and T. Ishihara. "Polarization dependence of transverse photo-induced voltage in gold thin film with random nanoholes". *Optics Express* 25.3 (2017), pp. 2143–2152.

[49] G. M. Mikheev and V.M. Styapshin. "Nanographite analyzer of laser polarization". *Instruments and Experimental Techniques* 55.1 (2012), pp. 85–89.

[50] P. Zheng, S. K. Cushing, S. Suri, and N. Wu. "Tailoring plasmonic properties of gold nanohole arrays for surface-enhanced Raman scattering". *Physical Chemistry Chemical Physics* 17.33 (2015), pp. 21211–21219.

[51] T. Rindzevicius, Y. Alaverdyan, B. Sepulveda, T. Pakizeh, M. Kll, R. Hillenbrand, J. Aizpurua, and F. J. Garca de Abajo. "Nanohole Plasmons in Optically Thin Gold Films". *The Journal of Physical Chemistry C* 111.3 (2007), pp. 1207–1212.

[52] T. Ohno, C. Wadell, S. Inagaki, J. Shi, Y. Nakamura, S. Matsushita, and T. Sannomiya. "Hole-size tuning and sensing performance of hexagonal plasmonic nanohole arrays". *Opt. Mater. Express* 6.5 (2016), pp. 1594–1603.

[53] S. D. Ganichev, W. Weber, J. Kiermaier, S. N. Danilov, P. Olbrich, D. Schuh, W. Wegscheider, D. Bougeard, G. Abstreiter, and W. Prettl. "All-electric detection of the polarization state of terahertz laser radiation". *Journal of Applied Physics* 103.11 (2008), p. 114504.